

Air Force Institute of Technology

AFIT Scholar

Theses and Dissertations

Student Graduate Works

3-17-2008

On-Board Thermal Management of Waste Heat from a High-Energy Device

Nathan D. Klatt

Follow this and additional works at: <https://scholar.afit.edu/etd>



Part of the [Aerospace Engineering Commons](#)

Recommended Citation

Klatt, Nathan D., "On-Board Thermal Management of Waste Heat from a High-Energy Device" (2008).
Theses and Dissertations. 2684.
<https://scholar.afit.edu/etd/2684>

This Thesis is brought to you for free and open access by the Student Graduate Works at AFIT Scholar. It has been accepted for inclusion in Theses and Dissertations by an authorized administrator of AFIT Scholar. For more information, please contact richard.mansfield@afit.edu.



**ON-BOARD THERMAL MANAGEMENT OF WASTE HEAT FROM
A HIGH-ENERGY DEVICE**

THESIS

Nathan D. Klatt, Captain, USAF
AFIT/GAE/ENY/08-M18

DEPARTMENT OF THE AIR FORCE
AIR UNIVERSITY

AIR FORCE INSTITUTE OF TECHNOLOGY

Wright-Patterson Air Force Base, Ohio

APPROVED FOR PUBLIC RELEASE; DISTRIBUTION UNLIMITED

The views expressed in this thesis are those of the author and do not reflect the official policy or position of the United States Air Force, Department of Defense, or the U. S. Government.

AFIT/GAE/ENY/08-M18

**ON-BOARD THERMAL MANAGEMENT OF WASTE HEAT FROM A HIGH-
ENERGY DEVICE**

THESIS

Presented to the Faculty

Department of Aeronautical and Astronautical Engineering

Graduate School of Engineering and Management

Air Force Institute of Technology

Air University

Air Education and Training Command

In Partial Fulfillment of the Requirements for the
Degree of Master of Science in Aeronautical Engineering

Nathan D. Klatt, B.S.

Captain, USAF

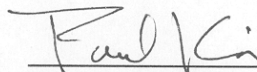
March 2008

APPROVED FOR PUBLIC RELEASE; DISTRIBUTION UNLIMITED.

ON-BOARD THERMAL MANAGEMENT OF WASTE HEAT FROM A HIGH-ENERGY DEVICE

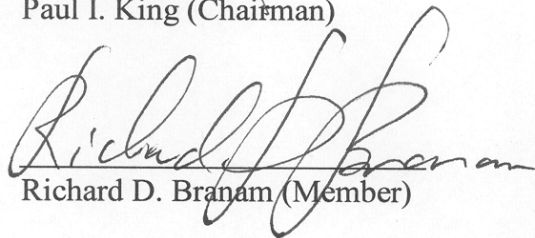
Nathan D. Klatt, B.S.
Captain, USAF

Approved:



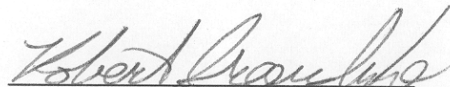
Paul I. King (Chairman)

13 Mar 08
date



Richard D. Branam (Member)

17 Mar 08
date



Robert B. Greendyke (Member)

13 Mar 08
date

Abstract

A method is presented that explores the primary design factors for an on-board high-energy laser or microwave-generated waste heat removal system and the trade space among the laser/microwave power, overall thermal efficiency, and duty cycle.

Methodology includes incorporation of single or cascaded vapor cycles (heat pumps) that transfer waste heat from a high-energy device into a heat exchanger installed in the bypass section a mixed-bypass turbofan engine of the type typically found on high performance aircraft. Analyzed are multiple bypass heat exchanger configurations that allow unimpeded air flow, minimizing friction and blockage losses. It is demonstrated that such an engine-heat exchanger combination can remove laser/microwave-generated waste heat with little to no effect on engine performance.

Acknowledgments

Special thanks to my advisor Dr. Paul King for allowing me to go off in a new direction with my research topic. My interest in this topic helped me thoroughly enjoy the research process and develop a new appreciation for the investigation of the world we live in. Dr. King's guidance kept me out of the metaphorical weeds and his encouragement motivated me through the long hours of work.

I'd like to thank Dr. Nicholas Kuprowicz at AFRL/RZTA for providing a variety of operationally oriented research topics. His inputs opened the door to a topic that I otherwise never would have considered. The background and technical support he provided gave me tremendous insight that kept my research focused.

My wife provided colossal support through many long days and nights of study and work. From bringing food during the all-nighters to keeping the home-front intact, she has been a model of help and encouragement. She has persevered through the lonely times when I was engrossed in studies and she never complained. I owe her an enormous debt.

To God be all the glory and honor, forever.

Table of Contents

	Page
Abstract.....	iii
List of Figures.....	vii
List of Tables	x
List of Symbols	xi
I. Introduction	1
<u>Objectives</u>	6
II. Background and Theory	7
<u>High-Energy Device</u>	7
<u>Thermal Storage Device</u>	7
<u>Heat Pump</u>	8
<u>Bypass Heat Exchanger</u>	12
<u>Engine Cycle</u>	19
<u>Chapter Summary</u>	25
III. Computational Setup	26
<u>Hardware</u>	26
<u>Software</u>	26
<u>Software Inputs</u>	26
<u>Code Validation</u>	28
IV. Results and Discussion	29
<u>Duty Cycle</u>	29
<u>Heat Pump</u>	30
<i>Temperature Profile</i>	30
<i>External Transfer Rates</i>	32
<i>Compressor Efficiency</i>	34
<u>Bypass Heat Exchanger</u>	36
<i>Single Heat Pump, Single Surface Heat Exchanger</i>	36
<i>Single Heat Pump, Dual Surface Heat Exchanger</i>	39
<i>Device Power Class and Bypass Length</i>	40
<i>Maximum Laser Class with Single Heat Exchanger</i>	42
<i>Maximum Microwave Class with Single Heat Exchanger</i>	43
<i>Cascaded Heat Exchanger</i>	44
<i>Maximum Laser Class with Cascaded Heat Exchanger</i>	46
<i>Maximum Microwave Class with Cascaded Heat Exchanger</i>	47
<i>Heat Transfer Rate into Bypass Air</i>	49
<i>Thermal Resistance in Bypass Heat Exchanger</i>	50
<i>Bypass Heat Exchanger Weight</i>	51
<u>Engine Cycle – Component Level</u>	52
<i>Bypass Duct</i>	53

<i>Additional Turbine Electric Power Requirement</i>	54
<i>Mixer</i>	57
<u>Engine Cycle – System Level</u>	59
<i>Uninstalled Thrust</i>	59
<i>Uninstalled Thrust Specific Fuel Consumption</i>	61
<u>Sensitivity Analysis</u>	63
<u>Flight Envelope</u>	65
<i>Off-Design Analysis</i>	65
<i>Device Power Class, at 100% Engine Throttle</i>	67
<i>Device Power Class, at 80% Engine Throttle</i>	70
V. Conclusions and Recommendations	72
<u>Conclusions</u>	72
<u>Recommendations</u>	74
Appendices	76
<u>Appendix A: General Results for Thermal Management Cycles</u>	77
<u>Appendix B: Engine Effects from the Thermal Management Cycles</u>	83
<u>Appendix C: Sensitivity Analysis Results</u>	85
<u>Appendix D: High-Energy Device and Engine Operation Envelopes</u>	89
<u>Appendix E: Discrete pressure values used in steam tables (psi)</u>	101
Bibliography	102
Vita	104

List of Figures

	Page
Fig. 1. Energy flow diagram	4
Fig. 2. T-s diagram for the heat pump showing external energy transfers	9
Fig. 3. Physical diagram of the heat pump showing component interfaces with the thermal storage device and the engine	10
Fig. 4. Engine schematic showing the layout of the heat exchanger	12
Fig. 5. Bypass heat exchanger segment cross section showing material configuration ...	15
Fig. 6. Simplified engine schematic showing section labels and dual surface heat exchanger	18
Fig. 7. Engine station numbering for reference in equations	20
Fig. 8. Correlation of input power and thermal transfer load	29
Fig. 9. Maximum temperature change of the vapor-compression cycle at a given phase change temperatures of the evaporator with an 80% efficient pump.....	31
Fig. 10. Maximum energy transfer rates of the condenser and the compressor with an 80% efficient pump.....	33
Fig. 11. Effects of compressor efficiency on phase change temperatures	34
Fig. 12. Effects of compressor efficiency on compressor exit temperature (T_2)	35
Fig. 13. Maximum energy transfer rates of the condenser with a 100kW laser and an 80% efficient heat pump compressor	38
Fig. 14. Heat exchanger lengths for a 100kW thermal management system at a range of evaporator temperatures.....	40
Fig. 15. Heat exchanger lengths for a 500 kW and a 1 MW thermal management system showing minimum evaporator temperatures.....	41
Fig. 16. Heat exchanger lengths for a thermal management system showing minimum evaporator temperatures for a variety of device power levels	42
Fig. 17. Cascade cycle showing multiple heat pumps	45
Fig. 18. Total heat transfer rate into the bypass air.....	49
Fig. 19. Thermal resistance at mean point between point 2p and 3, for a single heat pump, single surface heat exchanger	50
Fig. 20. Total pressure and total temperature ratios for the engine bypass section with a dual surface, single heat pump at the reference flight condition	53
Fig. 21. Thermal transfer rate at the bypass heat exchanger as a function of device power class.....	55

Fig. 22. Total temperature ratio across low-pressure turbine showing affects of heat pump power requirements.....	56
Fig. 23. Total pressure ratio across low-pressure turbine showing affects of heat pump power requirements.....	57
Fig. 24. Total temperature ratio across the mixer showing affects of the thermal management system.....	58
Fig. 25. Total pressure ratio across the mixer showing effects of the thermal management system.....	58
Fig. 26. Uninstalled thrust showing the change in a non-afterburning engine performance as a result of the thermal management system.....	60
Fig. 27. Uninstalled thrust showing the change in a afterburning engine performance as a result of the thermal management system.....	61
Fig. 28. Uninstalled thrust specific fuel consumption showing the change in a non-afterburning engine performance as a result of the thermal management system.....	62
Fig. 29. Uninstalled thrust specific fuel consumption showing the change in an afterburning engine performance as a result of the thermal management system.....	63
Fig. 30 Off-design points used for flight regime device operating limits.....	66
Fig. 31. Mach number vs. altitude plot of maximum supportable laser power [MW] at 100% engine throttle.....	68
Fig. 32. Achievable device power class for a single surface bypass heat exchanger, single heat pump, at reference flight conditions.....	77
Fig. 33. Achievable device power class for a dual surface bypass heat exchanger, single heat pump, at reference flight conditions.....	77
Fig. 34. Achievable device power class for a single surface bypass heat exchanger, cascaded heat pumps, under reference conditions.....	78
Fig. 35. Achievable device power class at given evaporator temperature for a dual surface bypass heat exchanger, cascaded heat pumps, under reference conditions.....	78
Fig. 36. Temperature profile at given power class for a single surface bypass heat exchanger, single heat pump, under reference conditions.....	79
Fig. 37. Temperature profile at given power class for a dual surface bypass heat exchanger, single heat pump, under reference conditions.....	79
Fig. 38. Temperature profile at given power class for a single surface bypass heat exchanger, cascaded heat pumps, under reference conditions.....	80
Fig. 39. Temperature profile at given power class for a dual surface bypass heat exchanger, cascaded heat pumps, under reference conditions.....	80
Fig. 40. Thermal resistance at the condenser mean phase change point for the single heat pump with a single surface heat exchanger.....	81

Fig. 41. Thermal resistance at the condenser mean phase change point for the single heat pump with a dual surface heat exchanger	81
Fig. 42. Thermal resistance at the condenser mean phase change point for the cascaded heat pumps with a single surface heat exchanger	82
Fig. 43. Thermal resistance at the condenser mean phase change point for the cascaded heat pumps with a dual surface heat exchanger.....	82
Fig. 44. Total temperature and total pressure ratios for the single heat pump, single surface heat exchanger.....	83
Fig. 45. Total temperature and total pressure ratios for the single heat pump, dual surface heat exchanger	83
Fig. 46. Total temperature and total pressure ratios for the cascade, single surface heat pump	84
Fig. 47. Total temperature and total pressure ratios for the cascade, dual surface heat pump	84
Fig. 48. Maximum laser power [MW] at 100% throttle	89
Fig. 49. Maximum microwave power [MW] at 100% throttle	90
Fig. 50. Maximum laser device cooling capacity [BTU/s] at 100% throttle	91
Fig. 51. Maximum microwave device cooling capacity [BTU/s] at 100% throttle	92
Fig. 52. Maximum laser power [MW] at 80% throttle	93
Fig. 53. Maximum microwave power [MW] at 80% throttle	94
Fig. 54. Maximum laser device cooling capacity [BTU/s] at 80% throttle	95
Fig. 55. Maximum microwave device cooling capacity [BTU/s] at 80% throttle	96
Fig. 56. Difference between 100% and 80% engine throttle for maximum laser device power [MW].....	97
Fig. 57. Difference between 100% and 80% engine throttle for maximum microwave device power [MW]	98
Fig. 58. Difference between 100% and 80% engine throttle for maximum laser device cooling rate [BTU/s]	99
Fig. 59. Difference between 100% and 80% engine throttle for maximum microwave device cooling rate [BTU/s].....	100

List of Tables

	Page
Table 1. Reference engine parameters and flight conditions	27
Table 2. Reference thermal managements parameters	27
Table 3. Maximum supported laser power using a single heat pump at the reference flight condition	43
Table 4. Maximum supported microwave power using a single heat pump at the reference flight condition.....	44
Table 5. Maximum supported laser power using cascaded heat pumps at the reference flight condition.....	47
Table 6. Cascade heat exchanger showing the maximum supported microwave system class for a given configuration.....	48
Table 7. Stagnation pressures and temperatures of reference engine high-energy device and thermal management system.....	54
Table 8. Sensitivity analysis for a single heat pump, single surface heat exchanger cooling a laser	64
Table 9. Sensitivity analysis for a single heat pump, single surface heat exchanger cooling a laser device.....	85
Table 10. Sensitivity analysis for a single heat pump, single surface heat exchanger cooling a microwave device.....	85
Table 11. Sensitivity analysis for a single heat pump, dual surface heat exchanger cooling a laser device.....	86
Table 12. Sensitivity analysis for a single heat pump, dual surface heat exchanger cooling a microwave device.....	86
Table 13. Sensitivity analysis for a cascaded, single surface heat pump cooling a laser device	87
Table 14. Sensitivity analysis for a cascaded, single surface heat pump cooling a microwave device	87
Table 15. Sensitivity analysis for a cascaded, dual surface heat pump cooling a laser device	88
Table 16. Sensitivity analysis for a cascaded, dual surface heat pump cooling a microwave device	88

List of Symbols

Acronyms

AFB	Air Force Base
AFIT	Air Force Institute of Technology
AFRL	Air Force Research Laboratory
AIAA	American Institute of Aeronautics and Astronautics
LCD	Liquid Crystal Display
NASA	National Aviation and Space Administration
NIST	National Institute of Standards and Technology
NOAA	National Oceanic and Atmospheric Administration
RAM	Random Access Memory

Symbols

A	Cross-sectional area [ft ²]
a	Speed of sound [ft/s]
C	Constant
C_p	Specific heat at constant pressure [BTU/lbm/R]
D	Diameter [ft]
e	Polytropic efficiency
f	Fuel-to-air mass flow ratio
F	Uninstalled thrust [lbf]
f_{DC}	Duty cycle factor
g_c	Newton's gravitational constant
h	Enthalpy [BTU/lbm]; Heat transfer coefficient [BTU/hr/ft ² /R]
h_{PR}	Heating value of fuel
k	Thermal conductivity [BTU/hr/ft/R]
\dot{m}	Mass flow rate [lbm/s]
M	Mach number
n_{pipes}	Number of coolant pipes in the bypass section
P_{input}	Input power to the laser system [W]
Pr	Prandtl number
p	Pressure [psf]
P	Power [BTU/s]
\dot{q}	Heat transfer rate per foot of bypass section [BTU/s/ft]
\dot{Q}	Heat transfer rate through the condenser into the engine [BTU/s]
Q	Total energy stored within the storage device [BTU]
R	Specific gas constant [ft*lbf/lbm/R]
Re	Reynolds number
SFC	Specific fuel consumption [1/hr]
S	Uninstalled thrust specific fuel consumption [1/hr]
T	Temperature [R]
t	Time, microwave emission or lase time [s]
U	Velocity [ft/hr]

Greek Symbols

α	Engine bypass ratio
α'	Mixer bypass ratio
β	Bleed air fraction
ε	Cooling air fraction
γ	Ratio of specific heats
η	Efficiency
η_{laser}	High-energy device system efficiency
μ	Dynamic viscosity [lbm/ft/hr]
π	Ratio of total pressure across a component
σ_h	Circumferential or hoop stress capacity of the conducting material
τ	Ratio of total temperature across a component
ρ	Density [lbm/ft ³]

Subscripts

0-9	Engine reference locations, see Fig. 8.
AB	Afterburner
b	Burner
BP	Bypass section
BypassSurface	Surface area of bypass air in contact with the heat exchanger
c	Heat pump compressor, engine compressor
cH	High pressure compressor (engine)
cL	Low-pressure compressor (engine)
condenser	Heat pump condenser at the bypass section
coolant	Heat pump coolant properties at the bypass heat exchanger
evaporator	Heat pump evaporator at the thermal storage device
f	Fan or fuel
fAB	Fuel at afterburner
g	Gas or air
gen	Waste heat generation rate
λ	Change in conditions from point zero to point four
laser	Laser device or microwave device
mix	Mixer
mL	Mechanical, low-pressure spool
mH	Mechanical, high-pressure spool
mPL	Mechanical, power takeoff shaft from low-pressure spool
pipes	Coolant pipe property
r	Freestream recovery
T	Stagnation conditions
t	Turbine
tL	Low-pressure turbine

tH
TOL

High pressure turbine
Power takeoff, low-pressure

ON-BOARD THERMAL MANAGEMENT OF WASTE HEAT FROM A HIGH-ENERGY DEVICE

I. Introduction

High energy devices like high-power lasers and microwave devices have become smaller and lighter than when first developed. Combining the mobility of an aircraft with the benefits of these technologies are continuing development, as discussed in Scott (2004:1-3). Today, low power lasers are used on many U.S. military aircraft within laser targeting pods. In the attempt to utilize lasers with higher power, one of the major challenges is handling the large amount of waste heat generated from a low system level efficiency.

Currently, high-energy laser systems are about 10% efficient, as described in (Perram et al., 2004:14). The remaining 90% of the input electric energy is converted into waste thermal energy that must be managed. The input power for a high-energy laser is typically greater than 100 kW and is sometimes in the megawatt-class. For a one megawatt laser, the thermal load is often 900 kW with a lase time of 6-20 seconds. For microwave emitters, the thermal load may be an approximately 5 megawatt-class with an efficiency of 20% for 5-15 seconds. The high amount of energy that must be moved is not the entire challenge. The device must be maintained at a specific temperature. Many high-energy lasers must be cooled at a temperature of approximately room temperature or between 527 and 536 R (67 – 76 °F). Microwave emitters may need to be cooled in the range of 617 to 626 R (158 – 167 °F). Ambient air temperatures may be near the device cooling temperature and will tend to increase the size of any direct device-air heat exchangers.

A variety of waste heat extraction systems have been examined. For instance, (Shanmugasundaram et al., 2005:1-14) examined a ram air heat exchanger to receive thermal energy from a single-phase coolant that drew energy from the laser system. Many cooling schemes have been examined for the rapid and direct cooling of the laser system itself as in (Wang et al., 2005:1-10) and (Shanmugasundaram et al., 2007:1-17).

Aircraft engines use the conversion of chemically stored energy (jet fuel) into thermal energy stored in the air (heat). This chemically stored energy is an economic and readily available source of energy. More and more of this energy is being used for purposes other than providing thrust, like cooling avionics, life-support, computers, radar, engine oil, etc. All of these devices create waste heat that must be cooled. Fuel has been used to cool aircraft devices prior to combustion. The additional thermal energy stored in fuel creates a favorable effect on the engine performance because less energy is required to initiate the reaction process during combustion. As the fuel thermal capacity has been reached by device cooling, the benefit from the preheating mechanism has been maximized for current jet fuels.

Storing the thermal energy within the fuel and recycling the hot fuel back into the fuel tanks is another thermal management scheme. Heat transfer through the wing surface could be attempted. The heat exchange through the wing surfaces may be very limited; however, if a low thermal signature is required. Additionally, storing energy within the fuel impacts the capacity of the other airframe systems that are already using the thermal capacity prior to fuel combustion, as previously described. Ultimately, the energy needs to escape the airframe.

Many aircraft today are required to maintain lower thermal signatures. This requirement limits options for thermal transfers from aircraft external surfaces with heat

exchangers. The air flowing through the airframe through either the engines or ram air scoop, in the engine inlet, remains viable options. Shanmugasundaram et al. (2005:1-14) have already published a scheme for a ram air heat exchanger. It was found that raising the device cooling temperature significantly reduced the mass of the heat exchanger. It was also found that using a layered plate-fin heat exchanger resulted in high pressure losses that, in some cases, exceeded the available dynamic pressure head. A fin-tube heat exchanger produced approximately 10% dynamic pressure head losses, increasing system drag. In order for a design choice to be made between thermal management schemes, an understanding of all of the options must be achieved. Both the capabilities of a heat pump and the impact on engine performance must be understood.

Waste heat will be drawn out of a high-energy device, such as a laser or microwave emitter, through a thermal storage device, a water-based heat pump, and a heat exchanger within the bypass section of a modern day jet fighter engine, mixed bypass turbofan. A set of guidelines will be provided for a starting point of design. The engine performance will be analyzed based to the effects of the thermal management system.

The laser or microwave device will be described with two terms. The first is the laser class that describes the total input power the system uses emitting a beam, expressed in Watts. This parameter is used for both the laser and microwave. The second term is the system level efficiency. This term describes the percentage of the system power that is in the final beam. The remaining power is converted to waste heat.

Due to the rapid generation of the waste heat, it is assumed a heat storage device will capture and hold the heat energy and allow for energy dissipation over a longer

period of time. It will also be assumed this device allows for enough surface area and temperature difference for a complete transfer of energy into a working fluid.

A closed system heat pump will be used for regenerative heat dissipation. The energy extracted from the thermal storage device and passed through the heat pump is transferred into the engine bypass air, through a single pass, counter-flow duct heat exchanger. The heat pump coolant temperature low point at the evaporator must be lower than the storage device medium. The coolant condenser exit temperature must be higher than the air in the engine bypass section. A basic schematic of the high-energy storage device, heat pump, and engine configuration is shown in Fig. 1.

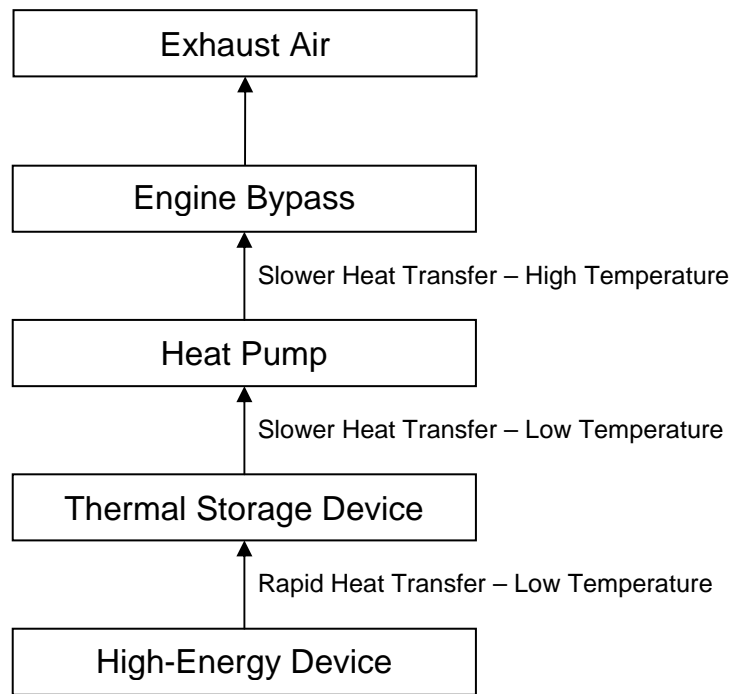


Fig. 1. Energy flow diagram

As the waste heat is transferred to the thermal storage device, the energy can begin transfer into a heat pump. The slower inflow rate of thermal energy will be greater

than outflow. Thus, a high-energy device can be used only for short periods of time during the dissipation cycles. A factor named the Duty Cycle Factor (f_{DC}) is the heat generation efficiency times the ratio of emitting time divided by the recovery time. The heat generation efficiency is one minus the total device efficiency. The time for the system to dissipate all of the stored heat, i.e., the time between the start of two consecutive device firings, is the recovery time. Thus, the device nominal power, say 1 MW, times f_{DC} is the energy rate that must be dissipated into the bypass air. Or viewed inversely, the maximum rate of energy dissipation in the bypass duct divided by f_{DC} is the maximum device power. Thus a small f_{DC} is desirable.

Objectives

The objective of this research is to understand the capabilities and limitations of the given thermal management system. The variables to be analyzed are:

1. Effect of f_{DC} on the thermal management system
2. Impact of maximum and minimum temperature within the heat pump on the thermal management system
3. Comparison of a single heat pump or cascaded heat pumps (two heat pumps in series)
4. Impact of thermal management system on engine performance
5. Influence of Mach number and altitude on the thermal management system and engine performance

II. Background and Theory

The underlying theory used for this analysis focuses on classical principals. This analysis is not intended to determine the state-of-the-art capabilities, but is intended to provide a baseline for design.

High-Energy Device

The starting point for this analysis begins with the waste heat generated by the high-energy device. Due to the rapid cooling rates and special requirements of the high-energy systems, the cooling of the device itself will not be analyzed. It will be assumed that the cooling has taken place and the thermal energy has been stored in a thermal storage device. The energy generated from a laser or microwave will be used synonymously as the source of the energy does not impact the thermal management system, only the amount of heat generation does. The requirements of each may be unique and will be analyzed separately but all the thermal management system does is process thermal energy. All of the high-energy system input power that is not an output within the directed energy is converted into waste heat. The waste heat generation rate is expressed,

$$\dot{Q}_{gen} = P_{input} (1 - \eta_{laser}) \quad (1)$$

The remainder of the analysis will utilize English units. The waste heat generation rate will be expressed in BTU/s. The high-energy device provides the energy for the thermal storage device.

Thermal Storage Device

The thermal storage device must extract the waste heat from the high-energy device quickly to prevent overheating of the laser lase medium. If the temperature of the lase medium is not carefully controlled, the medium will fracture and disable the system. The microwave must be protected from overheating in the same way.

The total energy stored within the storage device is determined by the product of the lasing time and the waste heat generation rate as shown in Eq. 2.

$$Q = \dot{Q}_{gen}(t_{lase}) \quad (2)$$

The total energy stored provides the basis for the time a given thermal management system is allowed to dissipate all of the stored energy.

Heat Pump

The design of the heat pump will include a traditional vapor compression cycle with an evaporator, compressor, condenser, and an expansion valve. The coolant type will be water due to its high critical point of 1,164 R. The critical point is the point where the liquid and vapor states are identical. The high critical point of water allows for a high maximum phase change temperature at the condenser exit and a high temperature difference with the bypass air. Other common coolant types such as ammonia, R-12, and benzene have a critical point temperature of 729.8 R, 692.4 R, and 1,012 R, respectively, and all have a lower critical point temperature than water.

The classical vapor-compression cycle is used for the heat pump design with the design points shown in Fig. 2.

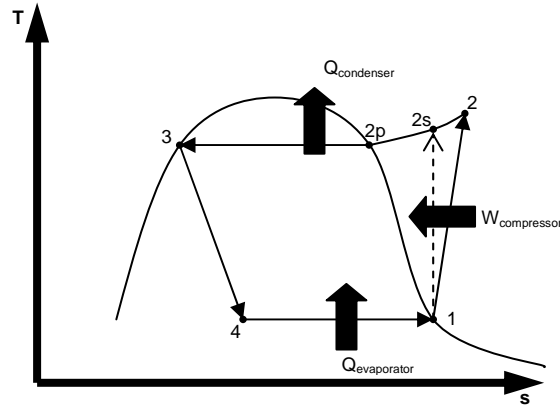


Fig. 2. T-s diagram for the heat pump showing external energy transfers

The curved line represents the vapor dome. The region to the left of the dome represents the liquid state. The region to the right of the vapor dome represents the pure vapor state, also known as the superheated vapor state. The area under the vapor dome represents a state of mixed liquid and vapor. The critical point is the point that is at the top of the dome or maximum temperature. The large arrows indicate where energy is added or removed from the coolant. The condenser provides the balance for the added energy to escape. Equation 3 shows the energy balance.

$$Q_{condenser} = Q_{evaporator} + Q_{compressor} \quad (3)$$

For a system limited by a fixed heat transfer rate at the bypass heat exchanger (condenser), added compressor work reduces the heat transfer capacity of the evaporator. The work added by the compressor increases the pressure and temperature of the coolant and should be kept to a minimum. Figure 2 shows the physical architecture associated with Fig. 1.

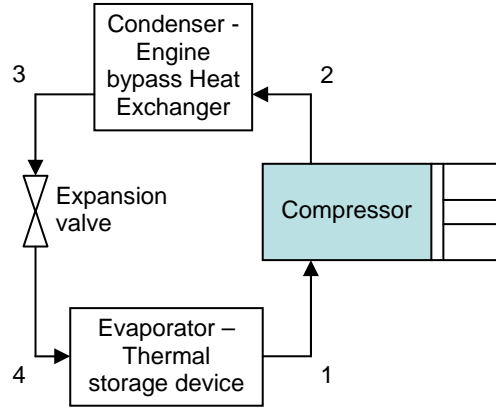


Fig. 3. Physical diagram of the heat pump showing component interfaces with the thermal storage device and the engine

The coolant loses energy through the condenser via the bypass heat exchanger.

The vapor compression cycle can be found based on the energy transferred in each component. As the heat is transferred from the thermal storage device to the coolant (point 4 – 1), the entropy is increased at constant pressure. At the exit of the evaporator, the coolant is completely vaporized into steam. The compressor increases the pressure (point 1 – 2). A small pressure drop occurs between points 2 and 3 but is assumed negligible due to the short length of the pipes in the bypass section. As the temperature is constant under the vapor dome, the phase change temperature (point 2p) is chosen as a design point. The pressure is found based on the phase change temperature. Point 2s is the point on the high pressure line with the same entropy as at the compressor entrance (point 1). Point 2 incorporates the inefficiencies in the compression process. The efficiency of compression process (Moran and Shapiro, 2004:492) is,

$$\eta_c = \frac{h_{2s} - h_1}{h_2 - h_1} \quad (4)$$

A low efficiency will increase the enthalpy from point 2s to point 2 and increase the temperature at a given pressure. All of the properties of the steam exiting the compressor at point 2 can now be determined.

As the pressure is constant between points 2 and 3, the coolant properties can be found at any point between 2 and 3. Lastly, the properties at point 4 can be found due to the constant enthalpy process down to the known low pressure (point 4).

Once the vapor-compression cycle is determined based on a low and high phase change temperature (T_1 and T_{2p}) and a compressor efficiency, sizing can be performed based on the heat transfer rate to the evaporator. The expression for the mass flow rate of the coolant (Moran and Shapiro, 2004:486) is,

$$\dot{m}_{coolant} = \frac{\dot{Q}_{evaporator}}{h_1 - h_4} \quad (5)$$

, where $\dot{Q}_{evaporator}$ is the energy transfer rate from the thermal storage device and h_1-h_4 is the energy storage capacity of water, between points 1 and 4, per unit mass. Because water has a relatively large heat of vaporization, the mass flow rates tend to be relatively small. For example, an evaporator heat transfer rate of 41.7 BTU/s and an enthalpy gain of 624.5 BTU/lbm will require a coolant mass flow rate of 0.0667 lbm/s. With a known coolant mass flow rate, the magnitude of the compressor work and the heat transfer through the condenser can be found. A more comprehensive review of non-idealized vapor-compression cycles can be found in (Çengel et al., 1994:591). The challenge now is the heat exchanger design in the engine bypass duct.

Bypass Heat Exchanger

The heat exchanger chosen is a counter-flow heat exchanger without fins. Fins were not included because the pressure losses from blockage and skin friction was not desirable. The counter-flow type of heat exchanger is used because of the requirement for the coolant temperature to be higher than the air. Since the magnitude of change in temperature of the coolant is much higher than the air, the lowest temperature of the coolant (during phase change) will be closest to the temperature of the air. Because the coldest air will be at the front of the bypass duct, the temperature difference will be greatest if the phase change temperature ($T_{2p}-T_3$) interacts with the bypass inlet temperature. The schematic in Fig. 4 shows the basic layout within the engine bypass section.

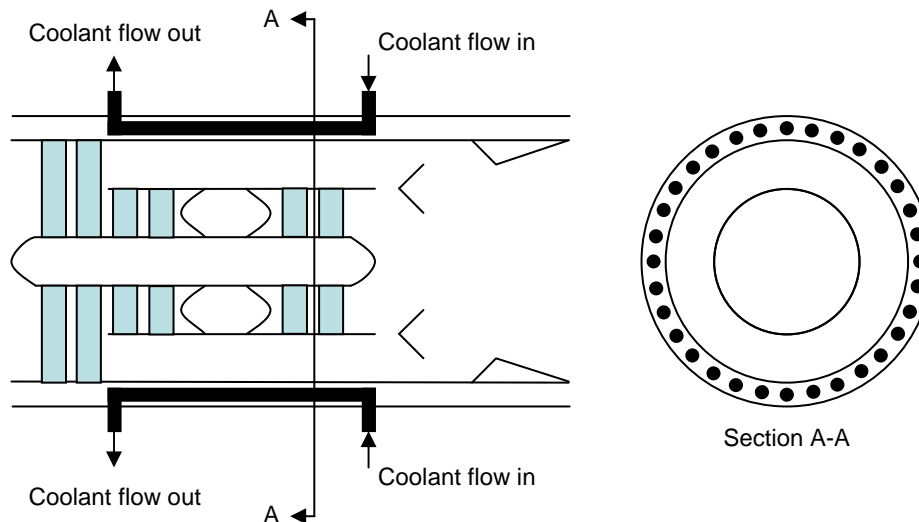


Fig. 4. Engine schematic showing the layout of the heat exchanger

Section A-A shows a large number of small diameter coolant pipes to create a nearly even temperature distribution across the surface of the bypass duct. This temperature distribution is necessary due to the requirement of the theory to have a constant wall

temperature. The pipes will be configured in parallel (no snaking of pipe flow), maintaining a constant temperature in each pipe at section A-A. The distance between pipe centers is twice the diameter. The number of pipes is the bypass circumference divided by the pipe spacing rounded down to the next whole number. As the intent of the heat exchanger is to transfer the thermal energy from the coolant into the bypass section air, the rate of heat transfer (Humble et al., 1995:133) is governed by Eq. 6.

$$\dot{q}_{condenser} = \frac{\dot{Q}_{condenser}}{L_{BypassSurface}} = \frac{T_{coolant} - T_{Tg}}{\frac{1}{h_{coolant} A_{PipeSurface} n_{Pipes}} + \frac{L_{metal}}{k_{metal} A_{BypassSurface}} + \frac{1}{h_g A_{BypassSurface}}} \quad (6)$$

Each fraction within the denominator is commonly referred to as the thermal resistance of each component of the heat exchanger. In this case, there is energy transferred from the steam into the walls of the pipe material, which flows through the pipe material and into the engine bypass air. The coolant temperature drops until the coolant is within the phase change regime. The transfer of energy to the bypass air causes a change in temperature to $T_{T,out}$.

$$T_{T,out} = \frac{\dot{Q}_{condenser}}{c_p \dot{m}_{13}} + T_{T,in} \quad (7)$$

The specific heat at constant pressure and the mass flow rate are assumed constant within the duct. Therefore, the temperature change ($T_{T,out} - T_{T,in}$) is dependent on the energy flow rate from Eq. 6. The heat transfer coefficients require a more in-depth analysis.

The heat transfer coefficient of the bypass air is from Humble et al. (1995:133). High-speed flow ($M > 0.4$) of hot gas in an enclosed channel can be described with the empirical relation,

$$h_g = 0.026k \left(\frac{\rho U}{\mu} \right)^{\frac{4}{5}} \left(\frac{1}{D} \right)^{\frac{1}{5}} \left(\frac{c_p \mu}{k} \right)^{\frac{2}{5}} \quad (8)$$

The temperature at the bypass inlet is assumed to be approximately 300 °F, variable of course, depending on operating conditions and compression. The heat transfer coefficient is dependent on both fluid properties and flow characteristics.

The coolant heat transfer coefficient incorporates pure vapor region (point 2 – 2p) and the mixed vapor/liquid region (point 2p – 3). Hill and Peterson (1992:129) shows,

$$h_{coolant} = 0.023k \left(\frac{\rho U}{\mu} \right)^{\frac{4}{5}} \left(\frac{1}{D} \right)^{\frac{1}{5}} \left(\frac{c_p \mu}{k} \right)^{\frac{1}{3}} \quad (9)$$

This empirical relation is valid for long smooth tubes. For the coolant in a pure vapor phase, Eq. 9 is directly applied. As heat is added or removed from the coolant during the phase change, the progression of fluid properties between the saturated liquid line and the saturated vapor line is linear, at a constant pressure. The averaged saturated liquid and vapor heat transfer coefficients are representative of the region under the vapor dome.

A high heat transfer coefficient is desirable as it will allow thermal energy to flow more rapidly. The online NIST publications on the thermophysical properties of water was used to determine the specific heat at constant pressure, dynamic viscosity, and the thermal conductivity of the coolant at a specified pressure and temperature.

The air density was calculated from the perfect gas law,

$$\rho = \frac{p}{RT} \quad (10)$$

The bypass air pressure, diameter, temperature, and velocity is determined based on the engine design and operating conditions and will be explained in more detail in the Engine Cycle section. The impact of the conducting material will be quantified.

The thermal conductivity of the heat exchange material is a material property and can change with temperature, depending on the material. As shown in Fig. 5, conducting material surrounds the coolant.

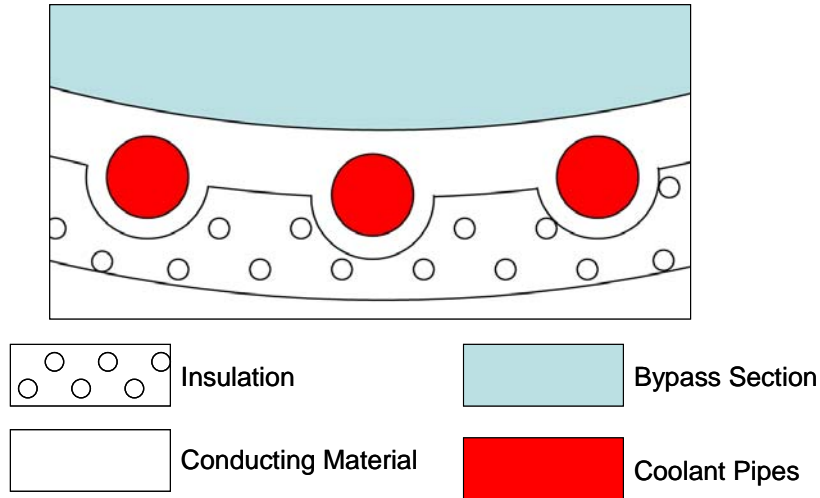


Fig. 5. Bypass heat exchanger segment cross section showing material configuration

One of the primary advantages of this geometry is the minimal impact of skin friction and flow blockage on the bypass air, while still allowing the coolant to flow within a pipe-shaped geometry. The minimum thickness of the conducting material between the coolant and the air or insulation is,

$$thickness_{pipe} = \frac{P_{Coolant} \left(\frac{D_{pipe}}{2} \right)}{\sigma_h} \quad (11)$$

Equation 11 is used to determine the hoop stress, σ_h , (Craig, 2000:587) in a material analysis and defines the applied stress. The stress capacity of the material used must be greater than σ_h . The stress capacity may be greatly reduced due to the high temperatures, caused by the coolant. The insulation may be a broad range of materials and is not

limited to heavy, solid ceramics. A thermal blanket may be a good choice. The purpose of the insulation is to contain the flow of thermal energy within the bypass section.

The shortest distance the energy must travel through the conducting material is equal to the pipe thickness between the coolant pipe and the bypass air. The maximum distance is half the circumference of the pipe plus the pipe thickness. The distance used for the thermal conductivity is the average of the maximum and minimum distances described above. Once the heat transfer rate into the bypass air is known, the length of the bypass heat exchanger can be found.

Determining the length of the heat exchanger is a process of equating the energy rate from the coolant (condenser) to the transfer rate through the heat exchanger. The heat exchanger process can be divided into two regimes. First is the phase change process where the air temperature is relatively constant and is approximated as such. Using the averaged phase change properties and constant coolant temperature and by dividing the energy required for the heat of vaporization by the heat transfer rate, the length of bypass required for the coolant to change phase can be found. The second regime occurs during the pure vapor portion (point 2 – 2p) of the heat exchange. Here the coolant temperature will not be constant. By discretizing this regime, a numerical approximation of the heat transfer rate at a small increment can be found. If the required length of bypass section is less than or equal to the length of the bypass section, the design is achievable.

Anderson (2003:113) provides a relationship for the effects of skin friction,

$$\frac{4fL_{BypassSurface}}{D_{outer}} + \frac{4fL_{BypassSurface}}{D_{inner}} = \left[-\frac{1}{\gamma M^2} - \frac{\gamma+1}{2\gamma} \ln \left(\frac{M^2}{1 + \frac{\gamma-1}{2} M^2} \right) \right]_{M_1}^{M_2} \quad (12)$$

The two terms to the left of the equal sign is to account for the inner and outer surfaces of the bypass section boundary. This expression is used to solve for the Mach number at the exit of the bypass section caused by skin friction.

Anderson (2003:104) also describes the relationship between the change in total temperature and Mach number due to the heat addition using,

$$\frac{T_{02}}{T_{01}} = \left(\frac{1 + \gamma M_1^2}{1 + \gamma M_2^2} \right) \left(\frac{M_2}{M_1} \right)^2 \left(\frac{1 + \frac{\gamma - 1}{2} M_2^2}{1 + \frac{\gamma - 1}{2} M_1^2} \right) \quad (13)$$

Equation 13 is derived from the compressible flow relations described later in the engine cycle section. Since the change in total temperature is computed from the heat addition, the exit Mach number, M_2 , can be solved. By combined change in Mach number from the friction and heat addition determined the Mach number at the exit of the bypass section.

Anderson (2003:113) gives the relation of the effect on stagnation pressure from the change in Mach number caused by heat addition and wall friction,

$$\frac{P_{02}}{P_{01}} = \frac{M_1}{M_2} \left[\frac{2 + (\gamma - 1)M_2^2}{2 + (\gamma - 1)M_1^2} \right]^{\frac{\gamma + 1}{2(\gamma - 1)}} \quad (14)$$

The stagnation pressure will decrease due to heat addition and skin friction. Care must be taken as to whether the initial Mach number is in the subsonic or supersonic regime. In each case, the Mach number will approach unity, as heat or friction is added. A more thorough description of the Rayleigh and Fanno curve theory can be found in Anderson (2003:109-116). Additional heat transfer capacity may be available by increasing the thermal transfer surface.

A second type of heat exchanger was investigated utilizing the outer and inner surfaces of the bypass section as shown in Fig. 6.

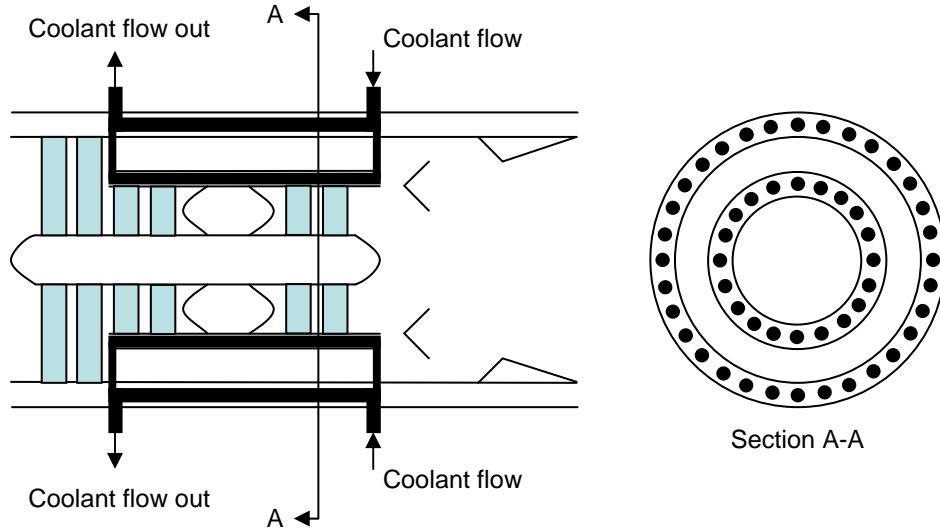


Fig. 6. Simplified engine schematic showing section labels and dual surface heat exchanger

The coolant is transferred to the inner pipes through the engine struts. This configuration can approximately double the heat exchanger surface contact area. The pipe diameters for the inner and outer surfaces are identical. Thus, the inner pipe spacing will be approximately equidistant with the outer pipe spacing.

Finally, an analysis of the boundary temperatures of the conducting material can be performed. Across a given heat exchanger surface, the temperature will drop from the highest temperature at the mean coolant temperature, to the wall material in contact with the coolant, to the wall material in contact with the air, and ending at the lowest temperature in the mean bypass air. The maximum temperature of the pipe material will be the surface (or the hot side of the wall) in contact with the coolant, shown with

$$T_{Wall,Hot} = T_{Coolant} - \frac{\dot{Q}_{condenser}}{hA} \quad (15)$$

This temperature can be used for analysis of material properties. Care must be taken when choosing a material to prevent melting and be of sufficient strength at the maximum temperature. Once the maximum temperature of the hot side of the wall is known, a corresponding minimum strength of material can be found. A high thermal conductivity is desired, but as the strength of the material decreases, the required thickness of the material increases and will increase some resistance to the flow of energy. A comparison of the thermal management systems must be performed to determine the overall system impact.

Engine Cycle

The engine model used to determine the engine performance and flow properties is based on a mixed bypass turbofan described in Mattingly et al. (2002:95). Each engine component changes the air properties flowing through the engine. These changes can be quantified in part with compressible fluid relations using total or stagnation temperature and pressure as in Eq. 16 and Eq. 17, respectively.

$$T_t = T \left(1 + \frac{\gamma - 1}{2} M^2 \right) \quad (16)$$

$$p_t = p \left(1 + \frac{\gamma - 1}{2} M^2 \right)^{\frac{\gamma}{\gamma - 1}} \quad (17)$$

A total pressure ratio, π , is defined as the ratio of exiting total pressure to entering total pressure. The total temperature ratio, τ , is defined as the ratio of exiting total temperature to entering air total temperature. A list of the total property ratios for each engine component and how they are determined can be found in Mattingly et al. (2002:102).

Figure 7 shows the nomenclature for a mixed bypass turbofan engine.

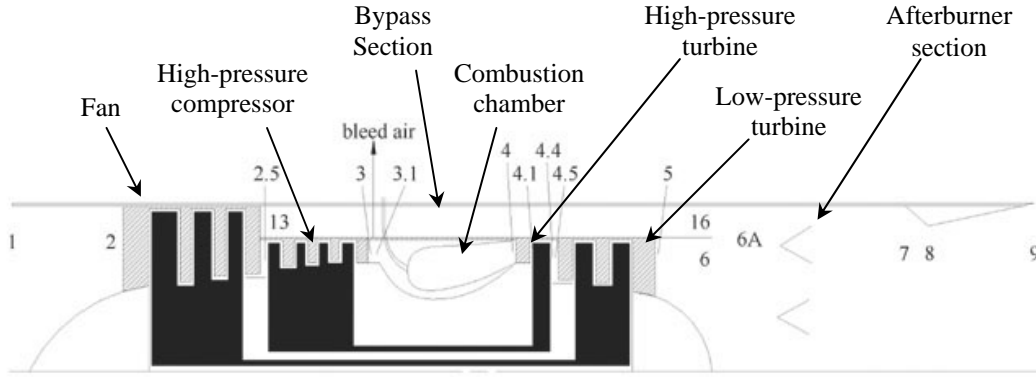


Fig. 7. Engine station numbering for reference in equations

Due to the symmetry, only the upper half is shown. Point zero, not shown, is the freestream conditions far ahead of the engine. The section between point 2.5 and point 6 is known as the core. The fan and the low-pressure compressor will have identical total temperature and pressure ratios. The mixer combines the flow from points 16 and 6 and ends at point 6A. In Mattingly et al. (2002), the assumption is that there is no stagnation pressure or temperature loss between points 13 and 16. However, changes to the total temperature and pressure outlined earlier were incorporated into the engine analysis presented here.

This analysis will incorporate the energy addition due to the heat exchanger and the losses due to friction on the bypass air. The air properties at the inlet of the bypass section can be found using Eqs. 18 – 20.

$$T_{T13} = T_0 \tau_r \tau_f \quad (18)$$

$$p_{T13} = p_0 \pi_r \pi_d \pi_f \quad (19)$$

$$\dot{m}_{13} = \alpha \frac{\dot{m}_0}{1 + \alpha} \quad (20)$$

These equations allow the bypass duct inlet conditions to be found. In addition, the bypass inlet Mach number and area size must be chosen. Mattingly et al. (2002:152) outlines a method to ensure the static air pressures are equal at both inlets to the mixer (points 6 and 16). The mass flow parameter is used to determine the cross-sectional area of the bypass section with Eq. 21.

$$MFP = \frac{\dot{m} \sqrt{T_T}}{P_T A} = M \sqrt{\frac{\gamma g_c}{R} \left(1 + \frac{\gamma - 1}{2} M^2 \right)^{\frac{\gamma + 1}{2(1 - \gamma)}}} = M \sqrt{\frac{\gamma g_c}{R} \frac{\sqrt{T_T / T}}{P_T / P}} \quad (21)$$

For this analysis, the area at the mixer inlet provides an approximation of the area of the bypass section.

For initial sizing, the Mach number and flow area at the bypass inlet was set equal to the computed exit area without the heat exchanger. After the effects of the heat exchanger are known, the Mach number at bypass exit can be recomputed. Now that the change in the bypass air from added heat and skin friction, the change to the low-pressure turbine air from the heat pump compressor power requirement will be examined.

Power can be drawn from the low-pressure turbine for the heat pump compressor. Electric power will only be extracted from the low-pressure turbine. Mattingly et al. (2002:112) defines a power takeoff coefficient, C_{TOL} , as,

$$C_{TOL} = \frac{P_{TOL}}{\dot{m}_0 c_{p0} T_0} \quad (22)$$

The power takeoff coefficient can be incorporated into a power balance between the power required for the engine low-pressure compressor and that provided by the low-pressure turbine. Mattingly et al. (2002:112) gives a relation for the stagnation

temperature and pressure ratios (τ_{iL} and π_{iL} respectively) across the low-pressure turbine as,

$$\tau_{iL} = 1 - \frac{\tau_r \{(\tau_{cL} - 1) + \alpha(\tau_f - 1)\} + (1 + \alpha) C_{TOL} / \eta_{mPL}}{\eta_{mL} \tau_\lambda \tau_{iH} \left\{ (1 - \beta - \varepsilon_1 - \varepsilon_2)(1 + f) + \left(\varepsilon_1 + \varepsilon_2 / \tau_{iH} \right) \frac{\tau_r \tau_{cL} \tau_{cH}}{\tau_\lambda} \right\}} \quad (23)$$

$$\pi_{iL} = \tau_{iL}^{\frac{\gamma_i}{(\gamma_i - 1) \varepsilon_{iL}}} \quad (24)$$

Equations 23 and 24 describe the changes to the core air that flows to the mixer.

The mixer combines the bypass and core air. The total temperature ratio can be determined from,

$$\tau_M = \frac{1 + \alpha' \left(\frac{\tau_r \tau_f \tau_{BP}}{\tau_\lambda \tau_{m1} \tau_{iH} \tau_{m2} \tau_{iL}} \right)}{1 + \alpha' C_{pc} / C_{pt}} \quad (25)$$

This equation was modified from the mixer equation shown in Mattingly et al.

(2002:153) to include T_{T16}/T_{T13} (τ_{BP}) not equal to unity. The method for determining the total pressure ratio across the mixer is not as direct, as shown in Eq. 26 and Eq. 27.

$$\pi_{M,ideal} = \frac{P_{t6A}}{P_{t6}} = (1 + \alpha') \sqrt{\tau_M} \frac{A_6}{A_{6A}} \frac{MFP_6}{MFP_{6A}} \quad (26)$$

$$\pi_M = \pi_{M,max} \pi_{M,ideal} \quad (27)$$

The frictional losses across the mixer is accounted for using $\pi_{m,max}$ as an input constant.

The losses due to fluid mixing is accounted for through $\pi_{m,ideal}$.

The engine characteristics that will be used to determine the overall impact from the thermal management system are uninstalled thrust and specific fuel consumption.

The uninstalled thrust or the total force exerted from the engine on the surrounding air is given by,

$$F = (\dot{m}_9 V_9 - \dot{m}_0 V_0) + A_9 (P_9 - P_0) \quad (28)$$

A derivation by Mattingly et al. (2002:110) shows a more useful form,

$$\frac{F}{\dot{m}_0 a_0} = \left(1 + f_0 - \frac{\beta}{1 + \alpha}\right) \frac{U_9}{a_0} - M_0 + \left(1 + f_0 - \frac{\beta}{1 + \alpha}\right) \frac{R_9}{R_0} \frac{T_9/T_0}{U_9/a_0} \frac{\left(1 - P_0/P_9\right)}{\gamma_0} \quad (29)$$

This form can be used for both afterburner on and off.

The uninstalled thrust specific fuel consumption (S) is a measure of the fuel economy of the engine. S can be computed using,

$$S = \frac{\dot{m}_f + \dot{m}_{fAB}}{F} = \frac{f_0}{F/\dot{m}_0} \quad (30)$$

S can be thought of as the fuel flow rate required to produce one unit thrust from the engine.

Sensitivity Analysis

A better understanding of the importance of the input parameters can be obtained through a modified discrete sensitivity analysis.

$$sensitivity = \frac{output_{final} - output_{initial}}{\left(\frac{input_{final} - input_{initial}}{input_{initial}} \right)} \quad (31)$$

This analysis examines the response to a non-dimensionalized input. Because the purpose of this paper is to understand the capabilities of the thermal management system and its impact on the engine, the engine and heat pump input parameters analyzed are: the heat pump compressor efficiency (η_c), the coolant pipe conductivity (k_{metal}), the coolant pipe yield strength (σ), outer diameter (D_{outer}) and length ($L_{BypassSurface}$) of the bypass section, friction factor of the surface in contact with the bypass air (f), mass flow rate of the inlet (\dot{m}_{13}), the aircraft power requirement excluding the heat pump compressor (P_{TOL}), engine bypass ratio (α), engine core compression ratio (π_c), and the bypass compression ratio (π_f). The heat pump operating temperatures are not included in the sensitivity analysis but are covered in the heat pump section within Chapter IV. The output parameters to be analyzed include maximum laser power class, uninstalled thrust and thrust specific fuel consumption, work required from the heat pump compressor, and rate of heat transfer into the bypass air. The sign of the sensitivity value will indicate the direction of the change. A positive value will produce a response in the same direction as the input. A negative value will produce a response in the opposite direction as the input.

Chapter Summary

Theory has been presented to determine the impact of high-energy device waste heat on engine performance. Using a heat pump, low temperature coolant can extract thermal energy and deposit it into bypass air at a high temperature. Due to the high temperature requirements, water was used as the coolant. The heat addition into the bypass air will impact the total temperature and pressure of the bypass air flow. The laser waste energy and required heat pump compressor power will impact the thrust and specific fuel consumption of the engine.

III. Computational Setup

Hardware

The hardware used for the computations performed for this project was a Windows XP based IBM personal computer. The system utilizes a Pentium® 4, 3.06 GHz processor, 2.00 GB of RAM, GeForce 8800 GTS Extreme Video Card, and a ViewSonic VX922 19" LCD Monitor.

Software

MATLAB® version 7.0.0.19920 (R14) was used for all calculations. None of the additional toolboxes or add-ons were needed as only the basic programming tools were utilized. Off-design parameters were found using AEDsys version 4.020, March 8, 2007.

Software Inputs

Based on the discussion within the Introduction section, on page 1, the laser and microwave thermal storage devices will assume a required coolant temperature of 527.5 R and 617.4 R, respectively. Because the designs of the thermal storage devices are presently not defined, the cooling temperature of the high-energy devices and their respective thermal storage devices will be identical.

The 1976 Standard Atmosphere tables (NOAA et al., 1976:53) were used for the far stream air pressure, temperature, and density. The resolution of the table was a set of values every thousand feet. A solver was created to linearly interpolate altitudes between one thousand foot increments.

A reference engine and flight condition used for comparison with the thermal management system are shown in Table 1.

Table 1. Reference engine parameters and flight conditions

π_c	36		η_{cL}	0.89	
π_f	3.5		η_{cH}	0.9	
T_{T4}	3200	[R]	η_{tH}	0.89	
T_{T7}	3600	[R]	η_{iL}	0.91	
α	0.4		η_{mPL}	0.98	
m_0	250	[lbm/s]	η_{mL}	0.99	
P_{TOL}	300	[kW]	η_{mH}	0.98	
M_5	0.4		β	0.01	[%]
C_{pc}	0.238	[BTU/lbm-R]	π_{AB}	0.96	
C_{pt}	0.295	[BTU/lbm-R]	η_{AB}	0.97	
γ_c	1.4		γ_{AB}	1.3	
γ_t	1.3		$\pi_{mix, max}$	0.97	
h_{PR}	18500	[BTU/lbm]	C_{pAB}	0.295	[BTU/lbm-R]
ϵ_1	0.05	[%]	P_0/P_9	1	
ϵ_2	0.05	[%]	M_0	0.8	
π_b	0.97		altitude	25000	[ft]
$\pi_{d, max}$	0.97		g_c	32.2	[ft/s ²]
π_n	0.98		η_b	0.98	
outer radius of bypass section			18.6	[in]	
length of bypass section			72.8	[in]	

This engine type could be for a high performance fighter aircraft. The bypass section outer radius and length were estimated based on the F110-GE-100 engine. The reference parameters for the thermal management system are shown in Table 2.

Table 2. Reference thermal managements parameters

coolant compressor efficiency	0.8	
pipe spacing	2x (D_{pipe})	
RefrigPipeDiameter	0.25	[in]
Thermal conductivity of pipe matl	15.8	[BTU/hr-ft-R]
Density of Pipe Matl	559.9	[lbm/ft ³]
Pipe matl strength at max temp	9300	[psi]
Max wall temp driven by mat'l properties	2259.67	[R]

The pipe properties in Table 2 describes the conducting material containing the coolant. As shown in Fig. 5, the material is not formed in a typical pipe shape but serves the same function.

The tabulated data from the NIST, Thermophysical Properties of Fluid Systems (<http://webbook.nist.gov/chemistry/fluid/>) tables were collected at selected pressures. The pressure increments increased with pressure. The selected discrete pressures increments used can be found in Appendix E. The maximum selected pressure of 3,190.83 psi is used because it is slightly less than the critical point for water (3,212 psi), allowing a mixed liquid vapor regime.

The NIST steam tables indicate a maximum temperature of 2,295 R, to avoid dissociation, and thus limits the maximum compressor outlet temperature (T_2) of the heat pump compressor. For modeling purposes, the maximum T_2 for the data used is 2,270 R to maintain accurate grid interpolation using four distinct table values.

Code Validation

The engine cycle portion of the code was validated by comparing the results with the parametric cycle analysis tool known as ONX, version 5.11, included with the AEDsys® software package, version 4.020, developed by Jack D. Mattingly and David T. Pratt. The results of the validation produced a maximum uninstalled thrust and uninstalled specific fuel consumption error of no more than 1%.

IV. Results and Discussion

Duty Cycle

Overall operational system requirements will set limitations on the size and performance of the thermal management system. The heat generated is assumed dissipated over a given period of time.

As explained in Chapter two, the duty cycle factor (f_{DC}) establishes the required heat removal rate in the bypass duct, which is determined by the product of f_{DC} and the laser class power.

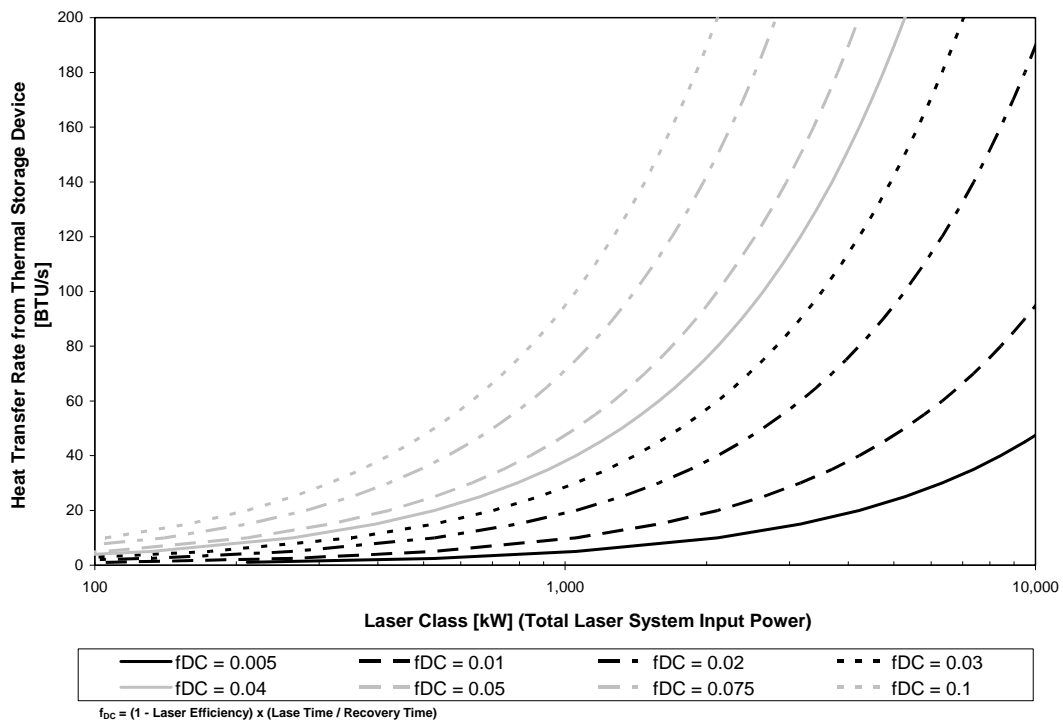


Fig. 8. Correlation of input power and thermal transfer load

Figure 9 allows for a quick understanding of the impact of the duty cycle factor and the trade space between the high-energy device power class and the load on the thermal

management system. For example, if an operational requirement for a high-energy device weapon program requires 20 seconds of lase time, 5 minutes of recovery time, and a system efficiency of 10%, the duty cycle factor will be 0.06. This example duty cycle factor will be used throughout this paper. If the desired high-energy device class is one Megawatt, then, from Fig. 9, the minimum heat transfer rate through the thermal management system is approximately 28.5 BTU/s. The x-axis is scaled in kilowatts because of the typical convention for high-energy weapons. Since the aircraft engine industry commonly uses English units, the y-axis heat transfer rates are in BTUs per second.

Heat Pump

An examination of the heat pump design parameters have been performed. The maximum temperature profile of compressor outlet temperature (T_2) and condenser phase change temperature (T_{2p}) will be shown at a range of thermal storage device coolant temperatures (T_1). The relationship between external energy transfer rates ($Q_{\text{compressor}}$, $Q_{\text{evaporator}}$, and $Q_{\text{condenser}}$) will be shown for the range of T_1 , used in the temperature profile section. The effects of the compressor efficiency on T_2 and T_{2p} will also be shown.

Temperature Profile

When designing a vapor-compression cycle, the phase change temperatures (T_1 and T_{2p}) are a design choice. For this study, the evaporator temperature range to be examined is from 525 – 1,125 R, which encompasses the cooling temperature of the thermal storage device cooling a laser and extends to within 39 R of the critical point.

For this range of evaporator phase change temperatures and an 80% compressor efficiency, the maximum changes in heat pump temperatures are shown in Fig. 10.

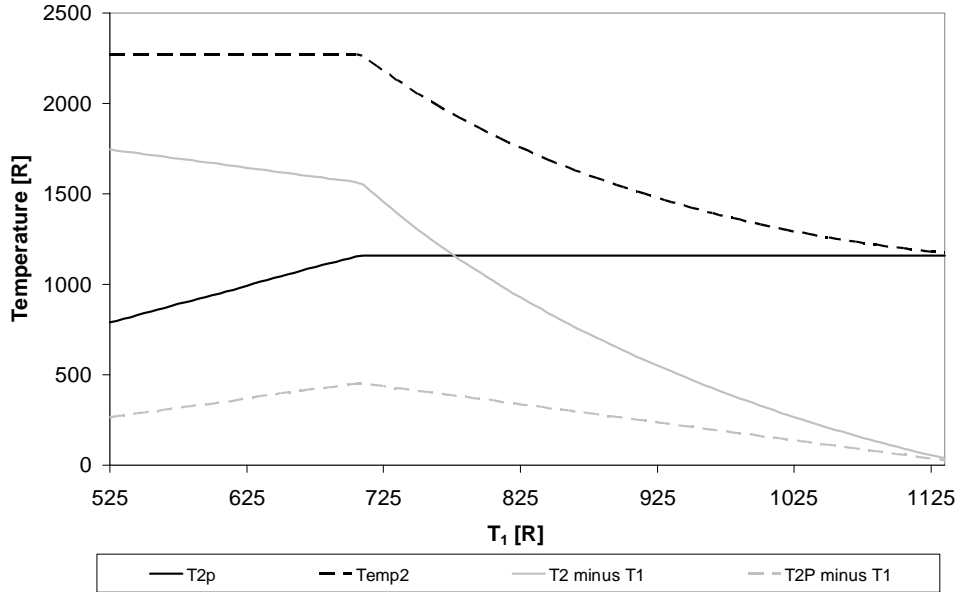


Fig. 9. Maximum temperature change of the vapor-compression cycle at a given phase change temperatures of the evaporator with an 80% efficient pump

Fig. 9 assumes a constant heat transfer rate at the evaporator ($Q_{\text{evaporator}}$) of 28.5 BTU/s.

The discontinuity at 705 R is because of the compressor outlet (T_2) equaling the maximum phase change temperature of water. As the evaporator phase change temperature (T_1) decreases below 705 R, the compressor outlet limitation of 2,270 R dominates the condenser phase change temperature (T_{2p}). As T_1 increases above 705 R, T_2 must decrease because of the T_{2p} constraint.

The $T_2 - T_1$ line shows the temperature change produced by the compressor. The cause of the $T_2 - T_1$ slope decreasing at 705 R is because T_2 will contribute to the slope change above 705 R, whereas T_1 is the sole cause of the change at T_1 less than 705 R.

The condenser phase change minus evaporator line ($T_{2p}-T_1$) shows T_{2p} increases at a greater rate than T_1 , at T_1 values less than 705 R. This is important because the difference in phase change temperatures (T_1 and T_{2p}) represents the maximum change in temperature the heat pump system can achieve. If T_{2p} is lower than the fluid being cooled, energy will flow into the condenser and cause a reversal in the cycle.

When T_1 is 705 R, the maximum phase change temperature (T_{2p}) and the compressor outlet temperature (T_2) will occur, at an 80% compressor efficiency. Below 705 R, the temperature difference across the condenser ($T_2 - T_3$) increases as T_1 decreases. Above 705 R, the T_2 will approach T_{2p} causing the condenser temperature difference ($T_2 - T_3$) to approach zero.

External Transfer Rates

Improving the heat transfer at the heat exchanger by maximizing the condenser temperature distribution ($T_2 - T_3$) may be counterproductive if the heat transfer rate at the condenser exceeds the heat exchanger capacity. The external energy transfer rates are shown in Fig. 11.

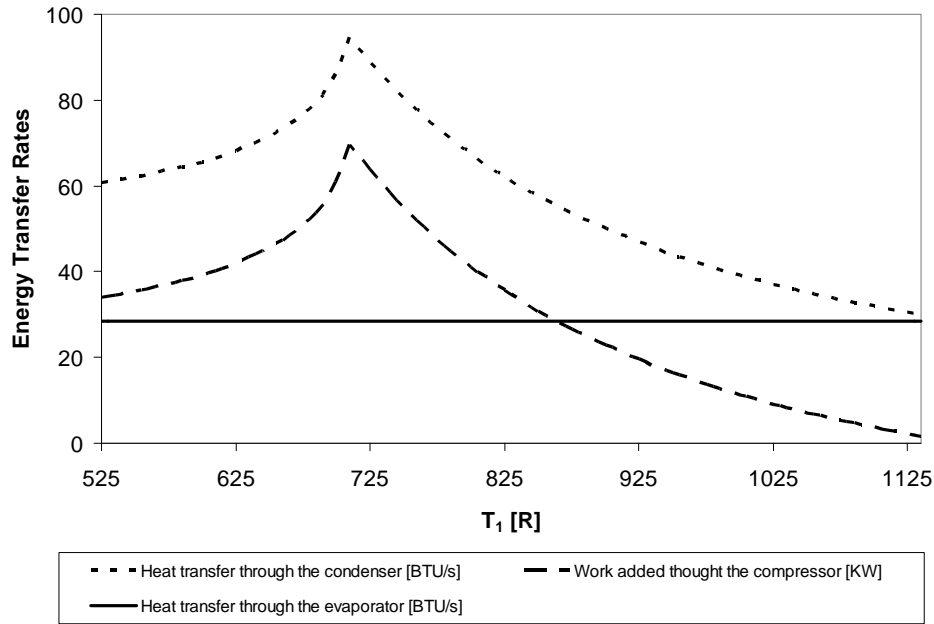


Fig. 10. Maximum energy transfer rates of the condenser and the compressor with an 80% efficient pump

The purpose is to show transfer rates that are required by the heat pump, without any constraints from the heat exchanger at the engine. Note that the compressor work is shown in kilowatts, whereas the heat transfer rates at the condenser and evaporator are shown in BTU/s. Figure 11 shows the compressor work impacts the heat transfer through the condenser. Below 705 R, the compressor work increases as the compressor exit pressure increases. At 705 R, the amount of compressor work is the greatest to maintain 28.5 BTU/s of cooling for the high-energy device. The T_1 value of 705 R correlates with the maximum condenser temperature profile from Fig. 9. As the evaporator temperature increases above 705 R, the difference between the two phase change pressures (from point 1 to point 2) decreases; reducing compressor work. The more efficient systems are those that input little work and transfer the required energy through the evaporator.

To put the compressor power in another perspective, the 40 kW compressor power is equivalent to approximately 56 horsepower. As a point of comparison, an outboard motor for a small boat is frequently rated at 50 HP.

Compressor Efficiency

A higher compressor efficiency will allow the compressor to achieve higher pressures at given work input. By generating a new refrigeration cycle at each T_1 at the given compressor efficiencies, the impact from the compressor efficiency on T_1 and T_{2p} can be examined in Fig. 12.

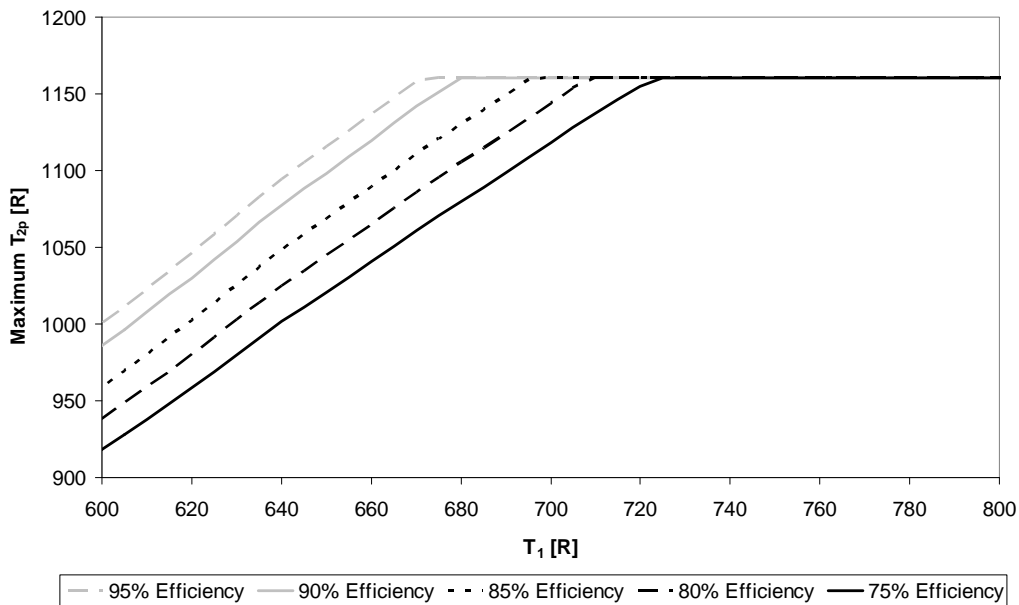


Fig. 11. Effects of compressor efficiency on phase change temperatures

When the maximum T_{2p} values reach the phase change limit for water of 1,160.2 R, each line becomes constant (horizontal). As the compressor efficiency increases, the maximum T_{2p} limit for water will be reached at a lower device cooling temperature (T_1).

At a given T_1 less than 670 R, an improvement of 5% (i.e. 85% to 90%) compressor efficiency will produce approximately 15 R increase to the maximum T_{2p} . At a given T_{2p} less than 1,160.2 R, an improvement of 5% compressor efficiency will produce approximately 14 R decrease the minimum T_1 . High T_1 values are desired for a high T_{2p} .

Using the same process as Fig. 11 and recording the T_2 values, the effect of the compressor efficiency and T_1 and T_2 is shown in Fig. 12.

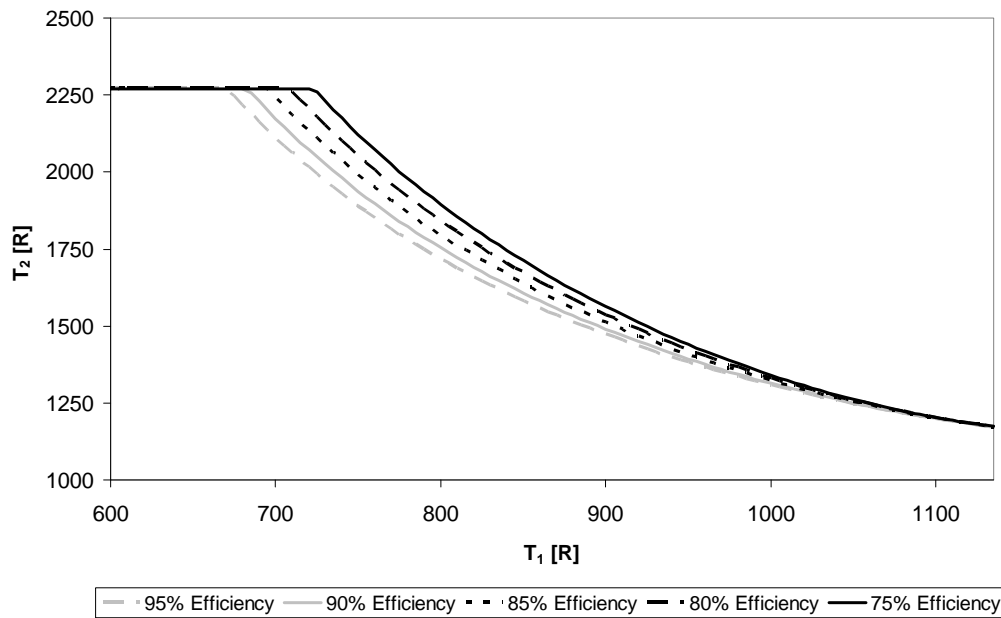


Fig. 12. Effects of compressor efficiency on compressor exit temperature (T_2)

The effects on the compressor exit temperature (T_2) become apparent at temperatures above 725 R. The lower evaporator temperatures are desired to achieve a high T_2 . Figures 11 and 12 must both be considered as both high T_{2p} and high T_2 are important for the transfer of energy into the bypass section, because they will be used for the $T_{coolant}$ term in Eq. 6. The optimum evaporator temperature is still not clear until the heat pump,

bypass heat exchanger, and engine cycle are all considered in the analysis. From this point on, the compressor efficiency will remain constant at 80%.

Bypass Heat Exchanger

Two heat exchanger and two heat pump configurations have been compared using the reference engine conditions. By using the outer (single surface) or both the inner and outer annulus surfaces (dual surface) of the bypass section for the transfer of energy from the coolant to the bypass air, the relationship between the length of bypass section required and supportable power classes has been found. Maximum power levels are shown for the respective cooling temperatures for the laser and microwave devices. The analysis is repeated for a cascaded heat exchanger (two heat exchangers in series). The required thermal transfer rates through the heat exchanger ($Q_{\text{condenser}}$) are shown at supportable device power classes. And finally, the thermal resistances of the coolant, pipe material, and the air has been compared.

Single Heat Pump, Single Surface Heat Exchanger

The heat exchanger in the engine bypass duct is the component of the thermal management that controls the flow of energy. The heat exchanger between points 4 and 1 is not part of this analysis because of the uncertainty in the thermal storage device design. All of the energy is assumed absorbed by the evaporator. Thus, the thermal transfer rate ($Q_{\text{evaporator}}$) is not constrained. Also, the mass flow rate of the coolant does not limit the device power class ($Q_{\text{evaporator}}$) because the mass flow rate can be increased to handle a larger $Q_{\text{evaporator}}$. Once the energy is transferred into the bypass air, the thermal energy

can flow out of the engine without any restrictions. All that remains of the thermal management cycle is to determine the thermal transfer rate of the heat exchanger at the bypass duct.

As shown in Eq. 6, the temperature difference ($T_{\text{coolant}} - T_{\text{Tg}}$) across the heat exchanger influences the rate of heat transfer. As an aircraft flies a mission, the atmospheric conditions, the fan total temperature ratio (τ_f) and the bypass section inlet Mach number impacts the temperature of the air entering the bypass section. For example, an engine operating at the reference conditions (Table 1), and with an operating altitude of 20,000 feet, a Mach number of 0.8, and a τ_f of 1.49, the temperature of the bypass section is approximately 700 R. The coolant temperature must be greater than the temperature of the bypass air. Since the lowest temperature of the steam occurs during the condenser phase change (point 2p – 3), the heat transfer from the mixed liquid/vapor will require the longest length of heat exchanger. As the temperature of point two (see Fig. 2) increases, the required heat exchanger length will continue to decrease.

At the design point of the engine (see Table 1), the length of a single surface heat exchanger required to transfer the waste heat from a 100 kW laser ($f_{\text{DC}} = 0.06$, $Q_{\text{evaporator}} = 5.69 \text{ BTU/s}$) is shown in Fig. 14.

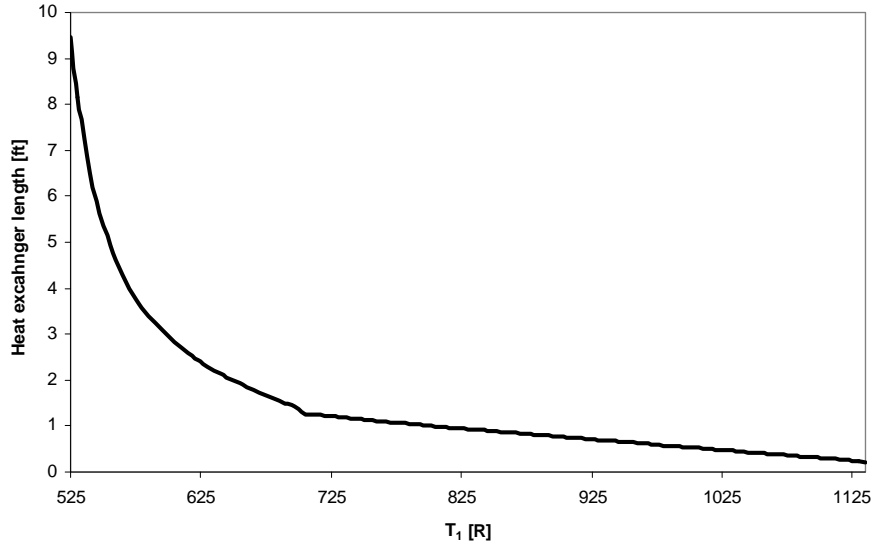


Fig. 13. Maximum energy transfer rates of the condenser with a 100kW laser and an 80% efficient heat pump compressor

The temperature profiles used for the evaporator, compressor exit, and condenser phase change was from Fig. 9. The bypass section length was computed at a given T_1 , by discretizing the heat exchanger into small increments, finding heat transfer rate of every increment (based on Eq. 6), and summing all of the lengths together. This heat exchanger is the single surface configuration shown in Fig. 4. The section length decreases with the increasing T_1 primarily because of the increased temperature profile between points 2 and 3 (Fig. 2). The required bypass length reduces more rapidly when T_1 is less than 705 R because of the maximized T_2 (at 2,270 R) and the increasing T_{2p} . When T_1 is increasing higher than 705 R, the primary cause of the reduction in bypass length is T_1 and T_2 approaching T_{2p} .

Because the length of the bypass section of the reference engine (see Table 1) is 6.07 feet, an evaporator temperature (T_1) less than 544 R (or 84 °F) will not dissipate all of the energy to complete the phase change and will not maintain the vapor-compression cycle's equilibrium. If the thermal storage device required T_1 to be less than 544 R and

the laser power is fixed at 100 kW, then the thermal load of 5.69 BTU/s must be lowered by using the duty cycle factor (f_{DC}) in Fig. 8 or by changing the heat exchanger type.

The discontinuity at 705 R is caused by the imposed limit of a maximum T_{2p} of 1,125 R. Although T_{2p} limit can be at the phase change temperature of water is 1,164 R, the T_{2p} limit was chosen to utilize the mixed liquid vapor region under the vapor dome (Fig. 2). The discontinuity is caused by an increase in the heat transfer coefficient of the coolant while the linear interpolation algorithm changed modes from a constant T_2 , increasing pressure (point 2), to a constant pressure (point 2) and decreasing T_2 . This effect will reoccur during the T_2 and the T_{2p} limit transitions.

Single Heat Pump, Dual Surface Heat Exchanger

The dual surface heat exchanger shown in Fig. 6 can be used to give additional energy transfer capability. Using the 100 kW laser ($f_{DC} = 0.06$, $Q_{evaporator} = 5.687$ BTU/s) from Fig. 13, Fig. 14 compares the dual surface heat exchanger with the single surface heat exchanger.

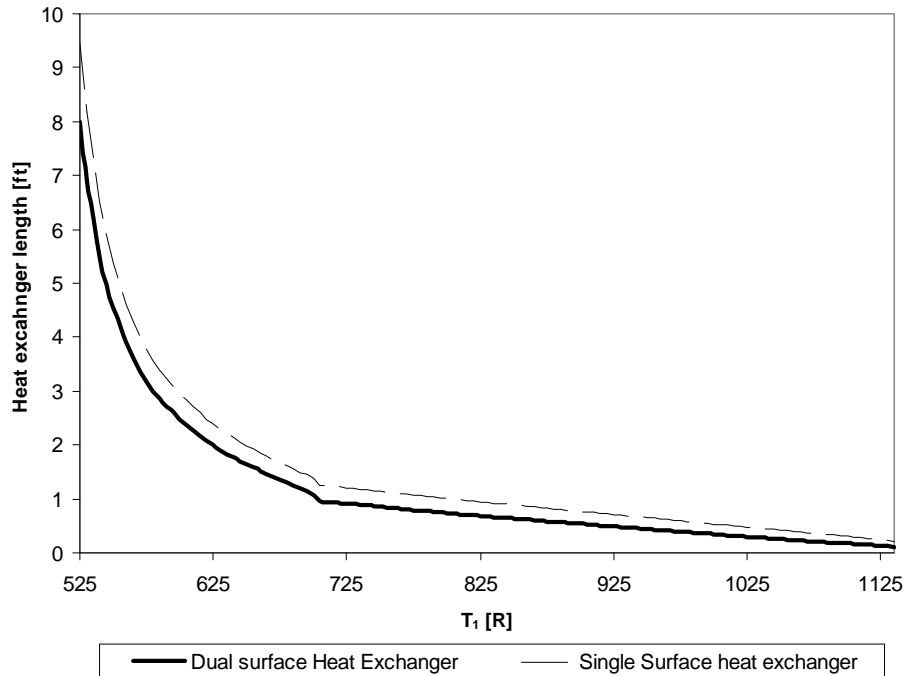


Fig. 14. Heat exchanger lengths for a 100kW thermal management system at a range of evaporator temperatures

The minimum evaporator temperature, for a 6.07 foot bypass, is now reduced from 544 R to 536 R (or 76.3 °F) for the dual surface heat exchanger. Even though surface area is almost doubled between the single and double heat exchangers, the required length of the dual surface heat exchanger is not half because the velocity is also halved, reducing the heat transfer coefficient and the net heat exchange.

Device Power Class and Bypass Length

The effects of increasing the device power class will be examined so that a maximum power class can be found for a range of T_1 and bypass length, instead of finding the bypass length with a 100 kW device power class. At the design point of the engine, a 500 kW and a 1 MW device with identical parameters are compared and are shown in Fig. 15.

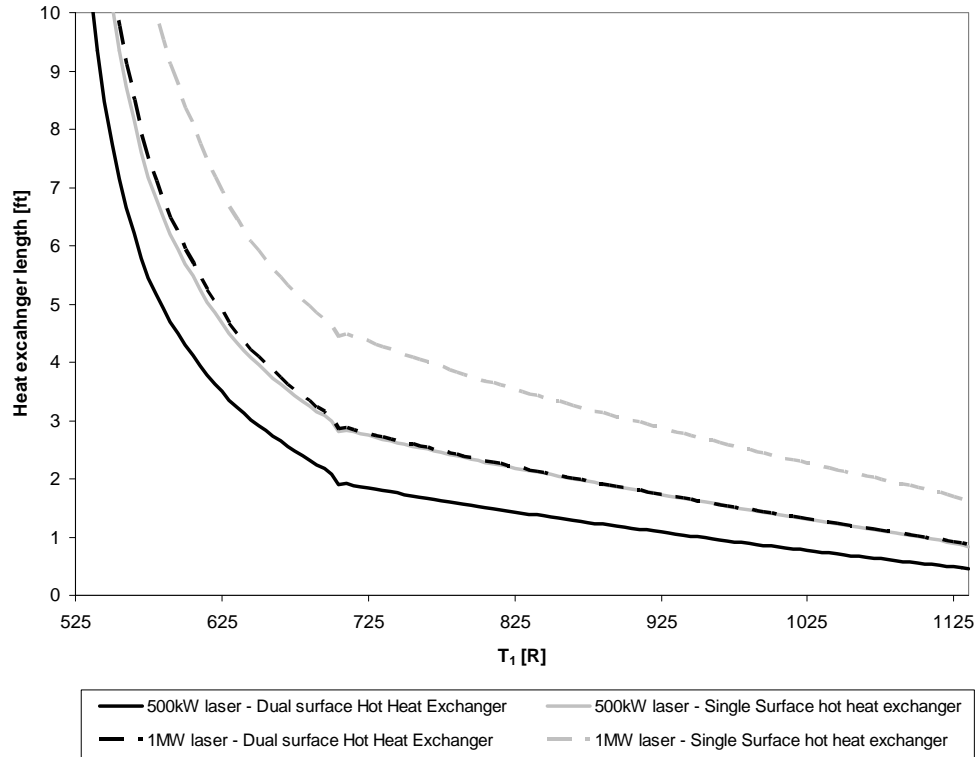


Fig. 15. Heat exchanger lengths for a 500 kW and a 1 MW thermal management system showing minimum evaporator temperatures

For a 6.07 ft bypass section length, a 1 MW device with a single surface heat exchanger can be cooled with a minimum T_1 of 645 R. A dual surface heat exchanger with the same bypass length can transfer the same amount of waste heat at a T_1 as low as 599 R. Increased power classes are shown in Fig. 16.

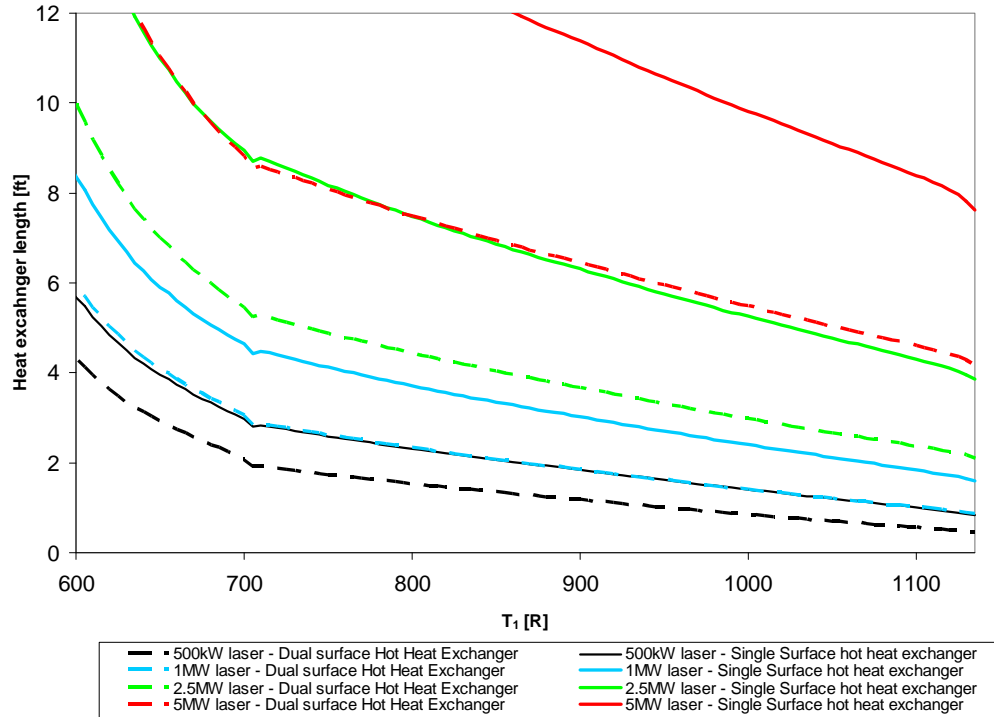


Fig. 16. Heat exchanger lengths for a thermal management system showing minimum evaporator temperatures for a variety of device power levels

The 5 MW device with a 6.07 ft bypass section cannot be cooled using a single surface heat exchanger, because the corresponding line in Fig. 16 does not extend below the 6.07 heat exchanger length at any T_1 . If a 5 MW device is needed, a dual surface heat exchanger or multiple engines with heat exchangers is required. Thus far, the data has been applied to a wide range of devices. A more specific case may be useful.

Maximum Laser Class with Single Heat Exchanger

To find a maximum laser device power class, the cooling temperature will be assumed to be 527.5 R, as defined on page 26. Setting the evaporator temperature (T_1) to 527.5 R and by using Fig. 9, the maximum temperature at the exit of the compressor (T_2) will be 2,270 R and the phase change temperature of the condenser ($T_{2p}-T_3$) will be 792.9 R. Using Fig. 16, the thermal management system at the engine design point (Table 1),

can support a 26 kilowatt device for a single surface heat exchanger. A dual surface heat exchanger can support a 46 kilowatt device as shown in Table 3.

Table 3. Maximum supported laser power using a single heat pump at the reference flight condition

Maximum laser class [kW]	26	45
Heat exchanger type	Single surface	Dual surface
Evaporator temperature, T_1 [R]	527.5	
Condenser phase-change temperature, T_{2p} [R]	792.9	
T_2 [R]	2,270	
Compressor work [kW]	1.8	3.0
Coolant mass flow rate [lbm/s]	1.881E-03	3.256E-03
heat transfer rate of condenser [BTU/s]	3.15	5.45

The maximum power classes were found by assuming a laser power and solving for the heat exchanger length. The device power level was adjusted until the heat exchanger length was approximately equal to the bypass section length. The maximum power class is 26 kW for the single surface heat exchanger and 45 kW for the dual surface heat exchanger. The maximum power class is relatively low because the low T_1 causes a low T_{2p} . The low T_{2p} causes a low temperature difference between the T_{2p} and the bypass air temperature, reducing the heat transfer rate in Eq. 6. If the coolant temperature (T_2) was further increased, the phase change temperature ($T_{2p}-T_3$) and the thermal transfer rate ($Q_{\text{condenser}}$) could both be increased.

Maximum Microwave Class with Single Heat Exchanger

For a typical microwave device, the coolant temperature at ($T_4 - T_1$) is 617.4 R, as defined on page 26. Because the microwave device coolant temperature ($T_1 = 617.4$ R) is higher than the laser coolant temperature ($T_1 = 527.5$ R), T_{2p} of the microwave heat pump will be higher than the laser T_{2p} . The higher T_{2p} causes an increased energy transfer at

the bypass heat exchanger (point 2 – 3) and an increased microwave device power class, as shown,

Table 4. Maximum supported microwave power using a single heat pump at the reference flight condition

Maximum microwave class [kW]	468	1,358
Heat exchanger type	Single surface	Dual surface
Evaporator temperature [R]	617.4	
Condenser phase-change temperature [R]	973.9	
T_2 [R]	2,270	
Compressor work [kW]	59.2	110.4
Coolant mass flow rate [lbm/s]	6.637E-02	1.237E-01
heat transfer rate of condenser [BTU/s]	97.54	181.85

The maximum power class for the microwave device is 468 kW and 1,350 kW with the single and dual surface heat exchanger, respectively. Reviewing from Table 3, the maximum laser power with a single heat pump is 26 kW and 45 kW with the single and dual surface heat exchanger, respectively. At the reference flight condition (Table 1), the microwave power is 18 and 30 times greater than the laser power, for the single and dual surface heat exchangers, respectively. However, there is another heat pump configuration capable of providing a higher temperature profile across the bypass heat exchanger (point 2 – 3) and maximum device power class.

Cascaded Heat Exchanger

By combining two heat pumps serially into what is known as a cascade cycle, the overall change in temperature, between the thermal storage device (T_1) and the bypass heat exchanger ($T_2 - T_3$), can be greatly increased.

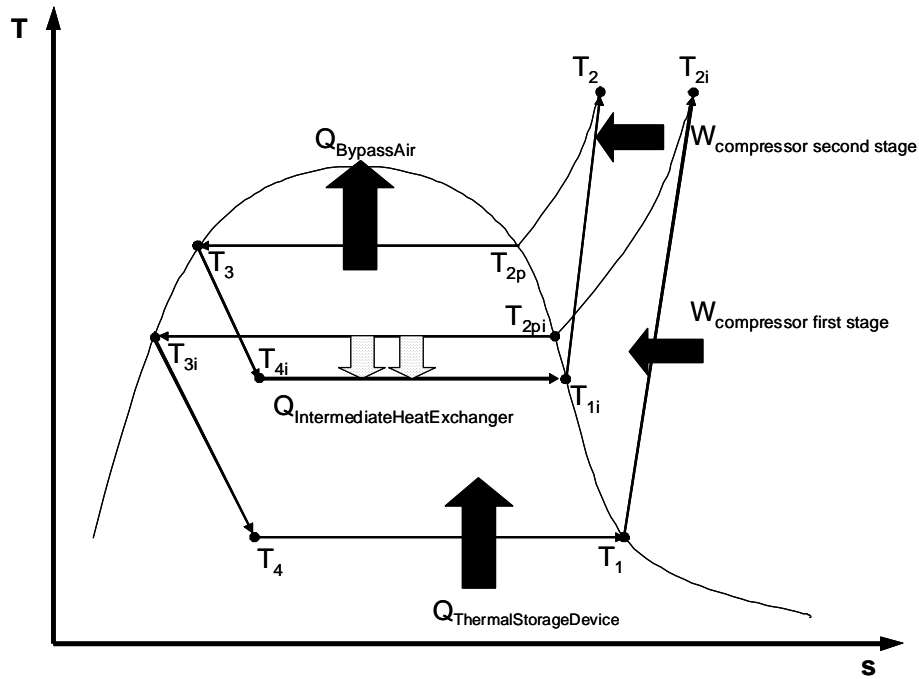


Fig. 17. Cascade cycle showing multiple heat pumps

The filled arrows show the external transfer of energy with devices outside of the cascaded heat pump, like compressor work, $Q_{\text{ThermalStorageDevice}}$, and $Q_{\text{BypassAir}}$. The dotted arrows show the internal transfer at the intermediate heat exchanger.

The first stage heat pump evaporator (point 4 – 1) will receive energy ($Q_{\text{ThermalStorageDevice}}$) directly from the thermal storage device. The first stage compressor (point 1 – 2i) will generate the maximum change in temperature to point (T_{2i}). The first stage condenser (point 2i – 3i) will exchange energy with the second stage evaporator (point 4i – 1i) at the intermediate heat exchanger. The energy transfer rate at the intermediate heat exchanger ($Q_{\text{IntermediateHeatExchanger}}$) will be higher than $Q_{\text{ThermalStorageDevice}}$ because of the added work from the first stage compressor (point 1 – 2i). The higher rate of thermal transfer at the second stage evaporator (point 4i – 1i) will required a higher coolant mass flow rate in the second stage heat pump. The coolant for the first and second-stage heat pumps will remain water. The second stage will use a second

compressor (point 1i – 2) and will exchange energy with the bypass heat exchanger (point 2 – 3). The first and second stage compressors can be physically integrated into a single axel compressor for both stages. Another benefit of this cycle is that the intermediate heat exchanger can be configured in a more efficient configuration for weight and volume than the bypass heat exchanger.

Maximum Laser Class with Cascaded Heat Exchanger

Cascaded heat pumps will be applied to the laser device requirements defined in the Maximum Laser Class with Single Heat Exchanger, on page 42. The first stage evaporator temperature ($T_4 - T_1$) will be 527.5 R. The coolant will enter the first stage condenser (T_{2i}) at 2,270 R and exit (T_{3i}) at 792.85 R. The second-stage heat pump evaporator (point 4i – 1i) will operate at a temperature of 750 R, causing a temperature differential of 42.85 R at the intermediate heat exchanger. As energy flows from hot to cold, the first-stage coolant will transfer energy to the cooler second-stage coolant at the intermediate heat exchanger. In this case, the second stage compressor outlet temperature (T_2) is identical (2,270 R) to the simple heat pump model first analyzed, but the pressure is higher. This higher pressure will increase the single heat pump T_{2p} from 792.9 R to the cascaded T_{2p} of 1,160.2 R. The increase of T_{2p} by 367.3 R will allow a higher rate of heat transfer into the engine bypass air. At the reference flight condition (Table 1), the maximum laser classes that can be supported by cascaded heat pumps for both a single bypass and a dual bypass surface heat exchanger are shown,

Table 5. Maximum supported laser power using cascaded heat pumps at the reference flight condition

		Maximum laser class [kW]	808	1,650
		Heat exchanger type	Single surface	Dual surface
First stage heat pump	Evaporator temperature, T_1 [R]	527.5		
	Condenser phase-change temperature, T_{2p} [R]	792.85		
	T_2 [R]	2,270		
	Compressor work [kW]	54.65	111.60	
	Coolant mass flow rate [lbm/s]	0.05835	0.11916	
	heat transfer rate of condenser [BTU/s]	97.75	199.61	
Second stage heat pump	Evaporator temperature, T_1 [R]	750.0		
	Condenser phase-change temperature, T_{2p} [R]	1,160.2		
	T_2 [R]	2,052		
	Compressor work [kW]	188.6	385.0	
	Coolant mass flow rate [lbm/s]	0.2776	0.5669	
	heat transfer rate of condenser [BTU/s]	276.5	564.6	

The cascaded heat pumps can support a maximum laser class of 808 kW and 1.65 MW for a single a double surface bypass heat exchanger, respectively. Reviewing from the single heat pump (Table 3), the laser power was limited to 26 kW and 45kW for the single and dual surface heat exchangers. At this flight condition, the power class was increased by a factor of approximately 35.

It should be noted that the supportable power class will span a wide range of values depending on the flight conditions (details found in the Flight Envelope section, page 65). It should also be noted that the laser class can be doubled when a heat exchanger is installed within each engine of a dual engine aircraft. The results shown in Table 5 are a very specific case for a high-energy device with a T_1 of 527.5 R.

Maximum Microwave Class with Cascaded Heat Exchanger

To further increase the supportable microwave power class, a cascade system can be applied. The results are shown in Table 6.

Table 6. Cascade heat exchanger showing the maximum supported microwave system class for a given configuration

		Maximum microwave class [kW]	1,108	2,239
		Heat exchanger type	Single surface	Dual surface
First stage heat pump	Evaporator temperature, T_1 [R]	617.4		
	Condenser phase-change temperature, T_{2p} [R]	974		
	T_2 [R]	2,270		
	Compressor work [kW]	90.06	181.98	
	Coolant mass flow rate [lbm/s]	0.10092	0.20394	
	heat transfer rate of condenser [BTU/s]	148.37	299.81	
Second stage heat pump	Evaporator temperature, T_1 [R]	925.0		
	Condenser phase-change temperature, T_{2p} [R]	1,160.2		
	T_2 [R]	1,476		
	Compressor work [kW]	101.3	204.7	
	Coolant mass flow rate [lbm/s]	0.3915	0.7912	
	heat transfer rate of condenser [BTU/s]	244.4	493.9	

The maximum supported high-energy devices, at the reference flight condition (Table 1), are 1.108 MW and 2.239 MW for a single surface and dual surface bypass heat exchanger, respectively.

For a more general set of achievable device power classes, a set of charts showing maximum power levels at a given device coolant temperature can be found in Fig. 32 – Fig. 35 within Appendix A. The 705 R transition point referred to on page 39 can be seen in Fig. 32 and Fig. 33.

The cascaded heat pump systems produce a decrease in the heat transfer coefficient of the coolant between points 2p and 3, causing a decrease in the maximum laser power between T_1 of 685 R and 710 R, as shown in Fig. 34 and Fig. 35. Once T_1 is greater than 710 R, the pressure at point 2 and the heat transfer coefficient between points 2p and 3 are constant and the maximum device power will increase with the increased device cooling temperature (T_1).

Temperature profiles showing the evaporator (T_1), compressor exit (T_{2i} and T_2), and condenser phase change temperatures (T_{2pi} and T_{2p}) for a range of device power classes are shown in Fig. 36 – Fig. 39 in Appendix A.

Heat Transfer Rate into Bypass Air

Energy transfer rate into the engine is quantified to model the engine performance. At reference conditions, the rate of energy transfer into the bypass air ($Q_{\text{condenser}}$) as a function of power class is shown,

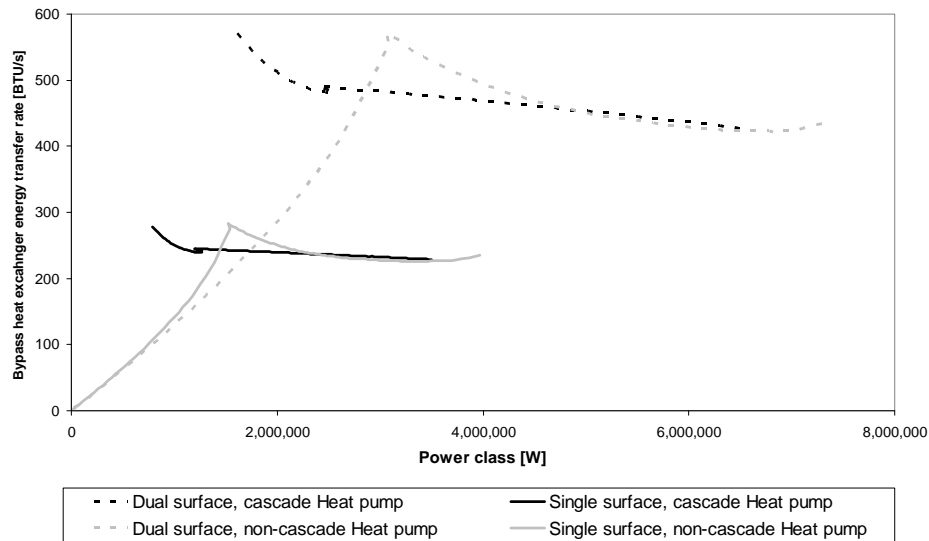


Fig. 18. Total heat transfer rate into the bypass air

The power class used is the previously developed maximum power that can be achieved at a given evaporator temperature. The behaviors of the cascaded thermal transfer rates may seem non-intuitive. As the transfer rates are heavily influenced by the temperature profile, the behavior becomes more intelligible. It is noted the highest power class does not produce the highest transfer rates. This is due, in part, to the heat pump compressor adding the greatest amount of work when T_2 and T_{2p} are at their respective maximum

values. The compressor will produce the greatest increase to temperature and pressure at this point and can be seen in Fig. 9 and Fig. 10.

Thermal Resistance in Bypass Heat Exchanger

A closer examination of the thermal resistance (page 13) preventing the transfer of energy through the air, the coolant, and the pipe material separating the two fluid flows will be performed. The results will provide an understanding of how to improve the performance of the heat exchanger. Within a single case, the thermal resistance of the coolant can decrease by 23% as it flows through the condenser. While comparing the resistance in each of the three materials (air, pipe, and steam), the mean phase change flow properties (between point 2p and 3) will be used to give an understanding of the relative levels of resistance. The thermal resistance of the single heat pump, single-surface heat exchanger was found by recording the thermal resistance value at the maximum power class at a given T_1 .

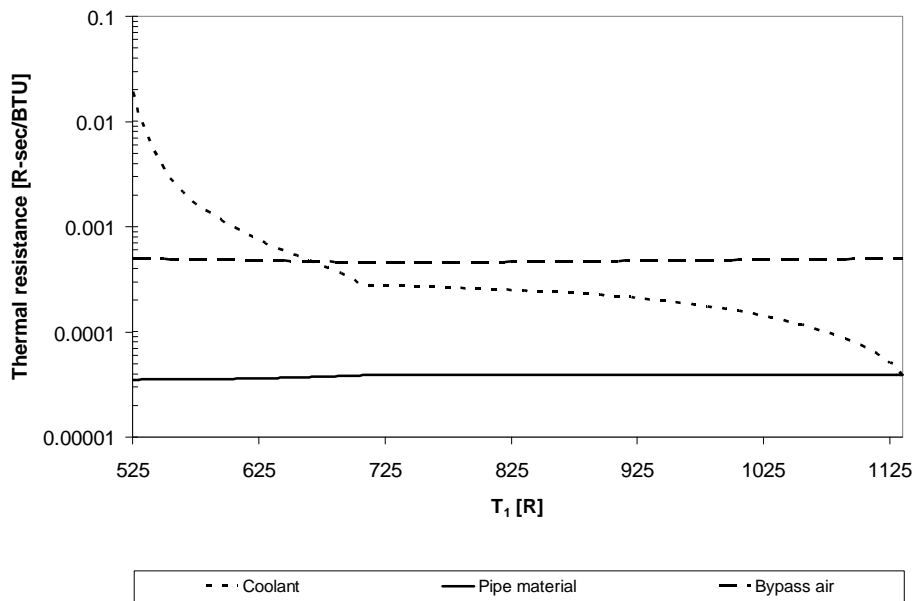


Fig. 19. Thermal resistance at mean point between point 2p and 3, for a single heat pump, single surface heat exchanger

The coolant provides the majority of the resistance to the heat transfer at low temperatures. Note that the y-axis is a log scale. The thermal resistance of the coolant decreases most rapidly below T_1 of 705 R. The discontinuity in the coolant resistance is caused by the same phenomenon discussed on page 39. Note that the solid pipe material separating the two fluids provides the least amount of resistance even though the thermal conductivity of a titanium alloy (~ 15.8 BTU/(hr-ft-R)) is not remarkably high compared with common heat exchanger materials, like copper (~ 232 BTU/(hr-ft-R)) or aluminum (~ 137 BTU/(hr-ft-R)). Due to the high temperatures and pressures to be examined in this paper ($T_2 = 2,270$ R, $P_2 = 3,190$ psi), a single material with high strength at high temperatures was selected. The thermal resistance of the complete set of thermal management system configurations, showing the resistance of the outer and inner bypass surfaces (Fig. 6), can be examined in Fig. 40 – Fig. 43, within Appendix A.

Bypass Heat Exchanger Weight

Using the geometry provided in Fig. 4 – Fig. 6, the density of the steam and pipe material (Table 2), and the reference engine (Table 1), the weight of the single surface heat exchanger pipe material is 220 pounds. If a thermal blanket like Fiberfrax® ceramic fiber blanket is used as the insulation material, the weight of the insulation is 88.6 pounds. The total weight of the coolant in both liquid and vapor form is approximately 162 pounds, leading to a total single surface heat exchanger weight of 470.6 pounds. The single surface heat exchanger has a weight of 77.57 pounds per foot of bypass section, parallel to the air flow. A dual surface heat exchanger will have a total weight of approximately 837 pounds and will have a unit weight of 138 pounds per foot length of bypass section.

Engine Cycle – Component Level

The effects of the thermal management system on the engine performance will be shown by first describing the changes on the engine components. The total temperature and total pressure of the bypass air will change because of the effects of the bypass heat exchanger. The amount of energy extracted from the core air, at the low-pressure turbine, will increase from the 300 kW (required by an airframe electrical systems, Table 1) to include the power required by the heat pump compressor. It will be shown how the changes to the bypass air and the low-pressure turbine air will impact the mixer, downwind of the bypass duct and the core. And the next section, Engine Cycle – System Level, will show how the component changes will impact the engine performance.

It should also be noted this analysis is an on-design analysis, other than the flight envelope. An on-design analysis assumes an engine optimized to operate at a single flight condition. The compression ratios, engine size, and component area ratios are calculated based on ideal operation. An off-design analysis would use a single engine design and vary the flight conditions, causing a change to many of the internal parameters like the compression ratios and bypass ratios. The on-design definition will be extended to include the effects of the high-energy device and thermal management system. The engine will be optimized to operate at the maximum power class for each coolant temperature (T_1).

Bypass Duct

The changes to the engine bypass air total pressure and total temperature represents the change to the bypass air energy, allowing the waste energy to be incorporated into the engine model. The changes in the bypass air total pressure and temperature are a combination of the effects of the heat addition from the heat exchanger (Eq. 7, 13, 14) and the skin friction caused by the bypass walls (Eq. 12 – 14). The net changes to the bypass air properties for the single heat pump, dual surface case are shown.

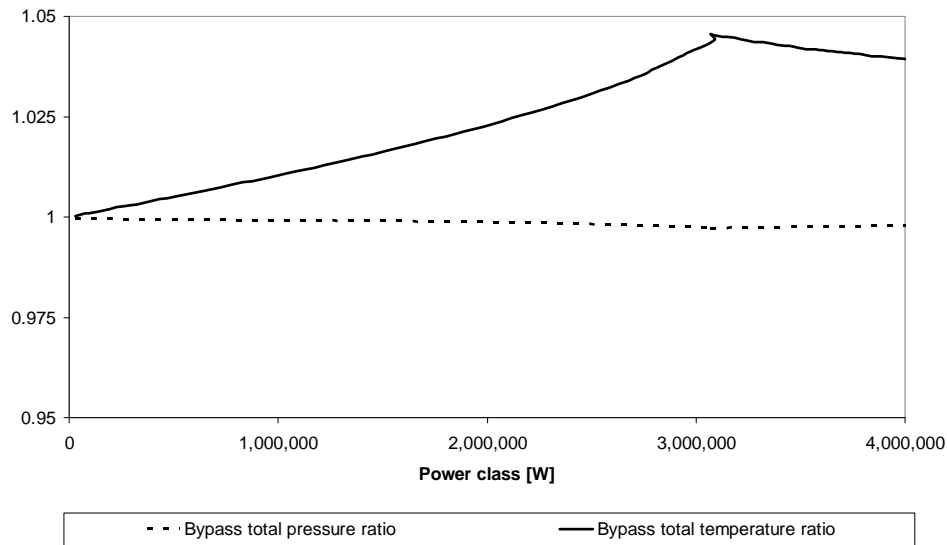


Fig. 20. Total pressure and total temperature ratios for the engine bypass section with a dual surface, single heat pump at the reference flight condition

At the reference engine condition (Table 1), the maximum total temperature ratio (τ_{BP}) is 1.046 (increase of 33 R) and the minimum pressure ratio (π_{BP}) is 0.9973 (decrease of 0.076 psi). The increase in stagnation temperature is a relatively low increase compared to other engine components. As a point of comparison, Table 7 shows the reference engine total temperatures and pressures at a variety of station numbers to show the magnitude of the changes in the stagnation air properties.

Table 7. Stagnation pressures and temperatures of reference engine high-energy device and thermal management system

Station Number	0	1	2	13	2.5	3	4	4.5	6	16	6A	7	9	
P_t	[psia]	8.3	8.3	8.1	28.3	28.3	290.7	281.9	86.1	28.3	28.3	27.1	26.0	25.5
T_t	[R]	485	485	485	725	725	1,518	3,200	2,369	1,875	725	1,254	3,600	3,600

For example, the total pressure ratio across the fan (π_f) can be found by dividing the total pressure at point 13 (28.3 psia) by point 2 (8.1 psia), equaling 3.5. The total pressure and temperature ratio (π_{BP} and τ_{BP}), at the laser device cooling temperature of 527.5 R, is 0.99905 and 1.00045, respectively. The microwave device cooling temperature of 617.4 R will cause a change in π_{BP} and τ_{BP} of 0.99897 and 1.014, respectively. The full set of total pressure and total temperature ratio graphs can be found in Fig. 44 – Fig. 47, within Appendix B.

The discontinuity in Fig. 20 at 3.1 MW is caused by the thermal conductivity and device power decrease discussed on page 48. The power levels in Fig. 20 correspond with the device cooling temperatures (T_l) as shown in Fig. 35, in Appendix A.

Additional Turbine Electric Power Requirement

An additional electrical requirement on the engine needed to drive the heat pump compressors. The additional power requirement for each type of thermal management system is shown in Fig. 21.

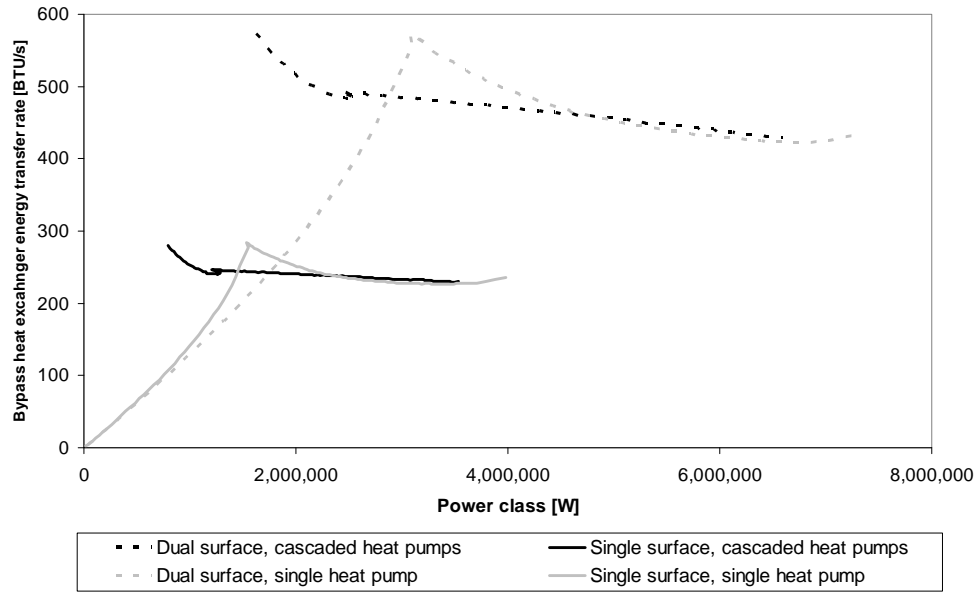


Fig. 21. Thermal transfer rate at the bypass heat exchanger as a function of device power class

Since the cascaded systems have two compressors, Fig. 21 combines both compressor’s requirements. The single heat pump systems are simply the single compressor workload. This data was recorded while the data for Fig. 44 – Fig. 47 was being generated. The decrease in the compressor work, for the single heat pump systems, is due to the maximum pressure at point 2, in Fig. 2, being achieved. The same phenomenon was observed in Fig. 10. The cascaded heat pump systems required the maximum compressor work at the lowest device coolant temperatures, T_1 .

In Fig. 21, the decreases in power in the cascaded systems are caused by the thermal conductivity and device power decrease discussed on page 48. The discontinuity in the single heat pump systems are caused by the phase change limit of water discussed on page 39. The power levels in Fig. 20 correspond with the device cooling temperatures (T_1) as shown in Fig. 35, in Appendix A.

The electric power to drive the compressor is generated from the energy within the air at station 4.5 (Fig. 7) via the low-pressure turbine, because electric power is

frequently generated from the low-pressure turbine in many current aircraft. The effects of the additional electric power requirement on the low-pressure turbine air, total temperature ratio (τ_{tL}), can be seen in Fig. 22.

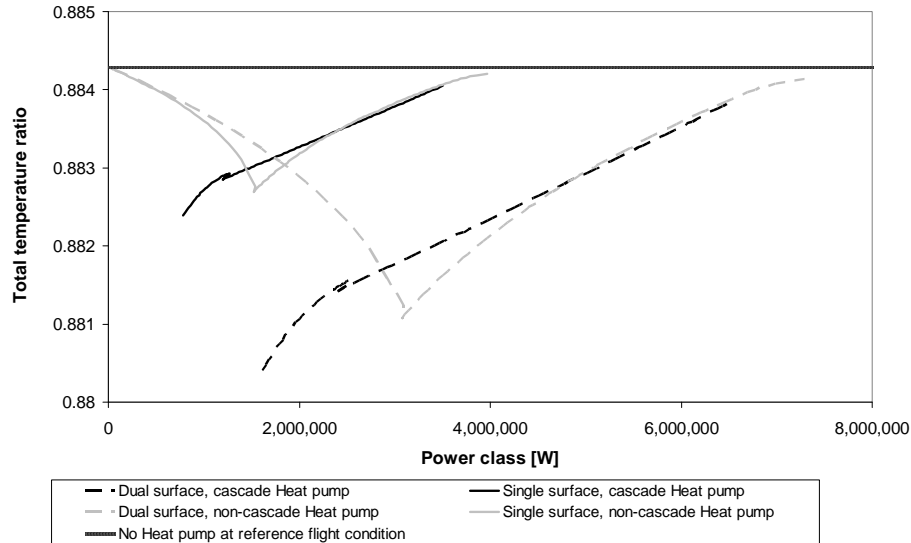


Fig. 22. Total temperature ratio across low-pressure turbine showing affects of heat pump power requirements

τ_{tL} for the reference engine without a high-energy device or thermal management system is shown by the horizontal line, at 0.8843. As the device power class increases from zero, the compressor work required for the single heat pump increases (Fig. 21). The required compressor work will remove additional thermal energy from the air and reduce τ_{tL} . Once the power class increases beyond the maximum compressor work point (Fig. 21), τ_{tL} will return to the reference engine condition without a high-energy device. Because the cascaded heat pumps required the greatest amount of compressor work at the lowest power classes, the τ_{tL} ratios will be at a minimum at the lowest power classes. The decrease in power in the cascaded systems and the discontinuity in the single heat pump systems are caused by the same phenomenon discussed for Fig. 21.

The total pressure ratios across the low-pressure turbine are shown,

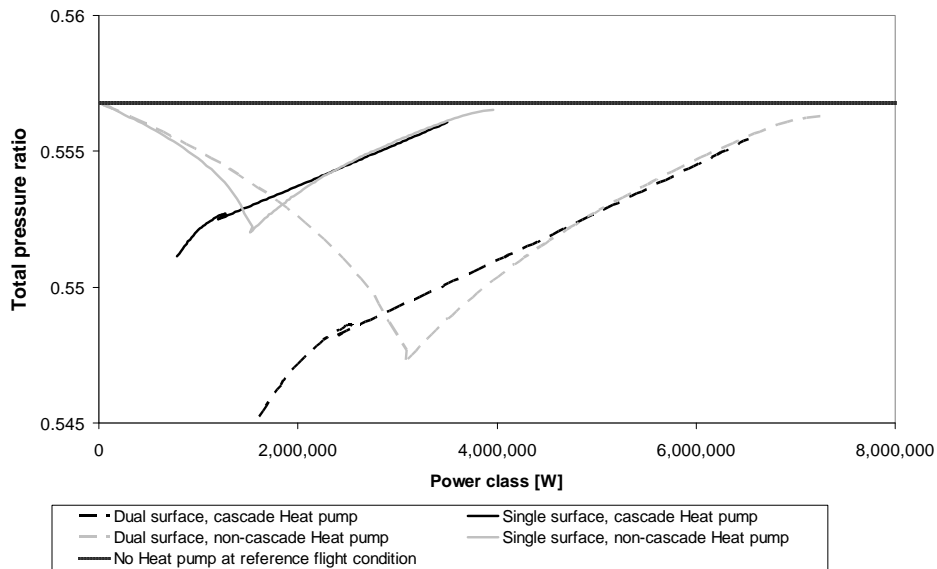


Fig. 23. Total pressure ratio across low-pressure turbine showing affects of heat pump power requirements

The effects on the total pressure are similar in shape to the total temperature case in Fig. 22 because π_{tL} is a function of τ_{tL} , as shown in Eq. 24. Note the small scale used for the y-axis in Fig. 22 and Fig. 23.

Mixer

Now that the changes in stagnation air properties across the low-pressure turbine and bypass air are found, understanding the mixer becomes essential in order to predict the change in engine performance. Based on Eq. 25, the total temperature ratio across the mixer is shown in Fig. 24.

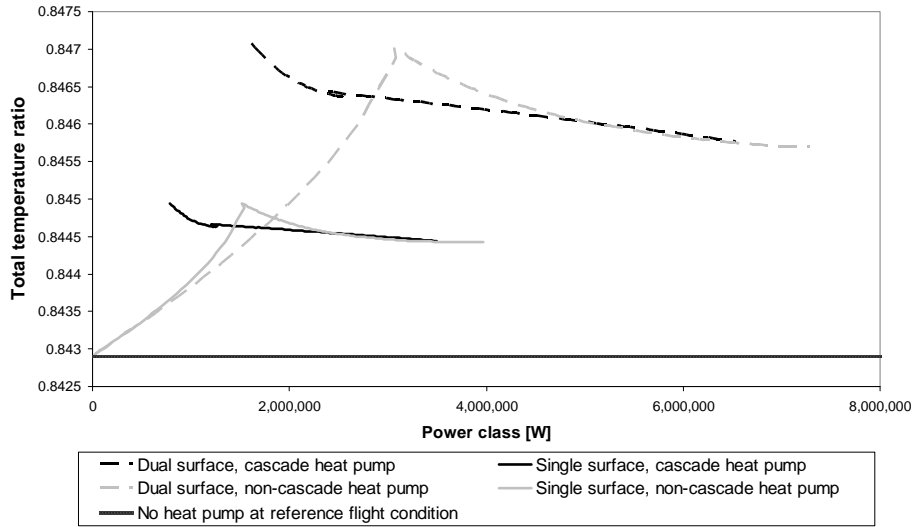


Fig. 24. Total temperature ratio across the mixer showing affects of the thermal management system

As the enthalpy of the air in the engine core is reduced and air in the bypass duct is increased (because of the change in τ_{L} and τ_{BP}), the term in the parenthesis of the numerator in Eq. 25 is increased. The increase in the value of the numerator causes an increase in the total temperature ratio of the mixer (τ_{mix}). The total pressure ratio across the mixer is found with Eq. 26 and Eq. 27,

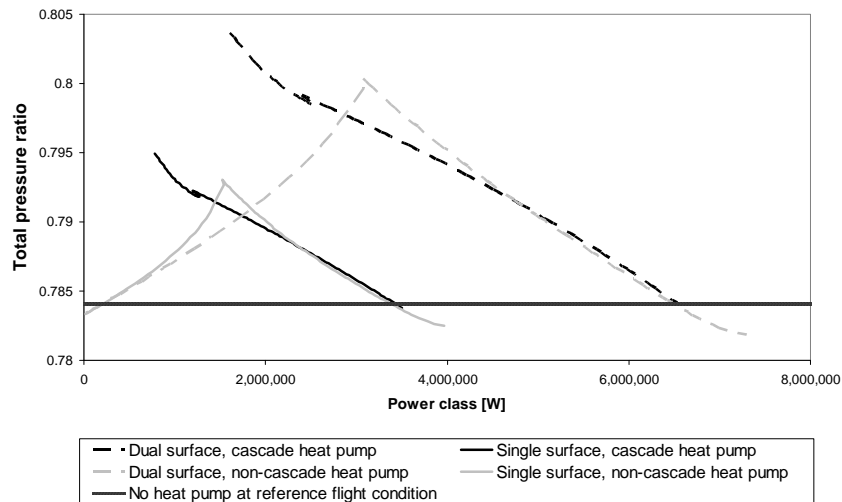


Fig. 25. Total pressure ratio across the mixer showing effects of the thermal management system

The total pressure ratio if the mixer (π_{mix}) is defined as the ratio of the total air pressure exiting the mixer (P_{6A}) divided by the total air pressure exiting the core (P_6). Since $\pi_{\text{m,max}}$ is a constant, $\pi_{\text{m,ideal}}$ causes the change in π_{mix} in Eq. 27. Eq. 26 shows the set of variables used to find $\pi_{\text{m,ideal}}$ are α' , τ_m , A_6/A_{6A} , MFP_6 , and MFP_{6A} , where α' is defined as the ratio of the mass flow rate of station 6 to 16 (Fig. 7). A_6/A_{6A} and MFP_{6A} are the terms that have the greatest relative change. However, the dominant term is A_6/A_{6A} causing the increase to $\pi_{\text{m, ideal}}$ and π_{mix} . An off-design analysis would not allow the area ratio to change, but as stated on page 52, this analysis is on-design enabling an engineer to choose an optimum operating condition, for a given cooling requirement at T_1 .

Engine Cycle – System Level

Two primary engine performance parameters commonly used to describe engine performance are uninstalled thrust and uninstalled thrust specific fuel consumption. Both parameters have been analyzed and the results will be presented.

Uninstalled Thrust

The total uninstalled thrust for both the afterburner on and off cases resulted in additional thrust compared to that produced at the reference engine parameters without the presence of a high-energy device. The non-afterburner case is shown in Fig. 26.

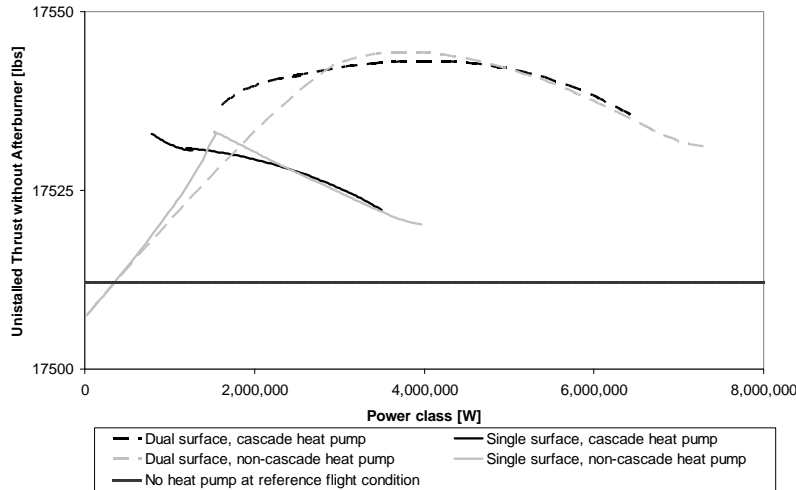


Fig. 26. Uninstalled thrust showing the change in a non-afterburning engine performance as a result of the thermal management system

The maximum increase in uninstalled thrust caused by the thermal management system is approximately 30 pounds (0.18% increase). The maximum decrease is approximately 5 pounds (0.028% decrease). The lowest power class (x-axis) in Fig. 26 is 32.88 kW. At 32.88 kW, the single heat pump systems cause a reduction in thrust, from the reference operating condition (Table 1), because the effect of the heat pump compressor is greater than the thrust increase from the heat addition. For all cases in Fig. 26, the thrust increases as the rate of heat transfer from the thermal storage device ($Q_{\text{evaporator}}$) increases and the total compressor work decreases.

In the engine performance figures, the decreases in power in the cascaded systems are caused by the thermal conductivity and device power decrease discussed on page 48. The decrease in the power at the discontinuity in the single heat pump systems are caused by the phase change limit of water discussed on page 39. The power levels, on the x-axis, correspond with the device cooling temperatures (T_1) as shown in Fig. 35, in Appendix A.

The uninstalled thrust produced in an afterburning engine can be seen in Fig. 27.

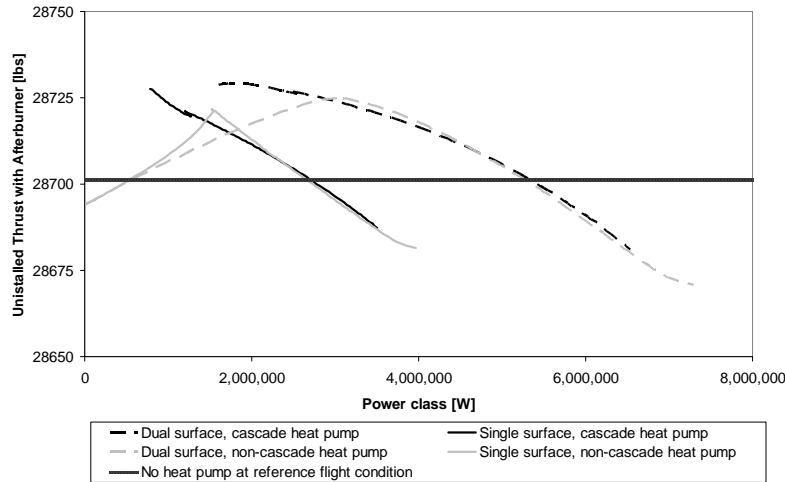


Fig. 27. Uninstalled thrust showing the change in a afterburning engine performance as a result of the thermal management system

The maximum increase in thrust from the reference engine operating condition is approximately 28 pounds (0.098% increase) and the maximum decrease is approximately 35 pounds (0.12% decrease). When comparing Fig. 27 and Fig. 26, the relative thrust in the afterburning case decreases to a lower thrust than the reference condition, at high device power levels. The high power levels in the non-afterburning case show an increase in power from the respective reference condition. Because of the additional thermal energy from the bypass section, the afterburner inlet (station 6A) will be a higher temperature than the reference condition, and the amount of fuel required to raise the temperature to the afterburner temperature limit (3,600 R) will decrease. Equation 28 shows the thrust as a function of the exit velocity (V_9). V_9 is found using $\tau_{\lambda AB} (h_{T7}/h_{T0})$, which is lower than the reference condition, for the high device power regime.

Uninstalled Thrust Specific Fuel Consumption

Typically, lower thrust specific fuel consumption, S , values are desirable because a decrease indicates a higher level of fuel efficiency. S is a measure of mass flow rate per

unit of thrust (Eq. 30). Using the thrust results from the preceding section, the main burner fuel mass flow rates are combined to create in Fig. 28.

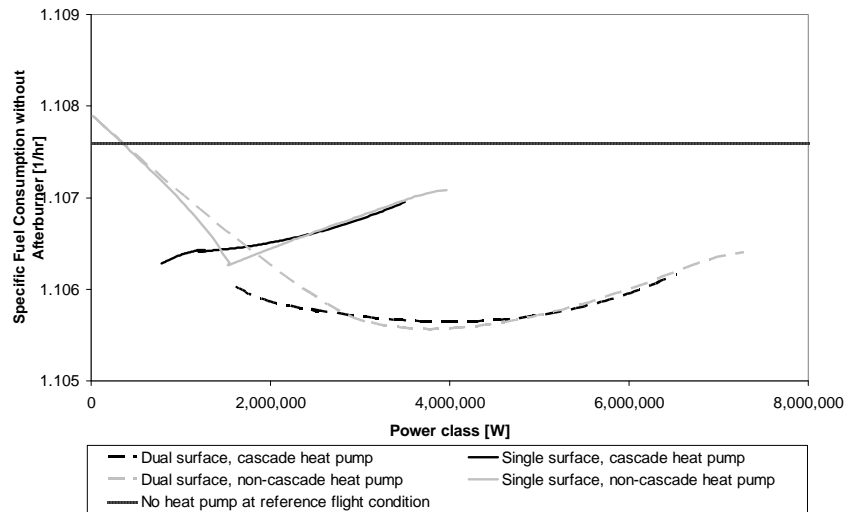


Fig. 28. Uninstalled thrust specific fuel consumption showing the change in a non-afterburning engine performance as a result of the thermal management system

The maximum response of S , in the non-afterburning case, is an increase of 0.00025 1/hr (0.23% increase) and a decrease of 0.002 1/hr (1.86% decrease). In all of the cases in Fig. 28, the main burner mass flow rates of the fuel are constant. Because of the constant fuel mass flow, when the thrust increases, S decreases. Therefore, the trend of S , in Fig. 28, is inversely proportional to the non-afterburning uninstalled thrust case, in Fig. 26.

S is shown for the afterburning engine in Fig. 29.

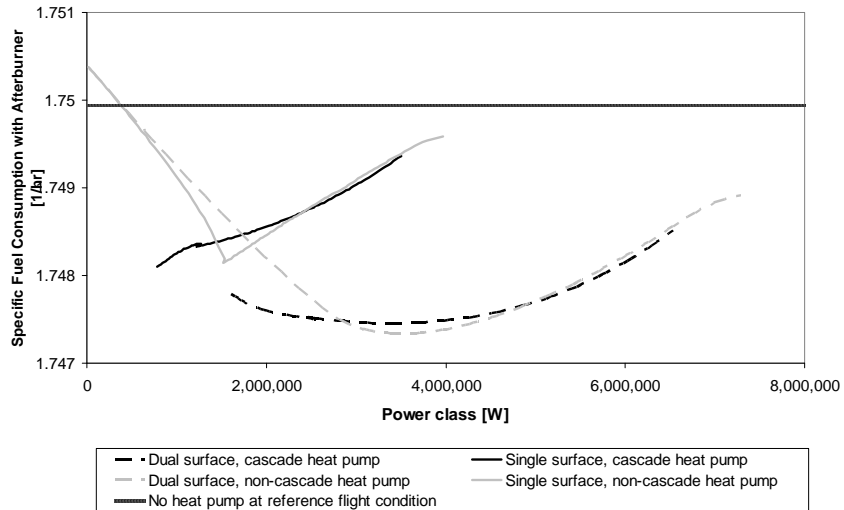


Fig. 29. Uninstalled thrust specific fuel consumption showing the change in an afterburning engine performance as a result of the thermal management system

The maximum response of S , in the non-afterburning case, is an increase of 0.0005 1/hr (0.028% increase) and a decrease of 0.0028 1/hr (0.16% decrease). In the afterburning case, the combustor fuel flow is constant. S is inversely proportional to the thrust produced (Fig. 27), except for the increase in the heat added to the afterburner inlet by the bypass heat exchanger ($Q_{\text{condenser}}$). As $Q_{\text{condenser}}$ increases (Fig. 21), S decreases because of a reduction in the afterburner fuel flow rate required to increase the afterburner inlet air temperature to the afterburner limit (3,600 R in this case).

Sensitivity Analysis

A sensitivity analysis was performed to give a basic understanding of how the primary performance parameters will respond to a change in an input variable. The primary performance parameters and the input variables are discussed on page 24. The sensitivity analysis includes the two high-energy devices and four heat pump configurations. The high-energy device cooling temperatures (T_1) are based on the laser

and microwave cooling requirements (527.5 R and 617.4 R, respectively). The heat pump configurations include the single and dual bypass heat exchange surfaces and the cascaded and single heat pump systems. The engine configuration is at the reference values (Table 1). Table 8 shows the results of the sensitivity analysis for the laser cooled by a single heat pump with a single surface heat exchanger.

Table 8. Sensitivity analysis for a single heat pump, single surface heat exchanger cooling a laser

Variable	Δ variable	Δ variable / variable _{init}	T ₁ [R]	LaserPower [W]	F _{noAB} [lbf]	F [lbf]	S _{noAB} [1/hr]	S [1/hr]	WorkComp [W]	QdotCond [BTU/s]
Compressor efficiency	0.020	0.025	527.5	4.28E+05	1.00E+02	2.92E+02	5.68E+00	5.16E+00	-3.59E-04	2.78E+01
Coolant pipe diameter	-0.00417	-0.200	527.5	-2.22E+05	-1.25E+01	-3.65E+01	-3.07E+00	-2.85E+00	1.94E-04	-1.52E+01
Coolant pipe conductivity	-0.80	-0.051	527.5	-2.08E+05	-4.94E+01	-1.44E+02	-2.91E+00	-2.75E+00	1.84E-04	-1.45E+01
Pipe yield strength	-300	-0.032	527.5	-3.27E+05	-7.75E+01	-2.26E+02	-4.57E+00	-4.31E+00	2.89E-04	-2.27E+01
Outer radius of bypass section	0.050	0.032	527.5	3.59E+05	7.75E+01	2.26E+02	1.11E+01	1.39E+01	-7.04E-04	2.49E+01
Length of bypass section	0.33	0.055	527.5	3.19E+05	4.55E+01	1.33E+02	-5.37E-01	-3.34E+00	3.40E-05	2.20E+01
Friction factor of surface in contact with bypass air	0.0090	9.000	527.5	1.17E+03	2.78E-01	8.11E-01	-5.51E+00	-8.31E+00	3.50E-04	8.15E-02
Mass flow rate of the inlet	20.0	0.080	527.5	1.32E+05	3.13E+01	9.12E+01	1.76E+04	2.87E+04	-3.45E-03	9.16E+00
Aircraft systems power requirement excluding the heat pump compressor	50.0	0.167	527.5	6.50E+04	1.50E+01	4.38E+01	5.86E+01	1.32E+02	-3.71E-03	4.52E+00
Engine bypass ratio (α)	0.050	0.125	527.5	1.00E+05	2.00E+01	5.84E+01	-2.43E+03	-2.38E+02	-1.54E-01	6.93E+00
Engine core compression ratio (π_c)	-4.00	-0.111	527.5	-1.07E+05	-2.25E+01	-6.57E+01	-2.44E+03	-6.22E+02	-7.17E-02	-7.42E+00
Engine bypass compression ratio (π_b)	-0.250	-0.071	527.5	-2.55E+05	-3.50E+01	-1.02E+02	1.45E+04	2.19E+04	-9.79E-01	-1.76E+01

In Table 8, each row lists an input variable (like the compressor efficiency, coolant pipe diameter, etc). The Δ variable column shows the change in the system input parameter when calculating the performance response. The Δ variable / variable_{init} column shows the non-dimensionalized form of the input parameter. The T₁ column shows the device cooling temperature used. Each of the remaining columns shows the response of a given variable to the change in the input (as defined in Eq. 31). If an increase in the supportable laser power is desired, the row, under the LaserPower column, with the highest absolute value would cause the greatest change in the laser class per unit of input variable.

For example, if the compressor efficiency is changed the performance parameter that will have the greatest response is the laser power (4.28×10^5) followed by the uninstalled thrust with afterburner (2.92×10^2). The performance parameter with the least response is the compressor work (-3.59×10^{-4}). The sensitivity analysis for the complete set of thermal management system configurations can be found in Table 9 – Table 16, in Appendix C.

Flight Envelope

High-energy device system capabilities have been examined for a variety of operating altitudes and Mach numbers. The bypass heat exchanger performance will change as the bypass section inlet conditions vary due to the modified flight conditions. Reviewing, the parameters upstream of the bypass section impacting the bypass inlet are the engine altitude, Mach number at station 0 (Fig. 7), inlet diffuser, bypass ratio, fan compressor ratio, and the bypass section inlet Mach number. The recovery factor is a function of the Mach number at station 0. As the Mach number increases, the recovery factor increases. The engine inlet diffuser is an inputted constant for the subsonic cases and increases with the Mach number in the supersonic cases. The equations and process for calculating the freestream recovery and the diffuser can be found in Mattingly et al. (2002:102).

Off-Design Analysis

Previously the bypass ratio, fan compression ratio, bypass inlet Mach number, altitude, and the freestream Mach number were specified for a given on-design reference

condition. Using the engine test module in the AEDsys® software package, version 4.020, developed by Jack D. Mattingly and David T. Pratt, the reference on-design engine parameters were used to find the off-design bypass inlet air properties. The off-design parameters that influence the bypass inlet airflow are the engine inlet mass flow rate, the bypass ratio, the fan compressor ratio, and the Mach number at the inlet of the bypass section. Because AEDsys assumes constant air properties through the bypass section, the computed Mach number at the bypass exit can be assumed that of the inlet. The on-design engine bypass ratio was modified from 0.4 to 1.4773 to allow the engine to operate at all conditions of interest (Mach number of 0.1 – 1.2, altitude of 0 – 40,000 ft). The engine bypass ratio was the only on-design parameter to change for the on-design analysis. The off-design parameters needed to compute the bypass inlet air properties were found at a series of points on a grid based on Mach number and altitude, shown in Fig. 30.

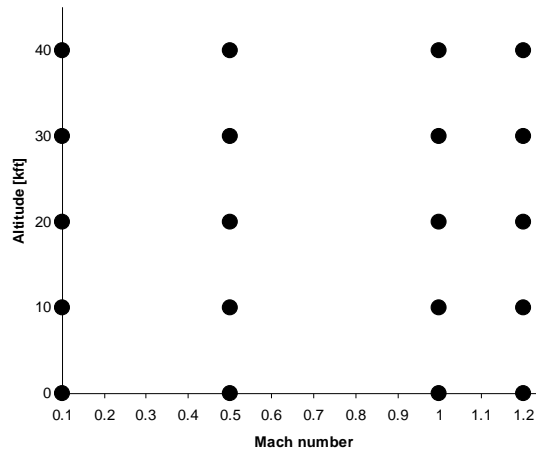


Fig. 30 Off-design points used for flight regime device operating limits

The altitudes and Mach numbers between points were approximated with a linear interpolation. This grid allowed for an approximation of a maximum high-energy device

power level at any point between a Mach number of 0.1 and 1.2 and from sea-level to 40,000 feet.

Using the bypass inlet air property approximations, the maximum device power was found based on the bypass section size as described on page 43. Additionally, the device cooling capacity was found for any generic device at the laser or microwave cooling temperatures (T_1). Since an engine may be cooling a device during take-off, descents, and combat, a set of solutions were found at an engine throttle setting of 80% and 100%, approximating engine idle and maximum thrust. Because the afterburner is downstream of the bypass section and will not influence the bypass section, the results of the afterburner case can be found in the 100% throttle results. More information regarding engine throttle and on-design and off-design analysis can be found in (Mattingly et al., 2002).

Because the difference between the maximum laser or microwave device power class between the 80% and the 100% throttle settings are not easily understood when examining the individual maximum power and cooling charts, a set of charts showing the difference between device power classes (80% power minus 100% power) have been added. A positive value on the difference charts corresponds with an increase in maximum laser power when the engine reduces the throttle.

Device Power Class, at 100% Engine Throttle

As an example, the 100% throttle, maximum laser power chart is shown in Fig. 31.

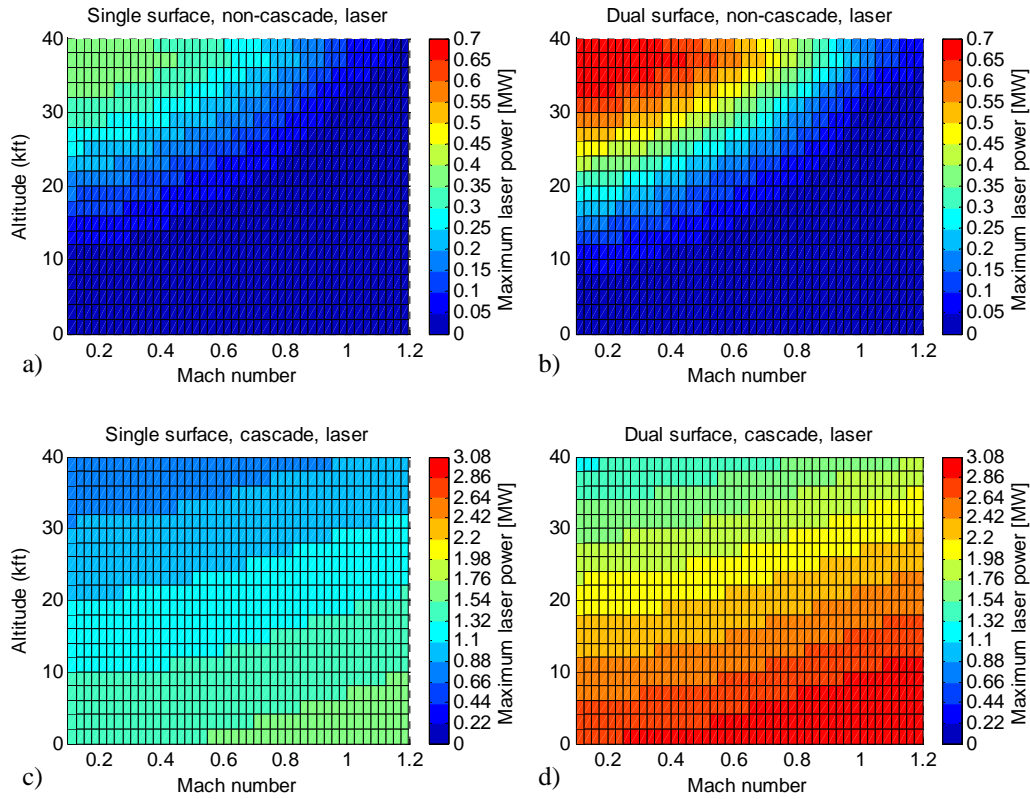


Fig. 31. Mach number vs. altitude plot of maximum supportable laser power [MW] at 100% engine throttle

The overall result for a laser device being cooled by a single heat pump is shown in Fig. 31 (a and b). Because the temperature difference between the bypass air and the coolant ($T_{2p} = 793$ R, Fig. 2) is greater at high altitudes and low Mach numbers (low bypass air inlet temperature), the higher powered lasers can be supported in this flight regime.

Because the cascaded system's heat exchanger coolant temperature ($T_{2p} = 1,125$ R, Fig. 17) is over 300 R higher than the single heat pump T_{2p} , the temperature difference does not dominate the supportable laser power with the cascaded heat pumps, shown in Fig. 31, c and d. As the engine increases altitude and decreases Mach number, the heat transfer coefficient of the bypass air decreases because of a decreasing bypass air density, velocity, and thermal conductivity, as shown in Eq. 8.

The set of 100% engine throttle Mach number versus altitude figures for the maximum power and cooling capacity of the laser and microwave devices are shown in Fig. 48 – Fig. 51, within Appendix D. The 80% throttle counterpart solutions are found in Fig. 52 – Fig. 55, within Appendix D. Finally, the difference between the 80% and 100% throttle settings of the device power and cooling capacity are shown in Fig. 56 – Fig. 59, within Appendix D.

The microwave device cooled by a single heat pump (Fig. 49, a and b) maintains a coolant temperature (T_{2p}) of 974 R. This T_{2p} does not allow either the temperature difference across the bypass heat exchanger or the coefficient of heat transfer of the bypass air to dominate the supportable power class, up to an altitude of approximately 32,000 feet or a Mach number less than 0.6. This altitude and Mach region supports a relatively constant supportable power class (± 50 kW).

A microwave device (Fig. 49, c and d) and laser device (Fig. 48, c and d) cooled by cascaded heat pumps respond to altitude and Mach number in a similar fashion in that the bypass air coefficient of heat transfer dominates the supportable device power class. Because the microwave T_1 and T_{2p} are higher than the laser device, the overall supportable microwave device power class is approximately 45% higher than the laser, with the cascaded heat pumps.

For all devices analyzed at an engine throttle setting of 100% (Fig. 48 – Fig. 51), the effect of increasing the heat exchanger surface area from a single to both sides of an annulus increased the cooling capacity by $88.58\% \pm 6.26\%$. The increase was found by comparing the single and dual sided heat exchanger at every Mach number and altitude point for each heat pump configuration.

Device Power Class, at 80% Engine Throttle

The effects of the reduction in engine throttle from 100% to 80% increased the maximum laser and microwave device power and laser operating region for the single heat pumps (Fig. 56 – Fig. 59, a and b). The maximum laser power remains in the high altitude, low Mach number region, and the maximum microwave power remains in the low altitude, low Mach number region. The constant microwave power region at 80% throttle (Fig. 53, a and b) is smaller than the 100% (Fig. 49, a and b) with a more gradual reduction in power level with increasing Mach number and altitude.

The maximum power with the single heat pump systems (Fig. 56 – Fig. 59, c and d) are more sensitive to the throttle setting than the cascaded heat pump systems (Fig. 56 – Fig. 59, a and b), because the reduction in throttle setting will reduce the fan compression ratio, reducing the bypass inlet temperature. For the cases of a single heat pump systems cooling a laser device (Fig. 56 and Fig. 58, a and b), the maximum device power will increase the most where T_{2p} and the bypass air temperature are equal.

The response to the throttle setting with the cascaded heat pumps (Fig. 56 – Fig. 59, c and d) are dominated by the heat exchanger temperature gradient and the coefficient of heat transfer of the air in opposite regions. The temperature gradient becomes more dominant in the high Mach number, low altitude regions, and causes the increase in maximum device power. The coefficient of heat transfer of the bypass air becomes more dominant in the low Mach number and high altitude regions, and causes the decrease in maximum device power.

The relative magnitude of the change in power class in the cascaded systems is far less than that of the single heat pump systems. For example, in Fig. 56, the maximum increase in power level in subplot b is 0.21 MW and in subplot d is 0.11. The increase in

subplot b was approximately 30%, whereas the increase in subplot d was approximately 4%.

V. Conclusions and Recommendations

Conclusions

This research explored the capabilities and effects of a thermal management system on a mixed bypass turbofan. Thermal energy was modeled from a storage device and through single and cascaded water-based, heat pumps. The energy was transferred into the bypass air through a single and dual surface heat exchanger.

A megawatt class high-energy laser can be cooled by a cascaded heat exchanger, within operationally relevant timeframes. Within the defined constraints, a single heat pump cannot generate the required increase in coolant temperature and pressure to be a feasible option. A megawatt class microwave emitter can be cooled by any of the thermal managements systems modeled. The dual surface bypass heat exchanger approximately doubles the heat transfer rate of the single surface heat exchanger. When choosing a specific thermal management system, the flight envelope has a significant impact on the optimum configuration.

It has been shown effects of the high-energy device and the thermal management system, including the power requirements of the heat pump compressors, have a minimal impact on the engine uninstalled thrust and uninstalled thrust specific fuel consumption.

A reduction from 100% to 80% (idle) engine throttle improved the laser and microwave device cooling performance of the single heat pumps systems. Cascaded heat pump cooling improved in the low altitude, high Mach number region and decreased in the high altitude, low Mach number region.

Additional engineering will need to be performed when designing an airframe for the thermal management system. Some examples may include a larger engine housing capable of supporting a larger and heavier engine, a larger fuselage to support the volumetric and weight requirements of a new thermal management system, and an overall higher weight and drag force caused by a potentially heavier airframe and larger fuselage. These design requirements are very real considerations that must be accounted for, but are outside the scope of this report.

Recommendations

A thermal management option was examined late within this project to exploit the full phase change properties of water and eject the spent vapor directly into the engine exhaust. A cooling temperature could be set with a precise vacuum pressure on stored water and a single or set of vacuum pumps could be used to draw the water through a thermal storage device, or potentially the high-energy device itself. The vaporized water could then be ejected into the engine exhaust, alleviating any need for a heat exchanger, high temperature and pressure compressor, and expansion valve. In this case, the lower the desired coolant temperature, the greater is the heat of vaporization of water and the less water is required to cool a given device. A preliminary analysis showed a pressure of 0.3632 psi would limit a device coolant temperature to 70 °F and the heat of vaporization to 1,053.9 BTU/lbm. A 1 MW laser with a 10% efficiency and 20 second lase time would produce 17,060 BTU. The mass of water required to absorb the given power is 16.19 lbm. The volume required to contain this amount of water is 0.260 ft³ or a 7.7in x 7.7in x 7.7in cube. With this little amount of mass used for each laser firing, many high-energy device firings could be cooled in a single mission. The benefits of this type of cooling scheme is a recovery time only limited by the flow rate of the water vapor. Additionally, the weight of the thermal management system is far less than a closed heat pump system. Finally, water provides good operational utility as it is readily accessible to support units, inexpensive to purify, and has negligible environmental impact.

The pipe geometry of the bypass heat exchanger was chosen to minimize the pressure losses due to skin friction and blockage of the airflow. The design weight could

be reduced by channeling the flow into traditional pipes running parallel to the airflow, within the heat exchanger airstream. The new configuration will also increase the surface area and the heat transfer rate. As the airflow will act as a boundary between the edges of the bypass section and the hot pipe, insulation material will not be needed. Due to the small distance between the inner and outer surfaces of the bypass section (may be 3 – 5 in) smaller pipes are desirable. However as the pipe diameter decreases, the pressure losses across the condenser will increase. The analysis of the trade-space between pipe diameter, flow velocity, and pipe configuration is useful for further optimization.

Water provides a good refrigerant medium at high temperatures. When examining cascaded heat pump systems for the colder first stage, a different coolant type, operating at a higher range on its vapor dome, could significantly increase the total system efficiency and high-energy device supported.

The heat pump compressor efficiency was identified as the most critical component to affect the maximum power class. An investigation of the maximum achievable compressor efficiency is useful. Additionally, the method of providing work to the heat pump compressor should be analyzed. In this report, the inefficiencies in converting the electrical energy generated at the low-pressure turbine back to mechanical energy at the heat pump compressor, and finally transferring the mechanical work into the coolant were not closely examined. It was suggested that a heat pump compressor could be used that has a turbine and two compressor stages on a single axel. There may be a benefit in using bleed air from the engine compressor to power a turbine at the heat pump compressor. Lastly, an assessment of the design choice between a piston compressor or an axial compressor at the heat pump should be performed.

Appendices

Appendix A: General Results for Thermal Management Cycles

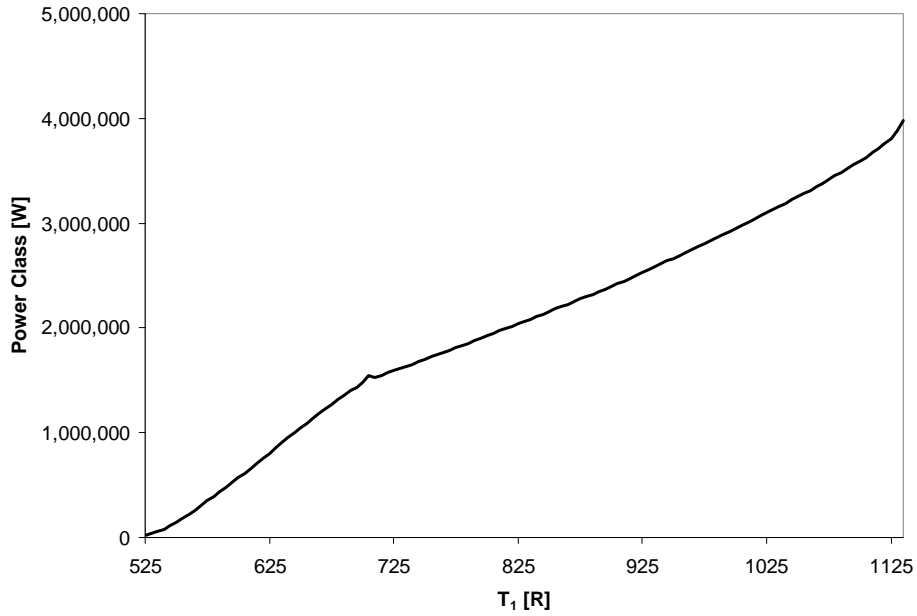


Fig. 32. Achievable device power class for a single surface bypass heat exchanger, single heat pump, at reference flight conditions

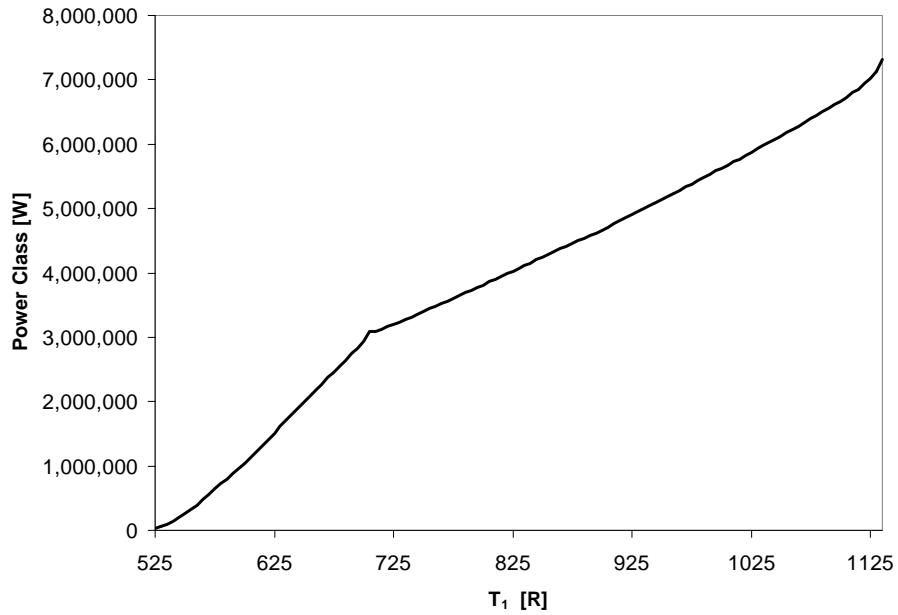


Fig. 33. Achievable device power class for a dual surface bypass heat exchanger, single heat pump, at reference flight conditions

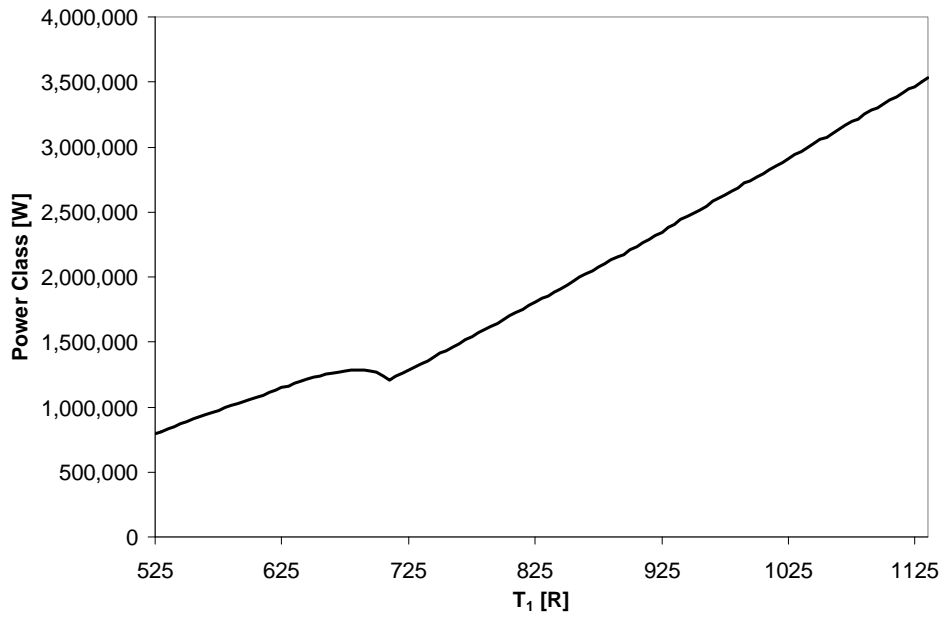


Fig. 34. Achievable device power class for a single surface bypass heat exchanger, cascaded heat pumps, under reference conditions

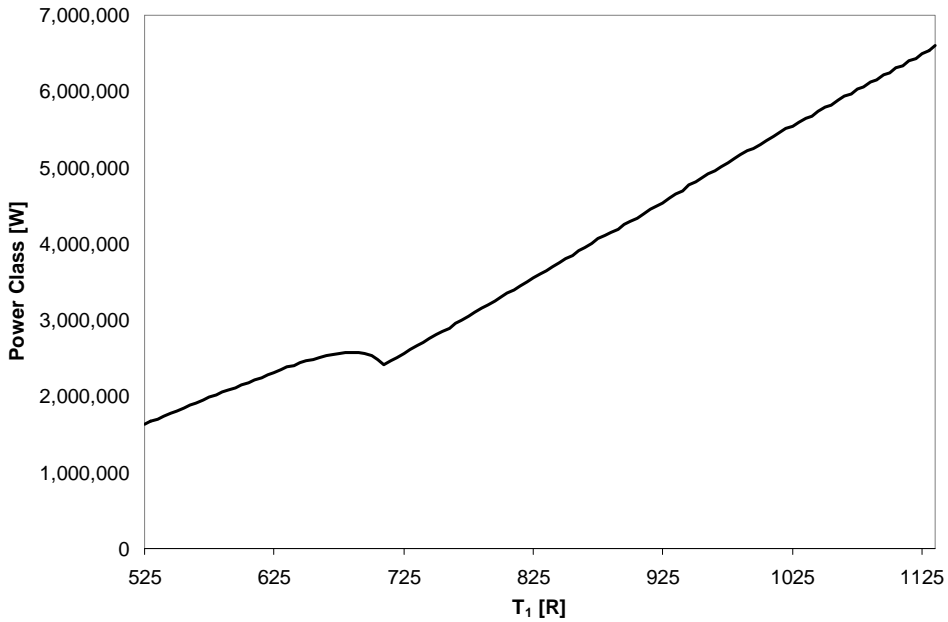


Fig. 35. Achievable device power class at given evaporator temperature for a dual surface bypass heat exchanger, cascaded heat pumps, under reference conditions

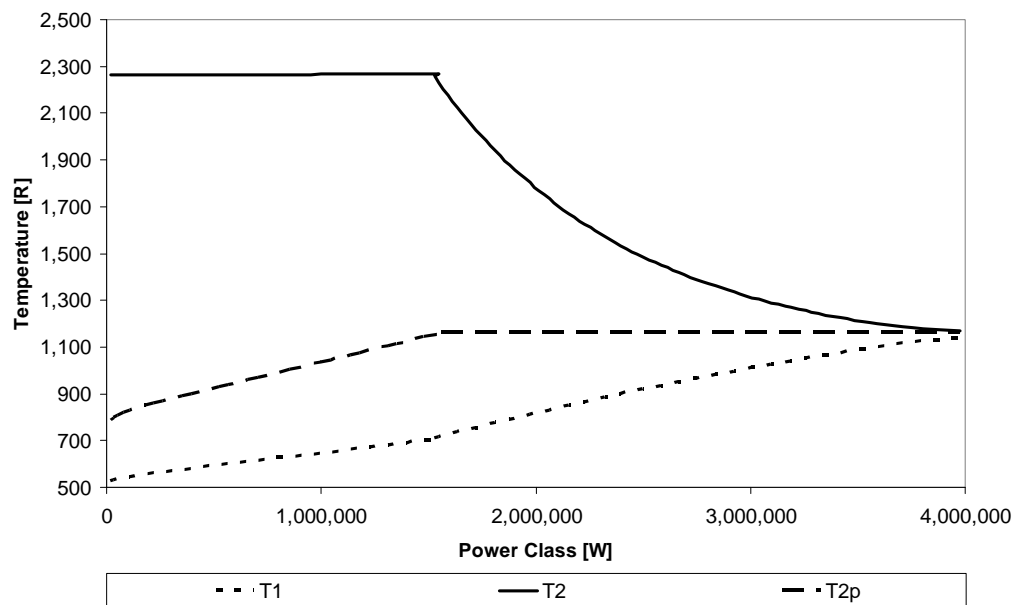


Fig. 36. Temperature profile at given power class for a single surface bypass heat exchanger, single heat pump, under reference conditions

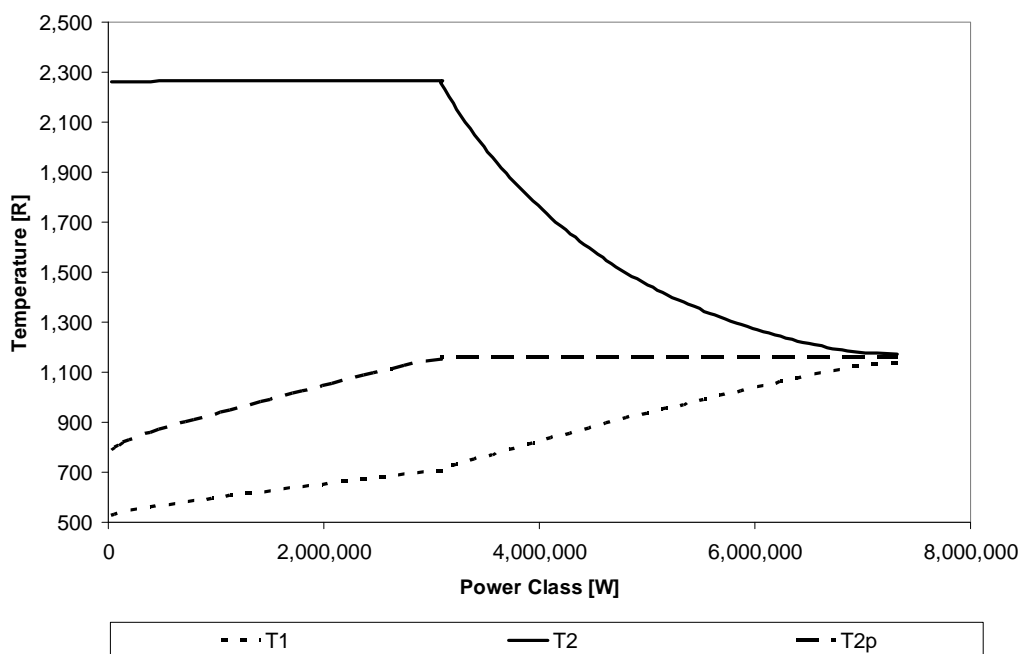


Fig. 37. Temperature profile at given power class for a dual surface bypass heat exchanger, single heat pump, under reference conditions

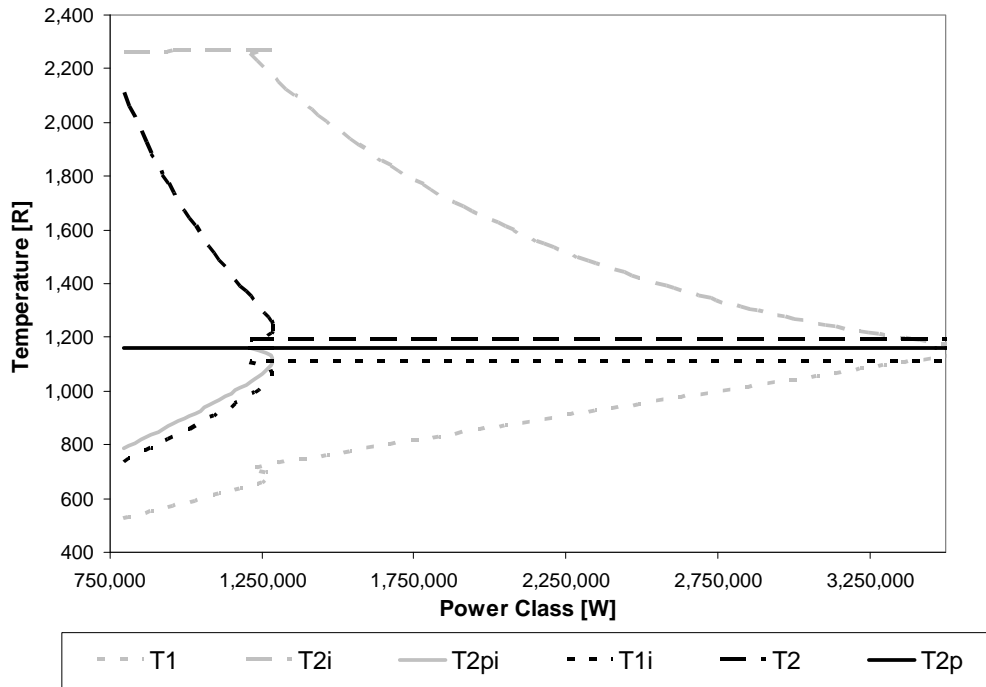


Fig. 38. Temperature profile at given power class for a single surface bypass heat exchanger, cascaded heat pumps, under reference conditions

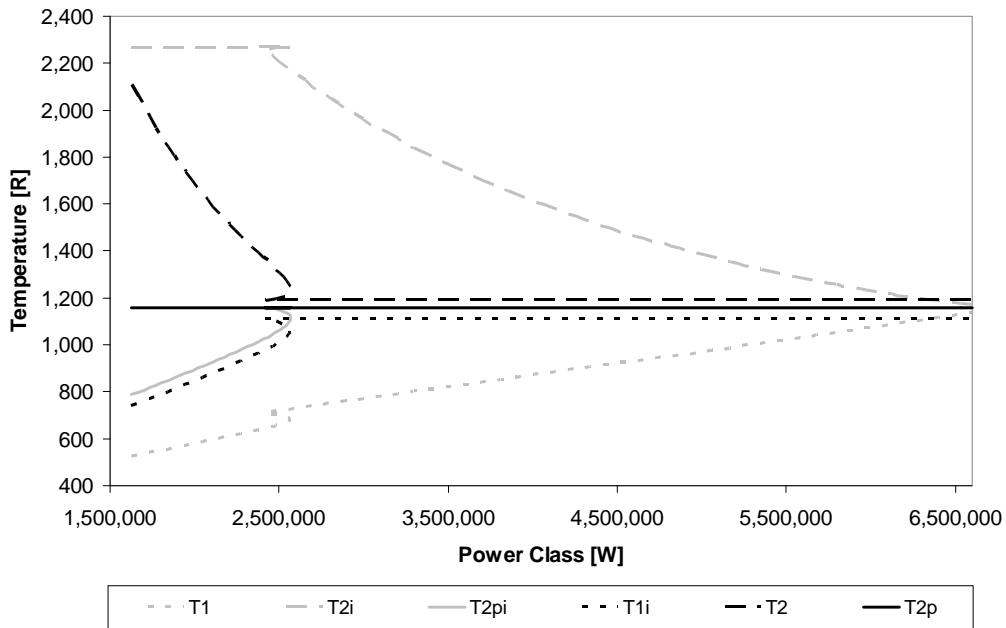


Fig. 39. Temperature profile at given power class for a dual surface bypass heat exchanger, cascaded heat pumps, under reference conditions

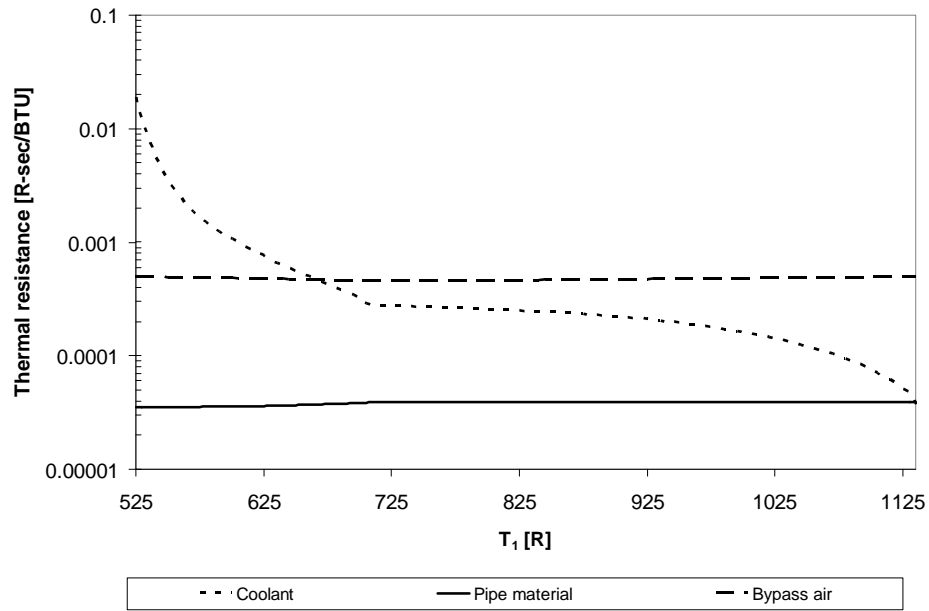


Fig. 40. Thermal resistance at the condenser mean phase change point for the single heat pump with a single surface heat exchanger

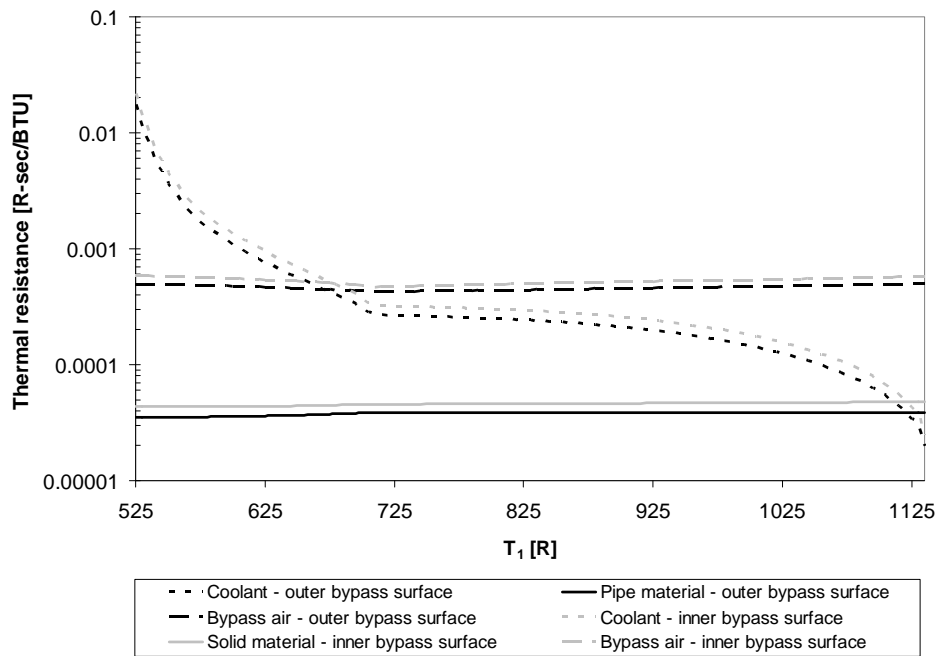


Fig. 41. Thermal resistance at the condenser mean phase change point for the single heat pump with a dual surface heat exchanger

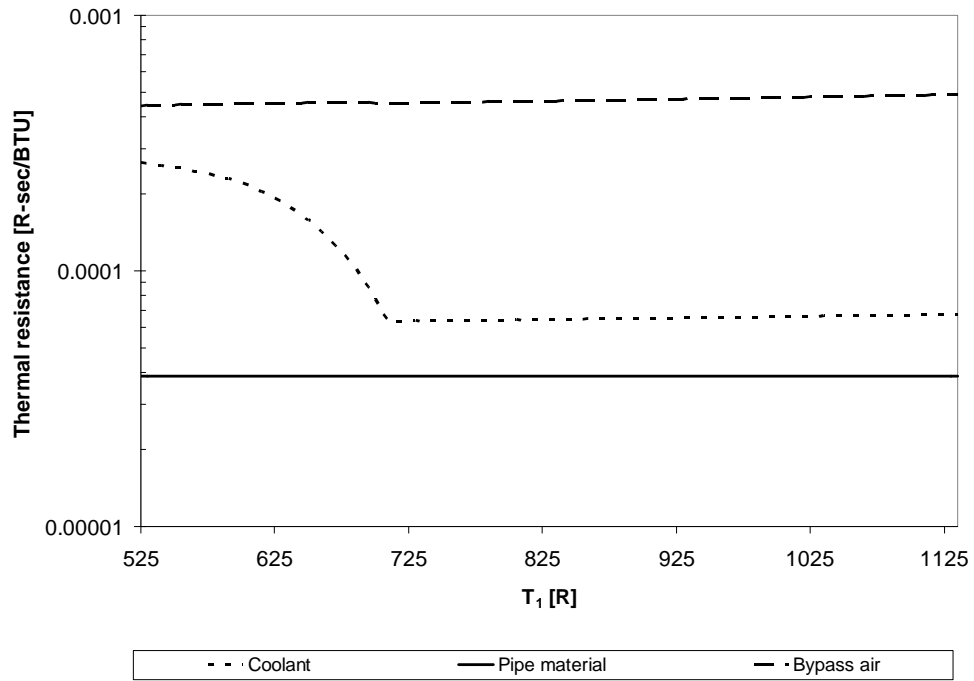


Fig. 42. Thermal resistance at the condenser mean phase change point for the cascaded heat pumps with a single surface heat exchanger

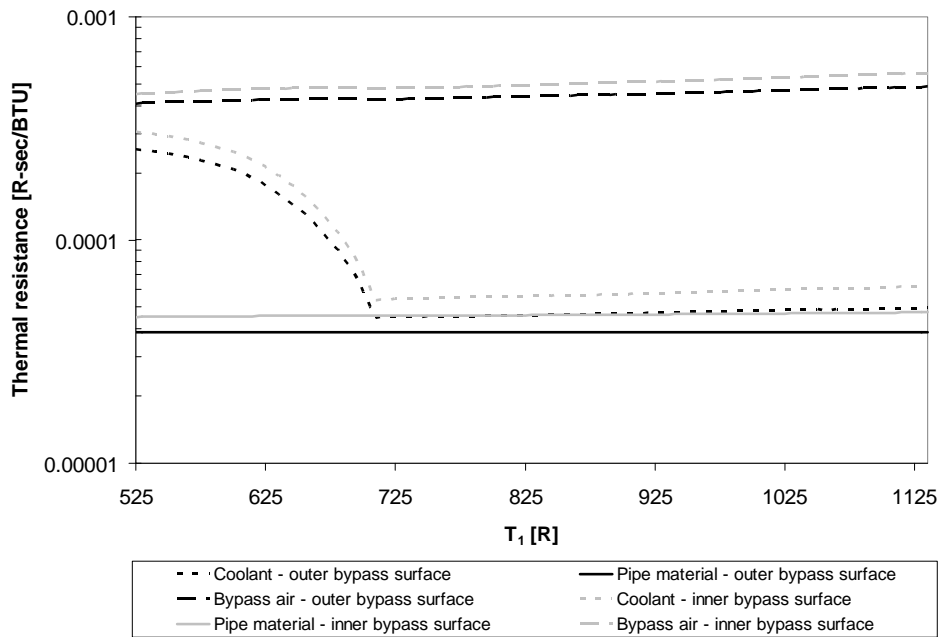


Fig. 43. Thermal resistance at the condenser mean phase change point for the cascaded heat pumps with a dual surface heat exchanger

Appendix B: Engine Effects from the Thermal Management Cycles

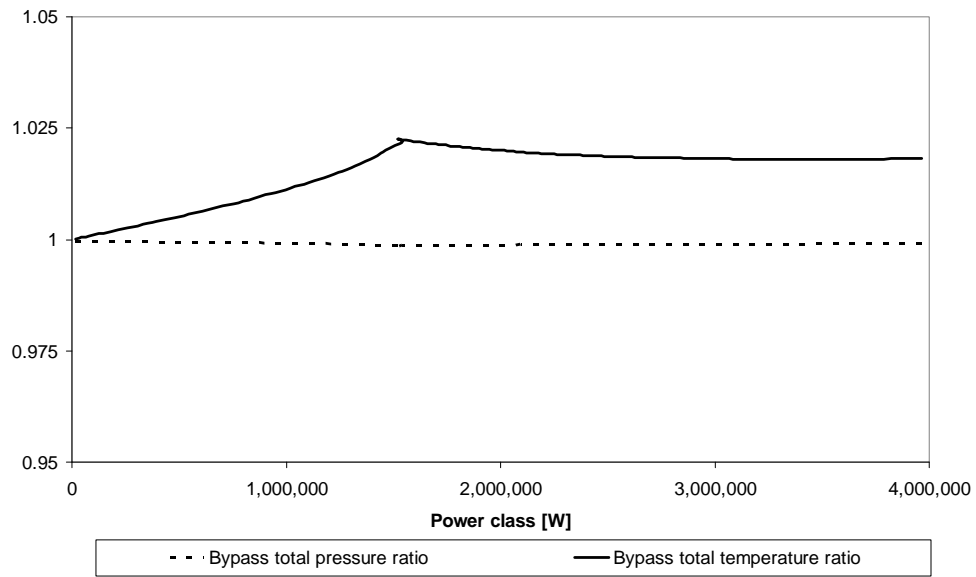


Fig. 44. Total temperature and total pressure ratios for the single heat pump, single surface heat exchanger

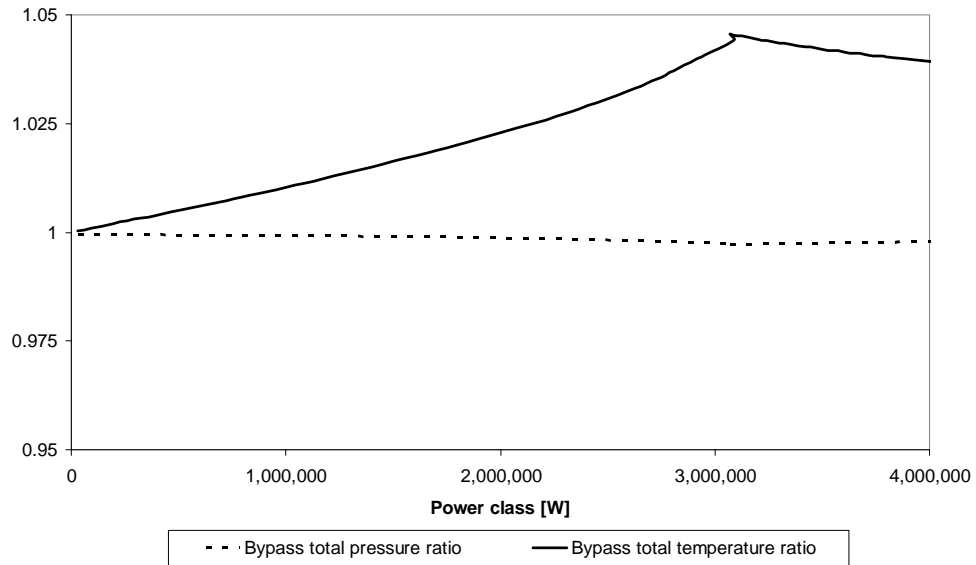


Fig. 45. Total temperature and total pressure ratios for the single heat pump, dual surface heat exchanger

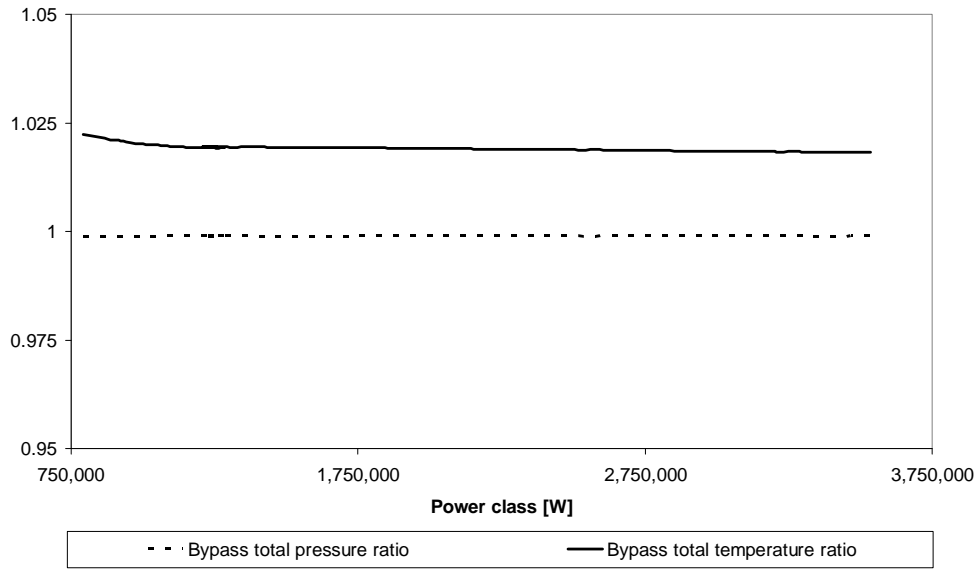


Fig. 46. Total temperature and total pressure ratios for the cascade, single surface heat pump

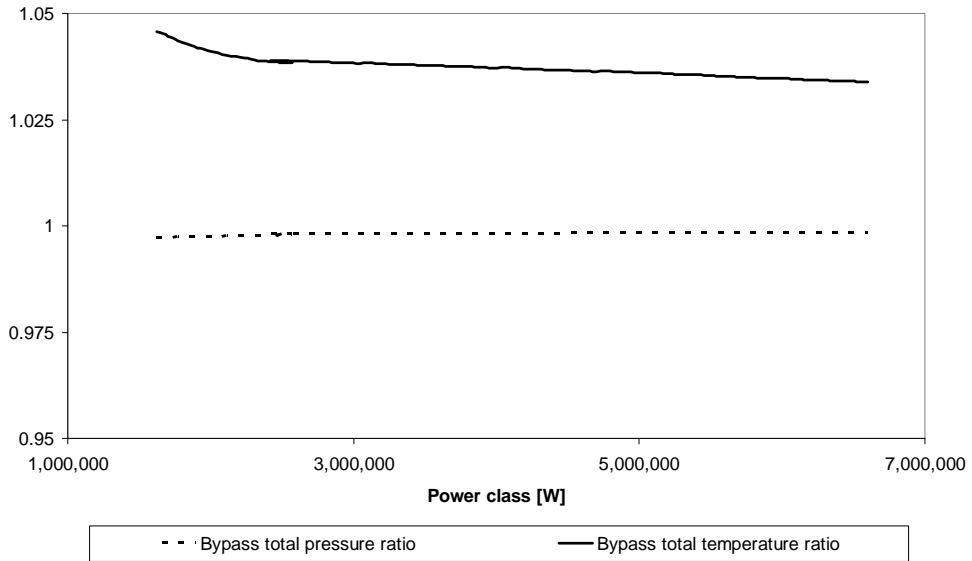


Fig. 47. Total temperature and total pressure ratios for the cascade, dual surface heat pump

Appendix C: Sensitivity Analysis Results

Table 9. Sensitivity analysis for a single heat pump, single surface heat exchanger cooling a laser device

Variable	Δ variable	Δ variable / variable _{init}	T ₁ [R]	LaserPower [W]	F _{noAB} [lbf]	F [lbf]	S _{noAB} [1/hr]	S [1/hr]	WorkComp [W]	QdotCond [BTU/s]
Compressor efficiency	0.020	0.025	527.5	4.28E+05	1.00E+02	2.92E+02	5.68E+00	5.16E+00	-3.59E-04	2.78E+01
Coolant pipe diameter	-0.00417	-0.200	527.5	-2.22E+05	-1.25E+01	-3.65E+01	-3.07E+00	-2.85E+00	1.94E-04	-1.52E+01
Coolant pipe conductivity	-0.80	-0.051	527.5	-2.08E+05	-4.94E+01	-1.44E+02	-2.91E+00	-2.75E+00	1.84E-04	-1.45E+01
Pipe yield strength	-300	-0.032	527.5	-3.27E+05	-7.75E+01	-2.26E+02	-4.57E+00	-4.31E+00	2.89E-04	-2.27E+01
Outer radius of bypass section	0.050	0.032	527.5	3.59E+05	7.75E+01	2.26E+02	1.11E+01	1.39E+01	-7.04E-04	2.49E+01
Length of bypass section	0.33	0.055	527.5	3.19E+05	4.55E+01	1.33E+02	-5.37E-01	-3.34E+00	3.40E-05	2.20E+01
Friction factor of surface in contact with bypass air	0.0090	9.000	527.5	1.17E+03	2.78E-01	8.11E-01	-5.51E+00	-8.31E+00	3.50E-04	8.15E-02
Mass flow rate of the inlet	20.0	0.080	527.5	1.32E+05	3.13E+01	9.12E+01	1.76E+04	2.87E+04	-3.45E-03	9.16E+00
Aircraft systems power requirement excluding the heat pump compressor	50.0	0.167	527.5	6.50E+04	1.50E+01	4.38E+01	5.86E+01	1.32E+02	-3.71E-03	4.52E+00
Engine bypass ratio (α)	0.050	0.125	527.5	1.00E+05	2.00E+01	5.84E+01	-2.43E+03	-2.38E+02	-1.54E-01	6.93E+00
Engine core compression ratio (π_c)	-4.00	-0.111	527.5	-1.07E+05	-2.25E+01	-6.57E+01	-2.44E+03	-6.22E+02	-7.17E-02	-7.42E+00
Engine bypass compression ratio (π_b)	-0.250	-0.071	527.5	-2.55E+05	-3.50E+01	-1.02E+02	1.45E+04	2.19E+04	-9.79E-01	-1.76E+01

Table 10. Sensitivity analysis for a single heat pump, single surface heat exchanger cooling a microwave device

Variable	Δ variable	Δ variable / variable _{init}	T ₁ [R]	MicrowavePower [W]	F _{noAB} [lbf]	F [lbf]	S _{noAB} [1/hr]	S [1/hr]	WorkComp [W]	QdotCond [BTU/s]
Compressor efficiency	0.02	0.025	617.4	2.82E+07	3.50E+03	7.04E+03	4.01E+02	3.82E+02	-2.54E-02	2.24E+03
Coolant pipe diameter	-0.00417	-0.200	617.4	-4.26E+06	-4.37E+02	-8.80E+02	-6.03E+01	-5.74E+01	3.81E-03	-3.46E+02
Coolant pipe conductivity	-0.80	-0.051	617.4	-1.38E+07	-1.73E+03	-3.47E+03	-2.00E+02	-1.92E+02	1.26E-02	-1.12E+03
Pipe yield strength	-300	-0.032	617.4	-2.18E+07	-2.71E+03	-5.45E+03	-3.15E+02	-3.03E+02	1.99E-02	-1.77E+03
Outer radius of bypass section	0.050	0.032	617.4	2.23E+07	2.71E+03	5.45E+03	3.28E+02	3.19E+02	-2.08E-02	1.82E+03
Length of bypass section	0.33	0.055	617.4	1.40E+07	1.59E+03	3.20E+03	1.96E+02	1.85E+02	-1.24E-02	1.14E+03
Friction factor of surface in contact with bypass air	0.009	9.000	617.4	7.80E+04	9.71E+00	1.95E+01	-4.37E+00	-7.20E+00	2.77E-04	6.36E+00
Mass flow rate of the inlet	20.0	0.080	617.4	8.73E+06	1.09E+03	2.20E+03	1.77E+04	2.89E+04	-1.08E-02	7.11E+02
Aircraft systems power requirement excluding the heat pump compressor	50.0	0.167	617.4	4.32E+06	5.24E+02	1.06E+03	1.07E+02	1.71E+02	-6.75E-03	3.52E+02
Engine bypass ratio (α)	0.050	0.125	617.4	6.67E+06	6.99E+02	1.41E+03	-2.43E+03	-2.84E+02	-1.55E-01	5.43E+02
Engine core compression ratio (π_c)	-4.00	-0.111	617.4	-7.09E+06	-7.87E+02	-1.58E+03	-2.46E+03	-6.00E+02	-7.04E-02	-5.77E+02
Engine bypass compression ratio (π_b)	-0.250	-0.071	617.4	-8.67E+06	-1.22E+03	-2.46E+03	1.12E+04	1.70E+04	-7.46E-01	-7.07E+02

Table 11. Sensitivity analysis for a single heat pump, dual surface heat exchanger cooling a laser device

Variable	Δ variable	Δ variable / variable _{init}	T ₁ [R]	LaserPower [W]	F _{noAB} [lbf]	F [lbf]	S _{noAB} [1/hr]	S [1/hr]	WorkComp [W]	QdotCond [BTU/s]
Compressor efficiency	0.02	0.025	527.5	-1.10E+06	-5.00E+02	-9.12E+02	-1.61E+01	-1.54E+01	1.02E-03	-8.15E+01
Coolant pipe diameter	-0.00417	-0.200	527.5	-1.66E+05	6.25E+01	1.14E+02	-2.20E+00	-2.00E+00	1.39E-04	-1.10E+01
Coolant pipe conductivity	-0.80	-0.051	527.5	5.50E+05	2.47E+02	4.50E+02	7.77E+00	7.27E+00	-4.91E-04	3.89E+01
Pipe yield strength	-300	-0.032	527.5	8.64E+05	3.88E+02	7.07E+02	1.22E+01	1.14E+01	-7.71E-04	6.10E+01
Outer radius of bypass section	0.050	0.032	527.5	-7.99E+05	-3.88E+02	-7.07E+02	-5.18E+00	-1.37E+00	3.28E-04	-5.66E+01
Length of bypass section	0.33	0.055	527.5	-2.78E+05	-2.28E+02	-4.15E+02	-8.98E+00	-1.13E+01	5.68E-04	-2.02E+01
Friction factor of surface in contact with bypass air	0.009	9.000	527.5	-3.10E+03	-1.39E+00	-2.53E+00	-5.57E+00	-8.37E+00	3.53E-04	-2.19E-01
Mass flow rate of the inlet	20.0	0.080	527.5	-3.55E+05	-1.56E+02	-2.85E+02	1.76E+04	2.87E+04	-3.00E-03	-2.50E+01
Aircraft systems power requirement excluding the heat pump compressor	50.0	0.167	527.5	-1.63E+05	-7.50E+01	-1.37E+02	5.50E+01	1.29E+02	-3.48E-03	-1.15E+01
Engine bypass ratio (α)	0.050	0.125	527.5	-1.89E+05	-1.00E+02	-1.82E+02	-2.44E+03	-2.46E+02	-1.54E-01	-1.34E+01
Engine core compression ratio (π_c)	-4.00	-0.111	527.5	2.22E+05	1.13E+02	2.05E+02	-2.43E+03	-6.15E+02	-7.22E-02	1.58E+01
Engine bypass compression ratio (π_t)	-0.250	-0.071	527.5	4.15E+05	1.75E+02	3.19E+02	1.44E+04	2.18E+04	-9.73E-01	2.92E+01

Table 12. Sensitivity analysis for a single heat pump, dual surface heat exchanger cooling a microwave device

Variable	Δ variable	Δ variable / variable _{init}	T ₁ [R]	MicrowavePower [W]	F _{noAB} [lbf]	F [lbf]	S _{noAB} [1/hr]	S [1/hr]	WorkComp [W]	QdotCond [BTU/s]
Compressor efficiency	0.02	0.025	617.4	5.08E+07	2.90E+03	5.83E+03	6.61E+02	5.96E+02	-4.18E-02	4.05E+03
Coolant pipe diameter	-0.00417	-0.200	617.4	-7.80E+06	-3.62E+02	-7.29E+02	-9.91E+01	-8.80E+01	6.26E-03	-6.36E+02
Coolant pipe conductivity	-0.80	-0.051	617.4	-2.48E+07	-1.43E+03	-2.88E+03	-3.29E+02	-3.00E+02	2.08E-02	-2.03E+03
Pipe yield strength	-300	-0.032	617.4	-3.92E+07	-2.24E+03	-4.52E+03	-5.18E+02	-4.73E+02	3.28E-02	-3.21E+03
Outer radius of bypass section	0.050	0.032	617.4	4.05E+07	2.24E+03	4.52E+03	5.38E+02	4.93E+02	-3.40E-02	3.31E+03
Length of bypass section	0.33	0.055	617.4	2.55E+07	1.32E+03	2.65E+03	3.26E+02	2.91E+02	-2.06E-02	2.08E+03
Friction factor of surface in contact with bypass air	0.009	9.000	617.4	1.40E+05	8.04E+00	1.62E+01	-3.63E+00	-6.57E+00	2.30E-04	1.15E+01
Mass flow rate of the inlet	20.0	0.080	617.4	1.55E+07	9.05E+02	1.82E+03	1.78E+04	2.89E+04	-1.56E-02	1.27E+03
Aircraft systems power requirement excluding the heat pump compressor	50.0	0.167	617.4	7.84E+06	4.34E+02	8.75E+02	1.37E+02	1.90E+02	-8.67E-03	6.41E+02
Engine bypass ratio (α)	0.050	0.125	617.4	1.22E+07	5.79E+02	1.17E+03	-2.44E+03	-3.40E+02	-1.54E-01	9.97E+02
Engine core compression ratio (π_c)	-4.00	-0.111	617.4	-1.30E+07	-6.52E+02	-1.31E+03	-2.46E+03	-5.62E+02	-7.01E-02	-1.06E+03
Engine bypass compression ratio (π_t)	-0.250	-0.071	617.4	-1.60E+07	-1.01E+03	-2.04E+03	9.20E+03	1.40E+04	-6.07E-01	-1.31E+03

Table 13. Sensitivity analysis for a cascaded, single surface heat pump cooling a laser device

Variable	Δ variable	Δ variable / variable _{init}	T ₁ [R]	LaserPower [W]	F _{noAB} [lbf]	F [lbf]	S _{noAB} [1/hr]	S [1/hr]	WorkComp [W]	QdotCond [BTU/s]
Compressor efficiency	0.02	0.025	527.5	2.56E+07	-1.10E+03	1.24E+04	9.21E+02	1.24E+03	-5.82E-02	6.97E+03
Coolant pipe diameter	-0.00417	-0.200	527.5	-3.45E+06	1.38E+02	-1.55E+03	-1.21E+02	-1.62E+02	7.62E-03	-9.67E+02
Coolant pipe conductivity	-0.80	-0.051	527.5	-1.22E+07	5.43E+02	-6.14E+03	-4.55E+02	-6.15E+02	2.88E-02	-3.49E+03
Pipe yield strength	-300	-0.032	527.5	-1.93E+07	8.53E+02	-9.63E+03	-7.17E+02	-9.68E+02	4.53E-02	-5.50E+03
Outer radius of bypass section	0.050	0.032	527.5	1.99E+07	-8.52E+02	9.63E+03	7.33E+02	9.88E+02	-4.63E-02	5.65E+03
Length of bypass section	0.33	0.055	527.5	1.24E+07	-5.01E+02	5.66E+03	4.32E+02	5.79E+02	-2.73E-02	3.48E+03
Friction factor of surface in contact with bypass air	0.009	9.000	527.5	6.92E+04	-3.06E+02	3.45E+01	-2.81E+00	-4.64E+00	1.78E-04	1.97E+01
Mass flow rate of the inlet	20.0	0.080	527.5	7.73E+06	-3.44E+02	3.88E+03	1.79E+04	2.91E+04	-2.09E-02	2.21E+03
Aircraft systems power requirement excluding the heat pump compressor	50.0	0.167	527.5	3.86E+06	-1.65E+02	1.86E+03	1.54E+02	2.54E+02	-9.70E-03	1.09E+03
Engine bypass ratio (α)	0.050	0.125	527.5	6.17E+06	-2.20E+02	2.49E+03	-2.54E+03	-4.36E+02	-1.48E-01	1.70E+03
Engine core compression ratio (π_c)	-4.00	-0.111	527.5	-6.44E+06	2.48E+02	-2.80E+03	-2.39E+03	-5.15E+02	-7.47E-02	-1.80E+03
Engine bypass compression ratio (π_b)	-0.250	-0.071	527.5	-7.30E+06	3.85E+02	-4.35E+03	6.72E+03	1.02E+04	-4.40E-01	-2.15E+03

Table 14. Sensitivity analysis for a cascaded, single surface heat pump cooling a microwave device

Variable	Δ variable	Δ variable / variable _{init}	T ₁ [R]	MicrowavePower [W]	F _{noAB} [lbf]	F [lbf]	S _{noAB} [1/hr]	S [1/hr]	WorkComp [W]	QdotCond [BTU/s]
Compressor efficiency	0.02	0.025	617.4	3.70E+07	2.30E+03	1.20E+04	8.28E+02	9.85E+02	-5.23E-02	3.33E+03
Coolant pipe diameter	-0.00417	-0.200	617.4	-4.80E+06	-2.87E+02	-1.50E+03	-1.08E+02	-1.28E+02	6.81E-03	-4.51E+02
Coolant pipe conductivity	-0.80	-0.051	617.4	-1.77E+07	-1.13E+03	-5.94E+03	-4.09E+02	-4.91E+02	2.58E-02	-1.67E+03
Pipe yield strength	-300	-0.032	617.4	-2.80E+07	-1.78E+03	-9.32E+03	-6.44E+02	-7.73E+02	4.07E-02	-2.64E+03
Outer radius of bypass section	0.050	0.032	617.4	2.88E+07	1.78E+03	9.32E+03	6.62E+02	7.93E+02	-4.18E-02	2.72E+03
Length of bypass section	0.33	0.055	617.4	1.78E+07	1.05E+03	5.48E+03	3.92E+02	4.64E+02	-2.47E-02	1.67E+03
Friction factor of surface in contact with bypass air	0.009	9.000	617.4	1.00E+05	6.38E+00	3.34E+01	-3.11E+00	-5.40E+00	1.97E-04	9.46E+00
Mass flow rate of the inlet	20.0	0.080	617.4	1.12E+07	7.18E+02	3.76E+03	1.78E+04	2.91E+04	-1.89E-02	1.06E+03
Aircraft systems power requirement excluding the heat pump compressor	50.0	0.167	617.4	5.58E+06	3.44E+02	1.80E+03	1.48E+02	2.28E+02	-9.33E-03	5.26E+02
Engine bypass ratio (α)	0.050	0.125	617.4	8.98E+06	4.59E+02	2.41E+03	-2.50E+03	-4.04E+02	-1.50E-01	8.40E+02
Engine core compression ratio (π_c)	-4.00	-0.111	617.4	-9.34E+06	-5.17E+02	-2.71E+03	-2.42E+03	-5.29E+02	-7.30E-02	-8.77E+02
Engine bypass compression ratio (π_b)	-0.250	-0.071	617.4	-1.16E+07	-8.04E+02	-4.21E+03	7.34E+03	1.12E+04	-4.81E-01	-1.10E+03

Table 15. Sensitivity analysis for a cascaded, dual surface heat pump cooling a laser device

Variable	Δ variable	Δ variable / variable _{init}	T _i [R]	LaserPower [W]	F _{noAB} [lbf]	F [lbf]	S _{noAB} [1/hr]	S [1/hr]	WorkComp [W]	QdotCond [BTU/s]
Compressor efficiency	0.02	0.025	527.5	5.50E+07	-1.70E+03	1.12E+04	1.03E+03	1.23E+03	-6.53E-02	1.44E+04
Coolant pipe diameter	-0.00417	-0.200	527.5	-7.35E+06	2.13E+02	-1.40E+03	-1.24E+02	-1.44E+02	7.86E-03	-1.99E+03
Coolant pipe conductivity	-0.80	-0.051	527.5	-2.63E+07	8.39E+02	-5.53E+03	-5.06E+02	-6.07E+02	3.19E-02	-7.22E+03
Pipe yield strength	-300	-0.032	527.5	-4.13E+07	1.32E+03	-8.67E+03	-7.94E+02	-9.52E+02	5.01E-02	-1.13E+04
Outer radius of bypass section	0.050	0.032	527.5	4.34E+07	-1.32E+03	8.67E+03	7.89E+02	9.33E+02	-4.99E-02	1.18E+04
Length of bypass section	0.33	0.055	527.5	2.67E+07	-7.74E+02	5.09E+03	4.48E+02	5.17E+02	-2.83E-02	7.25E+03
Friction factor of surface in contact with bypass air	0.009	9.000	527.5	1.48E+05	-4.72E+00	3.11E+01	-2.52E+00	-4.68E+00	1.60E-04	4.06E+01
Mass flow rate of the inlet	20.0	0.080	527.5	1.64E+07	-5.31E+02	3.50E+03	1.79E+04	2.92E+04	-2.41E-02	4.50E+03
Aircraft systems power requirement excluding the heat pump compressor	50.0	0.167	527.5	8.25E+06	-2.55E+02	1.68E+03	1.40E+02	2.06E+02	-8.82E-03	2.25E+03
Engine bypass ratio (α)	0.050	0.125	527.5	1.29E+07	-3.40E+02	2.24E+03	-2.73E+03	-7.66E+02	-1.36E-01	3.46E+03
Engine core compression ratio (π_c)	-4.00	-0.111	527.5	-1.35E+07	3.83E+02	-2.52E+03	-2.24E+03	-2.46E+02	-8.43E-02	-3.66E+03
Engine bypass compression ratio (π_b)	-0.250	-0.071	527.5	-1.68E+07	5.95E+02	-3.92E+03	4.39E+03	6.73E+03	-2.85E-01	-4.68E+03

Table 16. Sensitivity analysis for a cascaded, dual surface heat pump cooling a microwave device

Variable	Δ variable	Δ variable / variable _{init}	T _i [R]	MicrowavePower [W]	F _{noAB} [lbf]	F [lbf]	S _{noAB} [1/hr]	S [1/hr]	WorkComp [W]	QdotCond [BTU/s]
Compressor efficiency	0.02	0.025	617.4	7.81E+07	1.70E+03	1.08E+04	1.14E+03	1.15E+03	-7.17E-02	6.94E+03
Coolant pipe diameter	-0.00417	-0.200	617.4	-1.01E+07	-2.12E+02	-1.35E+03	-1.43E+02	-1.44E+02	9.02E-03	-9.33E+02
Coolant pipe conductivity	-0.80	-0.051	617.4	-3.74E+07	-8.37E+02	-5.32E+03	-5.57E+02	-5.74E+02	3.52E-02	-3.48E+03
Pipe yield strength	-300	-0.032	617.4	-5.91E+07	-1.31E+03	-8.35E+03	-8.76E+02	-9.00E+02	5.53E-02	-5.49E+03
Outer radius of bypass section	0.050	0.032	617.4	6.16E+07	1.31E+03	8.35E+03	8.89E+02	9.03E+02	-5.61E-02	5.72E+03
Length of bypass section	0.33	0.055	617.4	3.75E+07	7.72E+02	4.90E+03	5.18E+02	5.14E+02	-3.27E-02	3.47E+03
Friction factor of surface in contact with bypass air	0.009	9.000	617.4	2.12E+05	4.71E+00	2.99E+01	-2.27E+00	-4.92E+00	1.44E-04	1.97E+01
Mass flow rate of the inlet	20.0	0.080	617.4	2.33E+07	5.30E+02	3.37E+03	1.79E+04	2.91E+04	-2.51E-02	2.16E+03
Aircraft systems power requirement excluding the heat pump compressor	50.0	0.167	617.4	1.18E+07	2.54E+02	1.62E+03	1.68E+02	2.14E+02	-1.06E-02	1.09E+03
Engine bypass ratio (α)	0.050	0.125	617.4	1.86E+07	3.39E+02	2.15E+03	-2.61E+03	-6.49E+02	-1.43E-01	1.72E+03
Engine core compression ratio (π_c)	-4.00	-0.111	617.4	-1.95E+07	-3.82E+02	-2.42E+03	-2.33E+03	-3.34E+02	-7.82E-02	-1.81E+03
Engine bypass compression ratio (π_b)	-0.250	-0.071	617.4	-2.53E+07	-5.94E+02	-3.77E+03	4.99E+03	7.71E+03	-3.24E-01	-2.36E+03

Appendix D: High-Energy Device and Engine Operation Envelopes

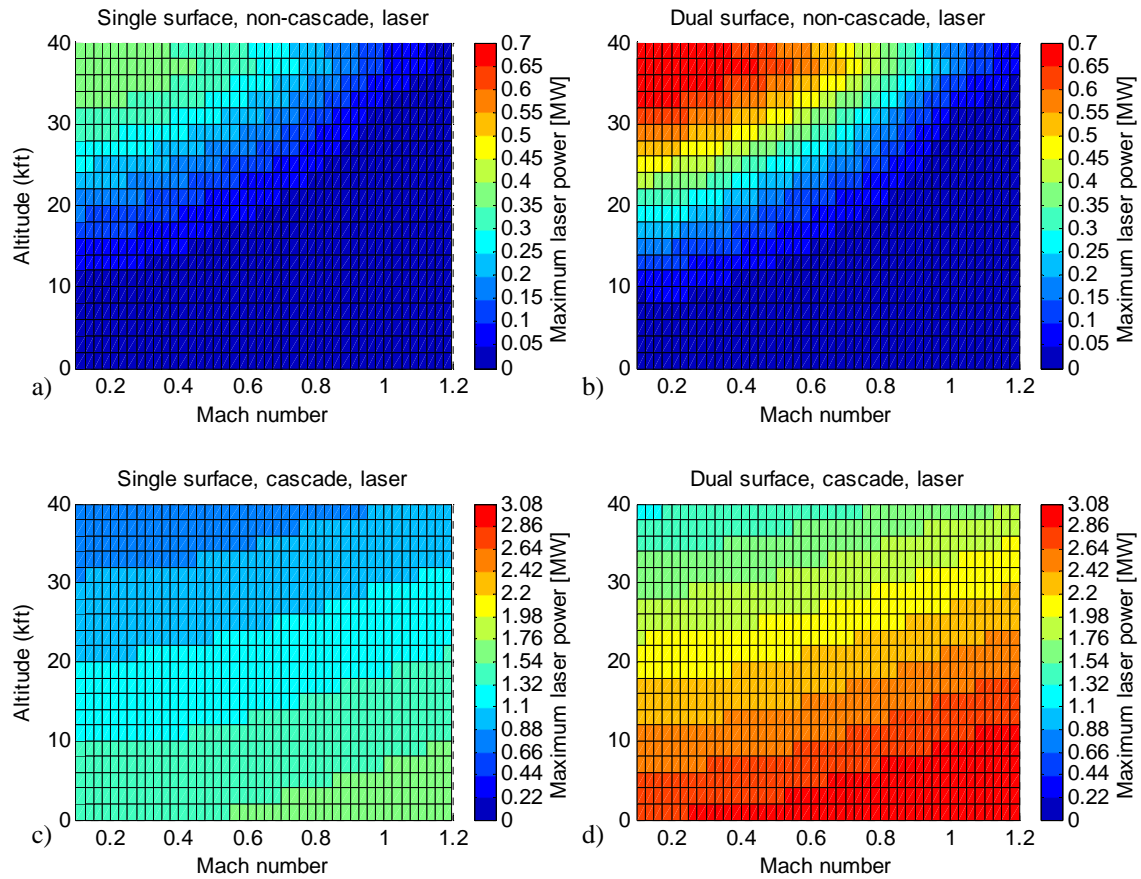


Fig. 48. Maximum laser power [MW] at 100% throttle

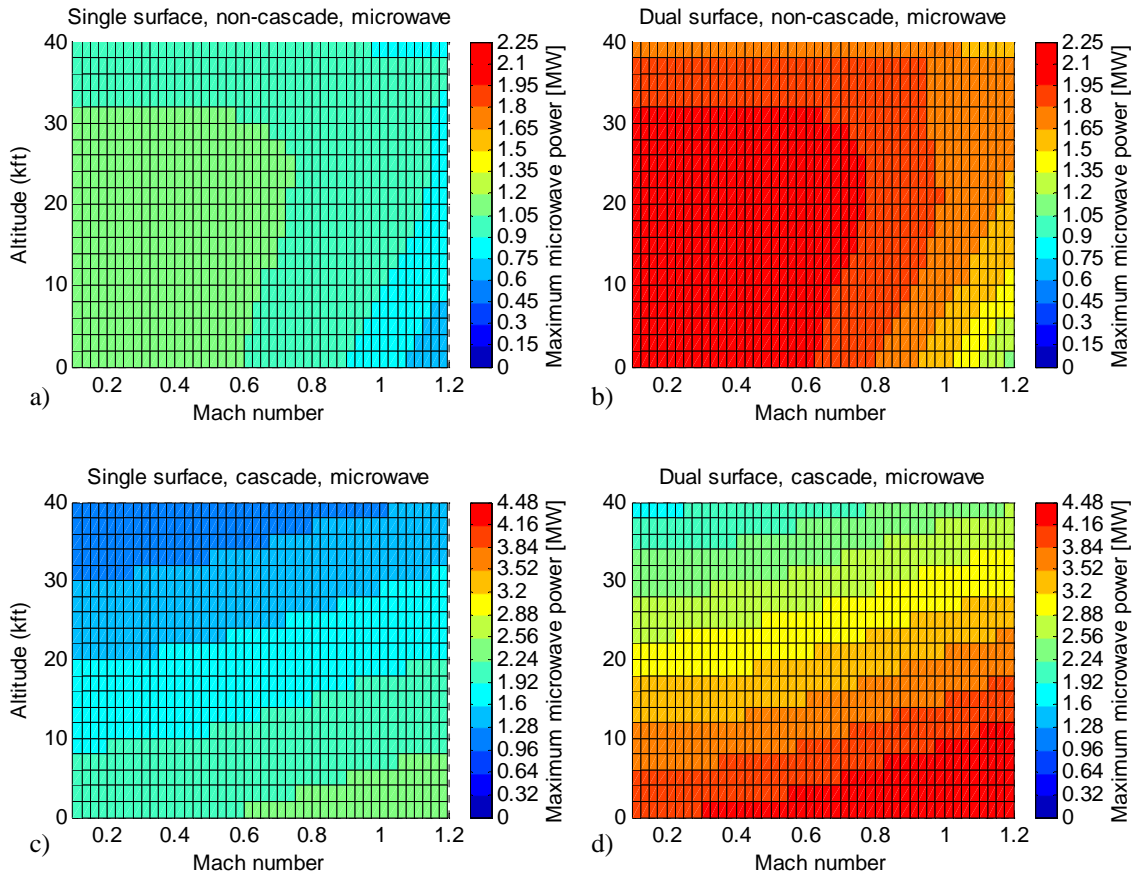


Fig. 49. Maximum microwave power [MW] at 100% throttle

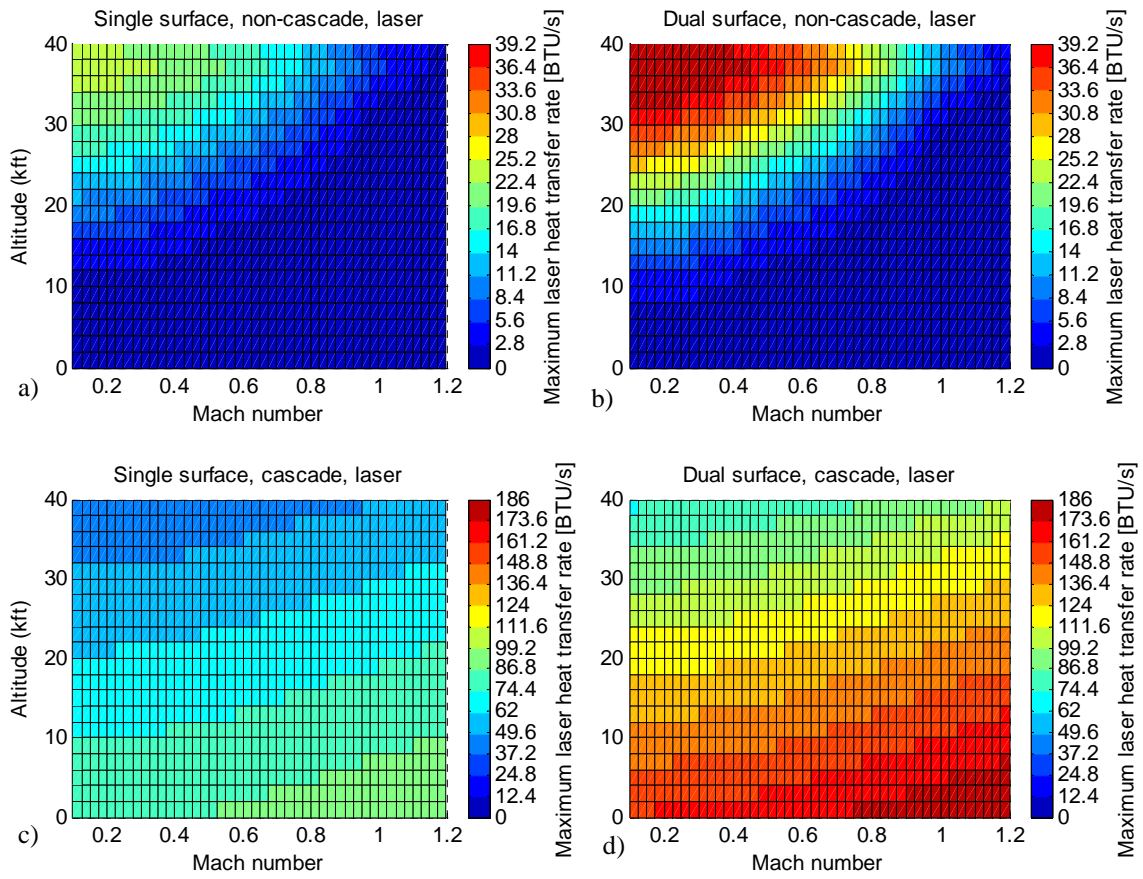


Fig. 50. Maximum laser device cooling capacity [BTU/s] at 100% throttle

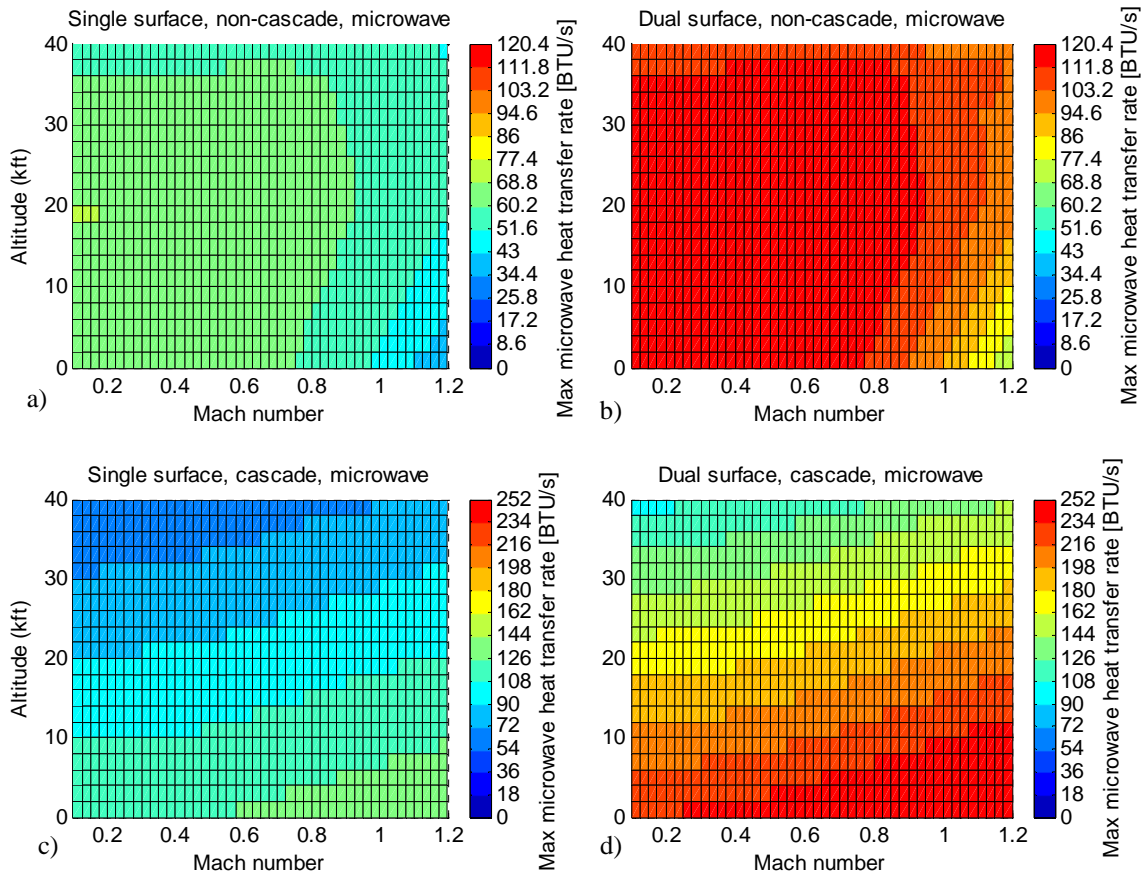


Fig. 51. Maximum microwave device cooling capacity [BTU/s] at 100% throttle

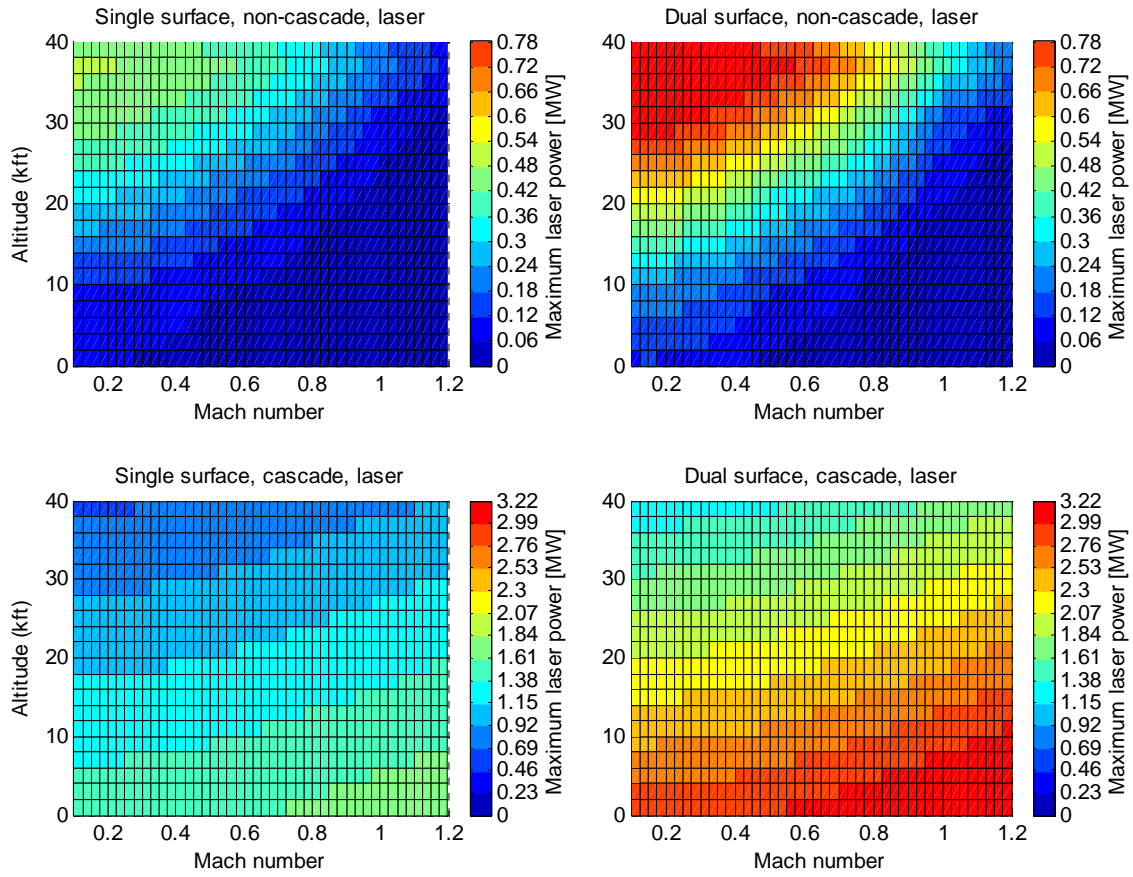


Fig. 52. Maximum laser power [MW] at 80% throttle

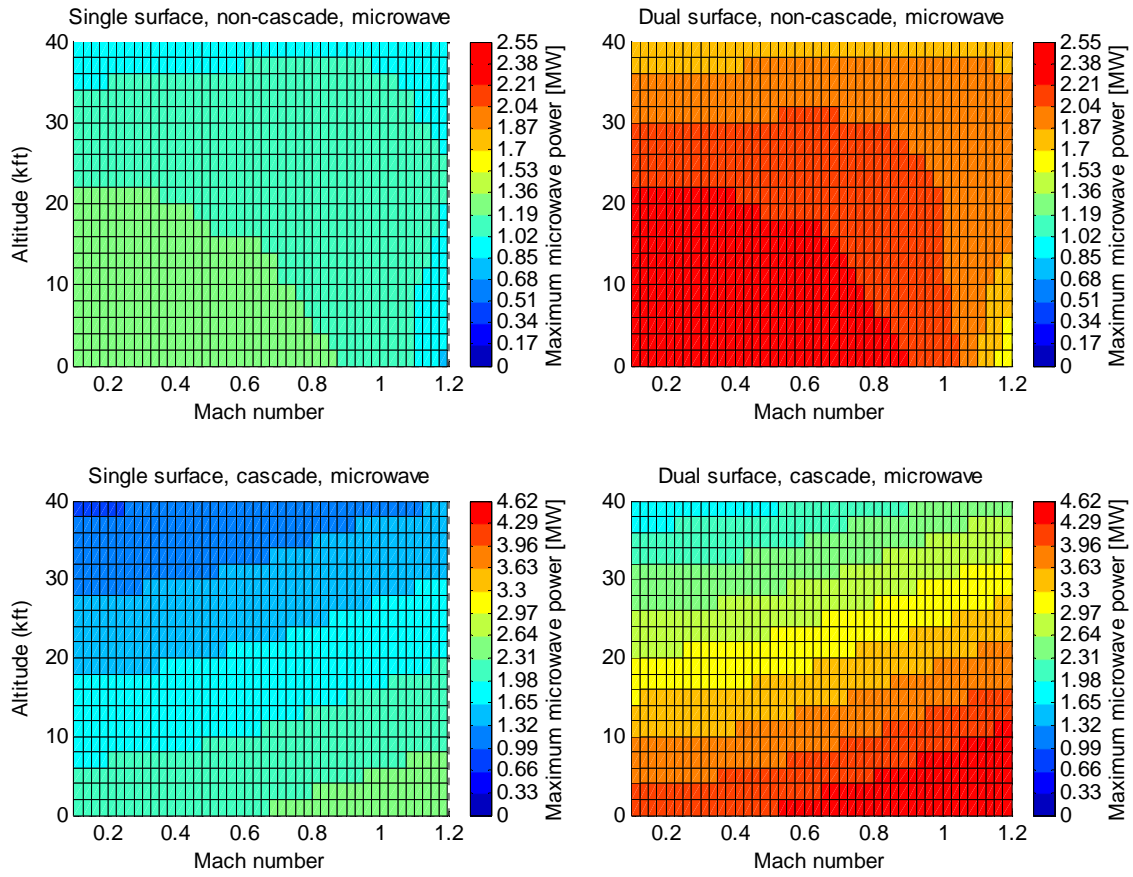


Fig. 53. Maximum microwave power [MW] at 80% throttle

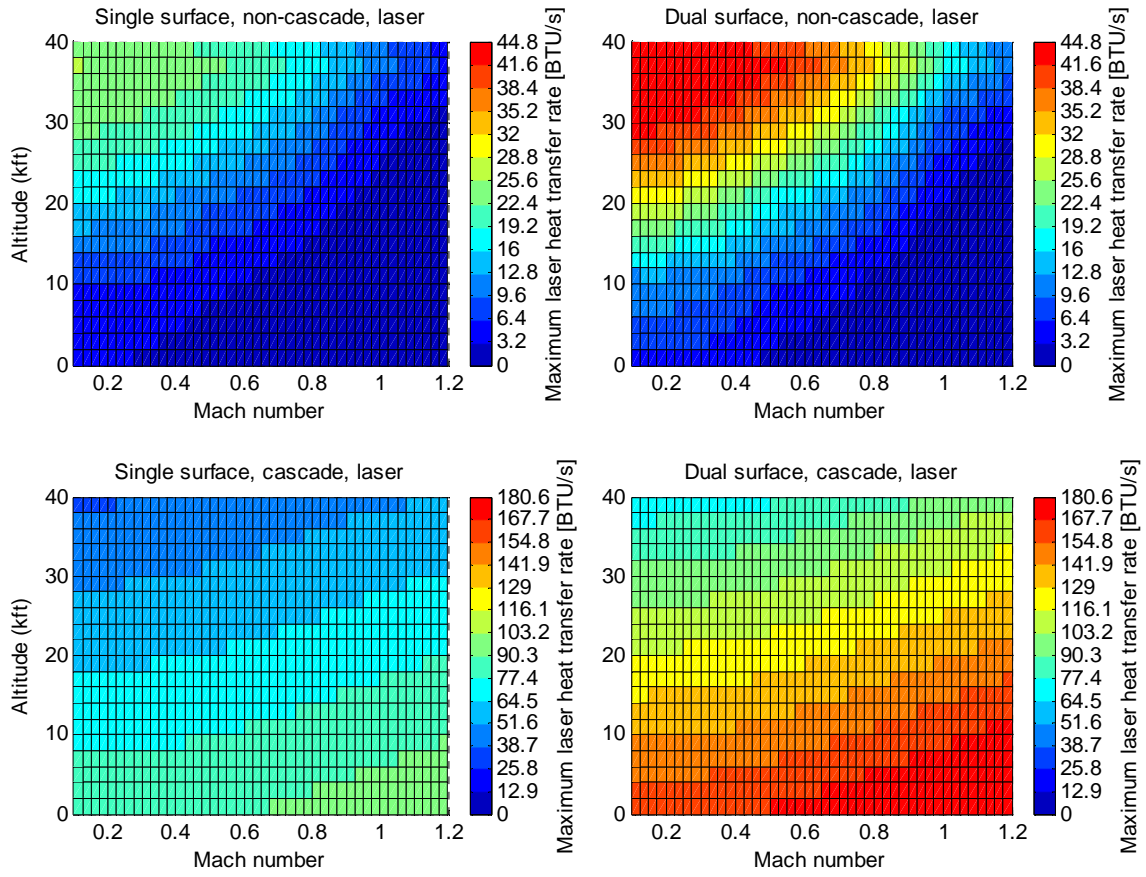


Fig. 54. Maximum laser device cooling capacity [BTU/s] at 80% throttle

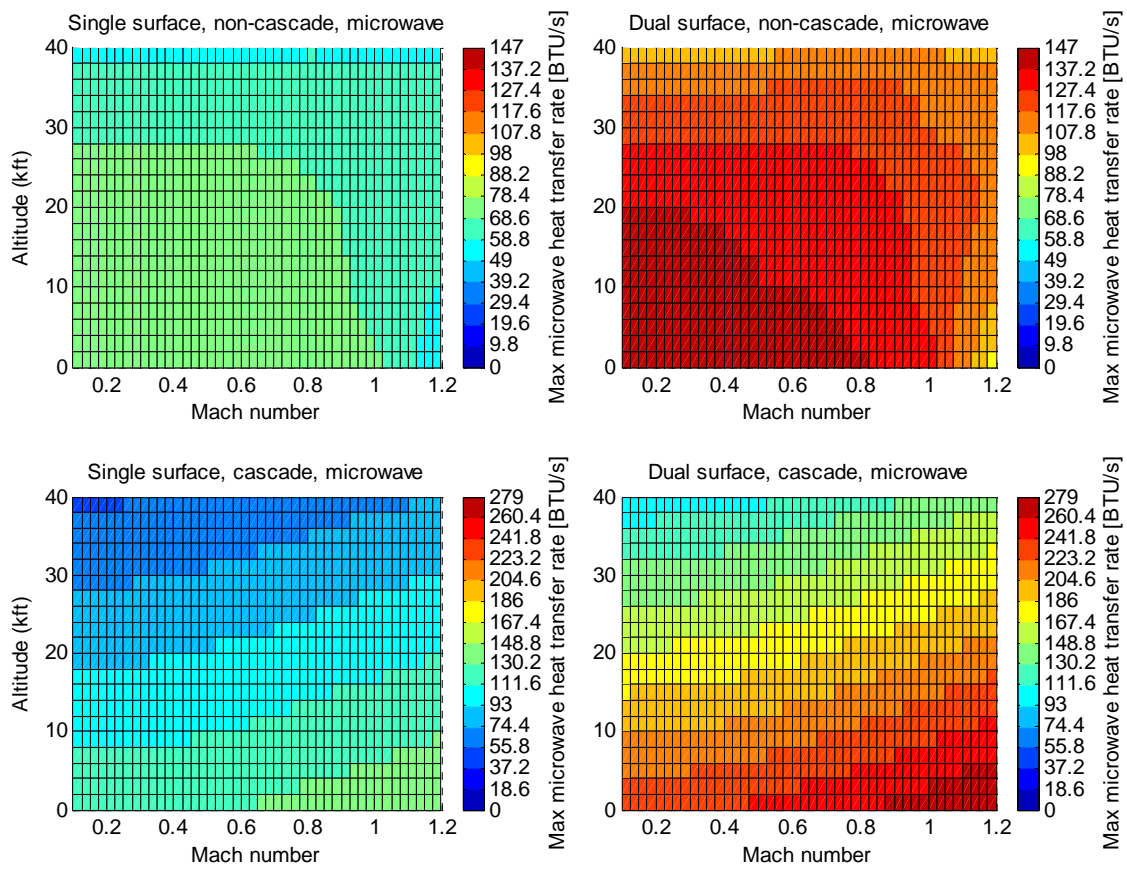


Fig. 55. Maximum microwave device cooling capacity [BTU/s] at 80% throttle

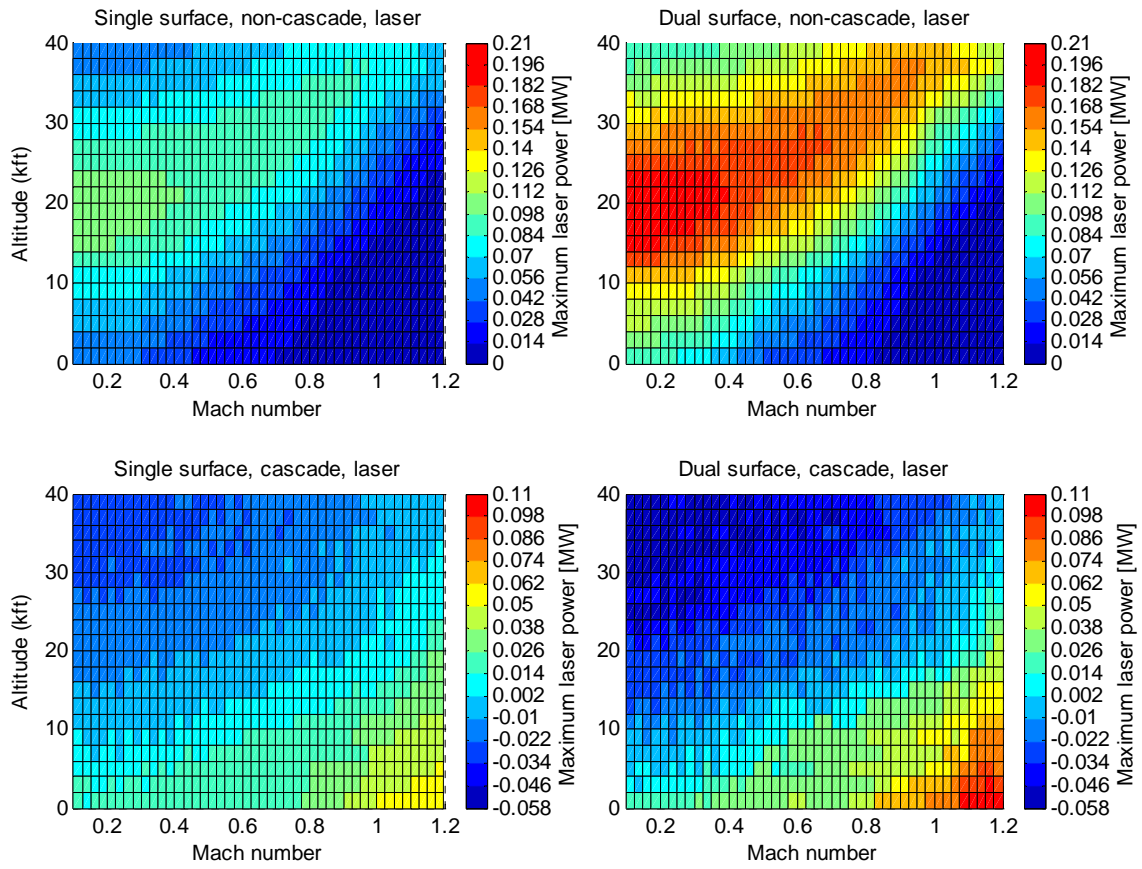


Fig. 56. Difference between 100% and 80% engine throttle for maximum laser device power [MW]

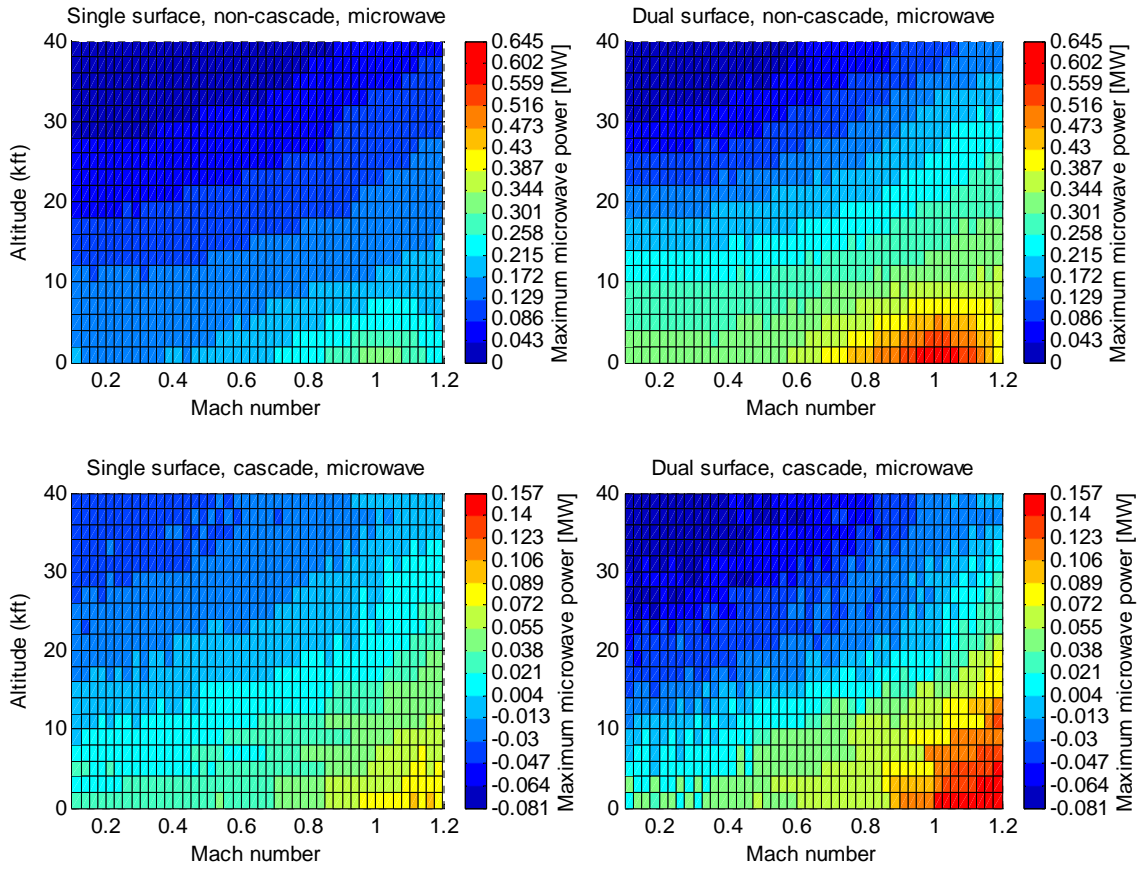


Fig. 57. Difference between 100% and 80% engine throttle for maximum microwave device power [MW]

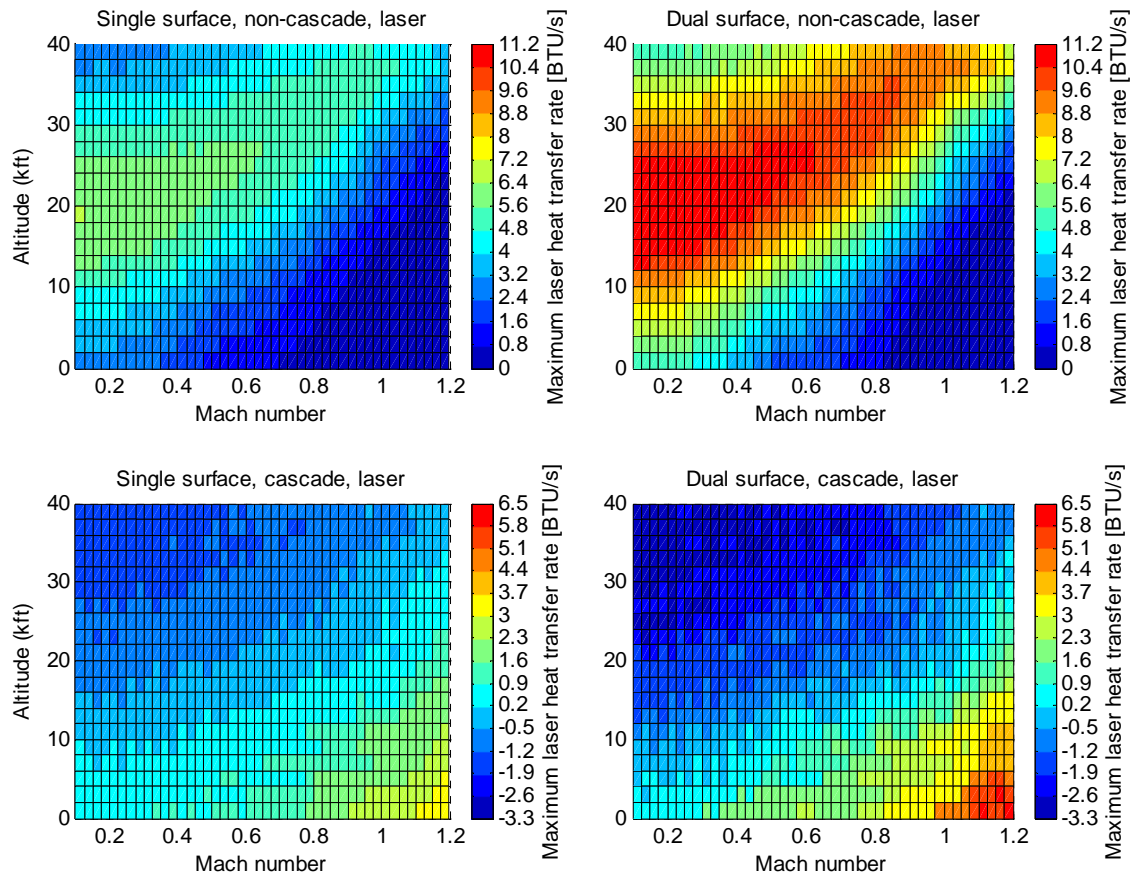


Fig. 58. Difference between 100% and 80% engine throttle for maximum laser device cooling rate [BTU/s]

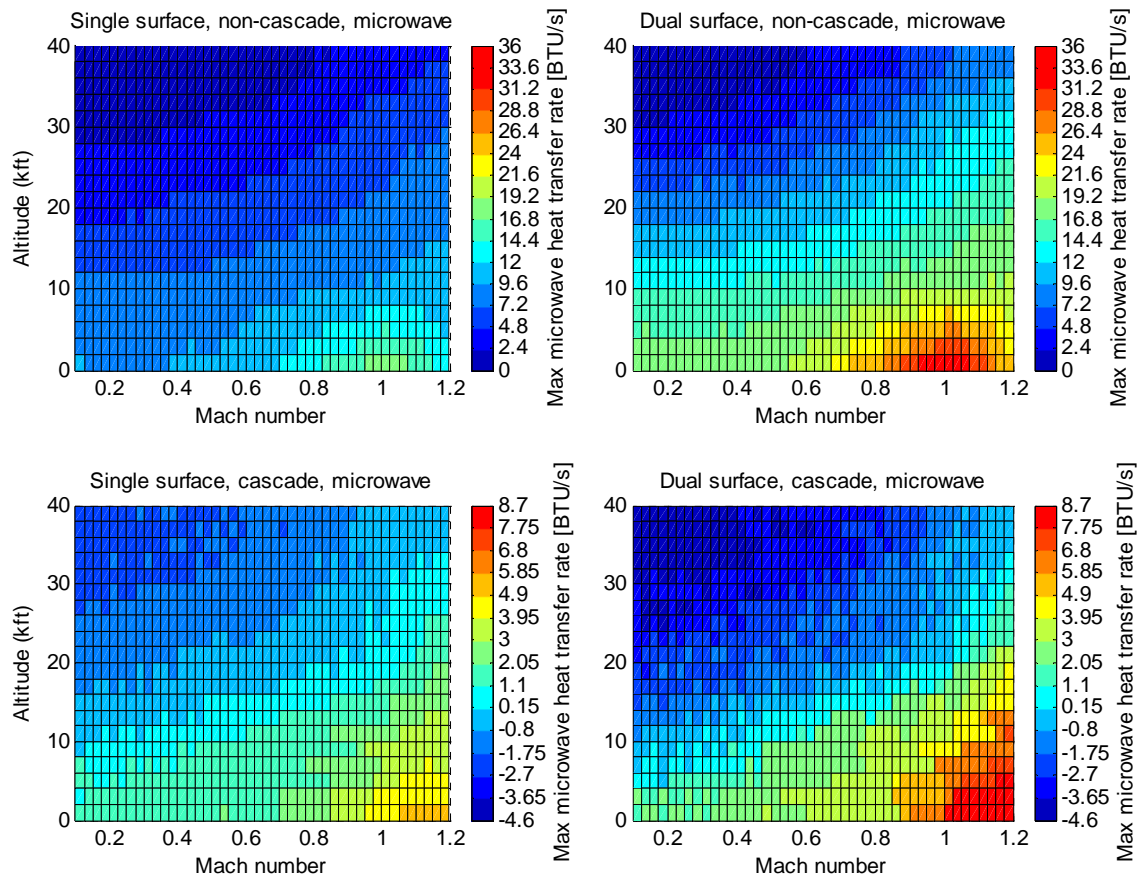


Fig. 59. Difference between 100% and 80% engine throttle for maximum microwave device cooling rate [BTU/s]

Appendix E: Discrete pressure values used in steam tables (psi)

0.1813
0.3626
0.7252
1.4504
7.2519
14.504
29.008
58.015
87.023
116.03
145.04
217.56
290.08
580.15
870.23
1160.3
1450.4
1740.5
2030.5
2320.6
2610.7
2900.8
3190.8

Bibliography

- Anderson, John D. *Modern Compressible Flow*. Boston MA: The McGraw-Hill Companies, Inc., 2003.
- Çengel, Yunus A. et al. *Thermodynamics: An Engineering Approach*. New York NY: The McGraw-Hill Companies, Inc., 1994.
- Craig, Roy R. *Mechanics of Materials*. New York NY: John Wiley & Sons, Inc., 2000.
- Hill, Philip G. and Carl R. Peterson. *Mechanics and Thermodynamics of Propulsion*. Reading MA: Addison-Wesley Publishing Company, Inc., 1992.
- Humble, Ronald W. et al. *Space Propulsion Analysis and Design*. New York NY: The McGraw-Hill Companies, Inc., 1995.
- Mattingly, Jack D. et al. *Aircraft Engine Design*. Reston VA: American Institute of Aeronautics and Astronautics, Inc., 2002.
- Moran, Michael J. and Howard N. Shapiro. *Fundamentals of Engineering Thermodynamics*. Hoboken NJ: John Wiley and Sons, Inc., 2004
- National Institute of Standards and Technology. "Thermophysical Properties of Fluid Systems." <http://webbook.nist.gov/chemistry/fluid/>. 05 October 2007.
- NOAA, NASA, and USAF. *U.S. STANDARD ATMOSPHERE, 1976*. NOAA-S/T 76-1562, October 1976.
- Perram, Glen P., Michael A. Marciniak, and Matthew Goda "High Energy Laser Weapons: Technology Overview," *A Critical Review - Laser Technologies for Defense and Security*. 1-25. Bellingham, WA: The International Society for Optical Engineering, 2004.
- Scott, William B. "Joint Office to Demo 25-kw. Laser Weapons," *Aviation Week & Space Technology*, 160:57-58 (June 2004)
- Shanmugasundaram, V., M. L. Ramalingam, B. Donovan, T. Mahefkey, and B. Hager "Analytical Investigation of Thermal Management Options for An Aircraft Based High Pulsed Power System Application," *3rd International Energy Conversion Engineering Conference*. 1213-1226. Reston, VA: American Institute of Aeronautics and Astronautics Inc., 2005.
- Shanmugasundaram, V., M. L. Ramalingam, and B. Donovan "Thermal Management System With Energy Storage for an Airborne Laser Power System Application," *5th*

International Energy Conversion Engineering Conference and Exhibit. 981-997. Reston, VA: American Institute of Aeronautics and Astronautics Inc., 2005.

Wang, J.R., J.C. Min, and Y.Z. Song “Forced convective cooling of a high-power solid-state laser slab,” *Applied Thermal Engineering*, 26:549-558 (April 2006)

Vita

Captain Nathan Klatt graduated from Mission Bay high School in San Diego, CA in May of 1996. He attended the University of Colorado at Boulder, where he graduated with a Bachelor of Science of Civil Engineering, with an emphasis in structural design, in December 2000. He was commissioned the same month through Detachment 105, Air Force ROTC.

Captain Klatt began active duty as a fill-in section commander and intelligence trainee at Mountain Home AFB, ID. There he learned about F-15C, F-15E, F-16CJ, B-1B, and KC-135 operations and unit support. After a short tour in Idaho, he began intelligence training at Goodfellow AFB, TX. After graduating tech school, he was reassigned to Osan AB, South Korea. He was worked at to the 51st Operations Support Squadron providing wing level support to A-10, F-16, U-2, HH-60, and C-12 squadrons stationed there. A year later he was reassigned to the U-2 squadron as the sole source of intelligence for the increased theater assets. In April 2004, he was reassigned to the Space Warfare Center, Detachment 2, at Langley AFB, VA. There, he provided engineering analysis and test support for a variety of programs furthering air and space integration. In May 2006, he entered the Air Force Institute of Technology Graduate School of Engineering and Management for his Masters of Science in Aeronautical Engineering. His emphasis was in air breathing and rocket propulsion. Upon graduation in March 2008, he will be assigned to the Air Force Research Labs at Kirtland AFB, NM.

REPORT DOCUMENTATION PAGE

Form Approved
OMB No. 074-0188

The public reporting burden for this collection of information is estimated to average 1 hour per response, including the time for reviewing instructions, searching existing data sources, gathering and maintaining the data needed, and completing and reviewing the collection of information. Send comments regarding this burden estimate or any other aspect of the collection of information, including suggestions for reducing this burden to Department of Defense, Washington Headquarters Services, Directorate for Information Operations and Reports (0704-0188), 1215 Jefferson Davis Highway, Suite 1204, Arlington, VA 22202-4302. Respondents should be aware that notwithstanding any other provision of law, no person shall be subject to a penalty for failing to comply with a collection of information if it does not display a currently valid OMB control number.

PLEASE DO NOT RETURN YOUR FORM TO THE ABOVE ADDRESS.

1. REPORT DATE (DD-MM-YYYY) 20-04-2008		2. REPORT TYPE Master's Thesis		3. DATES COVERED (From - To) Jan 07-Mar 08		
4. TITLE AND SUBTITLE ON-BOARD THERMAL MANAGEMENT OF WASTE HEAT FROM A HIGH-ENERGY DEVICE				5a. CONTRACT NUMBER		
				5b. GRANT NUMBER		
				5c. PROGRAM ELEMENT NUMBER		
6. AUTHOR(S) Klatt, Nathan D., CAPT, USAF				5d. PROJECT NUMBER		
				5e. TASK NUMBER		
				5f. WORK UNIT NUMBER		
7. PERFORMING ORGANIZATION NAMES(S) AND ADDRESS(S) Air Force Institute of Technology Graduate School of Engineering and Management (AFIT/EN) 2950 Hobson Way WPAFB OH 45433-7765				8. PERFORMING ORGANIZATION REPORT NUMBER AFIT/GAE/ENY/08-M18		
9. SPONSORING/MONITORING AGENCY NAME(S) AND ADDRESS(ES) AFRL/RZTA Attn: Dr. Nick Kuprowicz 1950 Fifth Street Wright-Patterson AFB, OH 45433				10. SPONSOR/MONITOR'S ACRONYM(S)		
				11. SPONSOR/MONITOR'S REPORT NUMBER(S)		
12. DISTRIBUTION/AVAILABILITY STATEMENT APPROVED FOR PUBLIC RELEASE; DISTRIBUTION UNLIMITED.						
13. SUPPLEMENTARY NOTES Advisor: Dr. Paul I. King, (937) 255-3636, ext 4628 paul.king@afit.edu						
14. ABSTRACT The use of on-board high-energy devices such as megawatt lasers and microwave emitters requires aircraft system integration of thermal devices to either rid waste heat or utilize it in other areas of the aircraft. Non-chemical lasers are among the most challenging applications due to the low cooling temperature requirements (67 °F) and high waste heat generation times of order 20 s. (Microwave devices will be cooled at 157.7 °F.) One plan calls for the rapidly generated waste energy to be stored prior to peripheral utilization, with subsequent removal of the heat over a 5-10 minute span. A method is presented that explores the primary factors in a laser-generated waste heat removal system to allow an understanding of the trade space between the laser power, overall thermal efficiency, and the duty cycle. Methodology includes incorporation of a single heat pump or cascaded heat pumps that transfer waste heat from the high-energy device into the bypass section of a mixed-bypass turbofan jet engine. Analyzed are multiple heat exchanger configurations that do not block the bypass air flow, minimizing friction losses. Some particulars of the waste heat removal system include a water coolant for the heat pump(s) and a maximum coolant temperature limited to 2,270 R. Results of an engine performance model used to determine the impact of the thermal management system are also presented.						
15. SUBJECT TERMS Mixed turbofan engine, turbofan, high-energy device, laser, microwave, cooling, bypass cooling, bypass duct, fan duct, heat pump, aircraft, cascaded, heat exchanger, annulus, refrigerant, water, steam, thermal storage, thermal management, heat dissipation						
16. SECURITY CLASSIFICATION OF:			17. LIMITATION OF ABSTRACT	18. NUMBER OF PAGES	19a. NAME OF RESPONSIBLE PERSON	
REPORT U	ABSTRACT U	c. THIS PAGE U	UU	120	Dr. Paul I. King	
			19b. TELEPHONE NUMBER (Include area code) (937) 255-6565, ext 4628; e-mail: paul.king@afit.edu			